



**TRANSFORMATION TO ZERO OFFSET**

by

**Thomas E. Jordan**

**Partially supported by the Consortium Project on  
Seismic Inverse Methods for Complex Structures**

**Center for Wave Phenomena  
Department of Mathematics  
Colorado School of Mines  
Golden, Colorado 80401  
Phone: (303)273-3557**



## ABSTRACT

Since its introduction in the late 1970's, dip moveout has firmly entrenched itself as part of the processing sequence for complex structure. Dip moveout compensates for reflection point dispersal, properly sorting events into zero offset traces containing reflections arising from common depth points. To this end, the dip moveout mapping has been well defined.

Dip-moveout amplitudes remain a mystery. The amplitude factors for conventional dip moveout arise from a Jacobian of traveltimes in going from finite offset to zero offset. To this extent, dip moveout is not a wave-equation based operation. Many questions remain regarding the proper distribution of amplitudes along the limbs of the operator.

A wave-equation based algorithm can be formulated by considering the transformation to zero offset to be a two-fold process - prestack migration/inversion followed by a zero offset forward model. The prestack migration/inversion defines the subsurface. The zero offset model transforms this subsurface into zero offset time data. This cascaded migration/modeling analogy can be utilized explicitly to formulate a wave-equation based dip moveout. By taking advantage of integral operators, a cascaded migration/modeling scheme can be defined and reduced analytically to an algorithm suitable for implementation on a digital computer.

In order to preserve amplitudes, an inversion algorithm can be

utilized in place of a migration in the cascaded migration/modeling system. An inversion algorithm offers the advantage of preserving amplitude information, and of compensating for the geometrical bias inherent in seismic data recording.

Prestack applications of such a transformation to zero offset include velocity analysis and amplitude versus offset processing in the presence of structure. In particular, amplitude offset analysis requires a certain degree of confidence in the amplitude preservation of the preprocessing sequence. With conventional dip moveout the amplitudes are given little attention and the resultant data contains questionable amplitude information. A wave-equation based dip moveout offers the possibility of generating data upon which reliable amplitude interpretation can be based.

This thesis will develop a dip-moveout algorithm based upon a cascaded inversion/modeling development. The resultant operator differs markedly from conventional dip-moveout. Examples are shown for both real and synthetic data.

## TABLE OF CONTENTS

	Page
ABSTRACT.....	i
TABLE OF CONTENTS.....	iii
LIST OF FIGURES.....	v
ACKNOWLEDGEMENTS.....	viii
GLOSSARY.....	x
BACKGROUND AND INTRODUCTION.....	1
1. WAVE EQUATION DIP MOVEOUT.....	5
1.1 Review of DMO by Fourier Transform.....	5
1.2 Why a New Dip-Moveout Formulation?.....	10
1.3 Wave Equation Dip-Moveout.....	12
2. INVERSION BACKGROUND.....	21
2.1 The Beylkin Transformation.....	21
2.2 The Inversion Geometry.....	28
2.3 Illuminating the Subsurface with Limited Aperture.....	31
3. THE TRANSFORMATION TO ZERO OFFSET.....	35
3.1 Overview.....	35
3.2 The 2.5 Solution.....	37
3.3 The TZO Impulse Response.....	40
3.4 Processing Applications.....	46
3.4.1 Velocity analysis.....	47
3.4.2 Amplitude versus offset.....	52
3.5 Stacking.....	54

3.6	When $v_0$ Is Not Equal To $v_m$ .....	56
3.7	Two or Three Dimensions?.....	58
3.8	Cost.....	60
	CONCLUSIONS.....	61
	REFERENCES.....	63
APPENDIX A:	2.5D TZO DERIVATION.....	67
APPENDIX B:	3D TZO DERIVATION - COMMON SHOT.....	85
APPENDIX C:	STATIONARY PHASE FORMULA.....	101
APPENDIX D:	TZO $\stackrel{?}{=} \text{NMO} + \text{DMO}$ .....	102
APPENDIX E:	DIP MOVEOUT AS INTERCEPT MAPPING.....	106
APPENDIX F:	LIMITS TO INTEGRATION.....	110
APPENDIX G:	CALCULATION OF DETERMINANT $h$ - 2.5D COMMON SHOT.....	113
APPENDIX H:	CALCULATION OF DETERMINANT $h$ - 3D COMMON SHOT.....	121
APPENDIX I:	CALCULATION OF DETERMINANT $h$ - 2.5D COMMON OFFSET.....	129
	FIGURES.....	135

## LIST OF FIGURES

Figure		Page
1.1	Reflector point dispersal.....	135
1.2	FK DMO impulse response.....	136
1.3	Example shot record raypath density.....	137
1.4	Geometrical interpretation of DMO impulse response	
	a. Pre-stack migration ellipse.....	138
	b. Rocca's smile-DMO impulse response.....	138
1.5	3D nature of DMO.....	139
2.1	Schematic of integral summation migration	
	a. Point diffractor generates hyperbola.....	140
	b. Output is superposition of guess hyperbolas.....	140
2.2	The nature of the wavevector $\mathbf{k}$ .....	141
2.3	Limits of recording aperture	
	a. Dip limits defined by recording geometry.....	142
	b. Corresponding wavevector limits defined by recording geometry.....	142
3.1	2.5D geometry.....	143
3.2	Berg DMO impulse response offset = 5,000 ft.....	144
3.3	Impulse response comparison-Berg vs. TZO common shot	
	a. Offset = 5,000 ft.....	145
	b. Offset = 10,000 ft.....	146
3.4	Shot record ray coverage.....	147
3.5	Zero offset ray coverage.....	147
3.6	The gradient of the phase as related to ray.....	148

3.7	Impulse response comparison-Berg vs. TZO common offset	
	a. Offset = 5000.....	149
	b. Offset = 10000.....	150
3.8	Domain of zero offset influence from shot records.....	151
3.9	Schematic of shot domain velocity analysis.....	152
3.10	Depth model for synthetic velocity analysis.....	153
3.11	Velocity analysis on model data.....	154
3.12	Gulf of Mexico salt dome - near trace display.....	155
3.13	Berg v. TZO velocity analysis comparison $v = 5,000 + 375t$ .....	156
3.14	Enlargements of Fig. 3.13	
	a. 0-1 seconds.....	157
	b. 1-2 seconds.....	158
	c. 2-3 seconds.....	159
3.15	Berg vs. TZO velocity analysis comparison $v = 5,600 + 1,050t$ .....	160
3.16	Enlargements of Fig. 3.15	
	a. 0-1 seconds .....	161
	b. 1-2 seconds.....	162
	c. 2-3 seconds.....	163
3.17	Berg vs. TZO velocity analysis comparison $v = 6,000 + 1,500t$ .....	164
3.18	Enlargements of Fig. 3.17	
	a. 0-1 seconds.....	165
	b. 1-2 seconds.....	166

	c.	2-3.....	167
3.19		Semblance analysis - Berg vs. TZO.....	168
3.20		Berg vs. TZO common offset comparison.....	169
3.21		Enlargements of Fig. 3.20	
	a.	0-1 seconds.....	170
	b.	1-2 seconds.....	171
	c.	2-3 seconds.....	172
3.22		Near trace display showing domain of stacked data.....	173
3.23		Comparison of Berg vs. TZO stack.....	174
3.24		Enlargements of Fig. 3.23	
	a.	0-1 seconds.....	175
	b.	1-2 seconds.....	176
	c.	2-3 seconds.....	177
3.25		Fresnel zone overlap for 3D data zone overlap for 3D data....	178
A-1		Geometrical interpretation of width of DMO ellipse.....	179
B-1		Out of plane speculars mapping to in-line data.....	180
B-2		3D Common shot geometry.....	181
D-1		Mapping geometry for DMO variables and TZO variables.....	182
E-1		Location of specular reflection for a given shot, geophone, and zero offset output point.....	183
E-2		Image source analysis to facilitate the computation of the location of the specular reflection point.....	184
F-1		Dip limits determined from geometry.....	185

All data are plotted relative amplitude scale unless otherwise noted.

## ACKNOWLEDGEMENTS

When a project of this magnitude is completed, it is too easy to forget the stumbling blocks along the way, and the countless contributions which helped to overcome them. Many people have contributed to my efforts. I have space to mention but a few.

Norm Bleistein has been a tremendous source of inspiration and guidance. His mathematical abilities are matched only by his enthusiasm and ongoing curiosity. It has been a rare privilege to be associated with him.

Jack Cohen first suggested the formulation of the problem as a system of cascaded operators. His early involvement in this project was critical to its success. Shuki Ronen lent his wealth of knowledge and experience on dip moveout. Shuki's ability to distinguish fact from artifact helped avoid many pitfalls. Brian Sumner wrote the graphics routines which made most of the figures possible. To Brian, a thousand thanks.

I am deeply indebted to the Center for Wave Phenomena for providing me with the support and academic freedom which made this project possible. In particular, the generous support of the sponsors of the Consortium Project on Seismic Inverse Methods for Complex Structures is greatly appreciated.

Barbara McLenon typed and prepared the manuscript. Her patience, professionalism and dedication made even the final harried days a

pleasant experience.

Most of all, thanks to my son, Matthew. Good friends are hard to find.



## GLOSSARY

$\omega$ :	zero offset (output) frequency
$\eta$ :	input frequency
$\xi_0$ :	zero offset trace location; $\xi_0 = (\xi_{01}, \xi_{02})$
$\xi_s$ :	shot location; $\xi_s = (\xi_{s1}, \xi_{s2})$
$\xi_g$ :	geophone location; $\xi_g = (\xi_{g1}, \xi_{g2})$
$\mathbf{x}$ :	$\mathbf{x} = (x, y, z)$ subsurface variables
$A_0^2(\mathbf{x})$ :	square of zero offset Green's function amplitude

$$A_0^2(\mathbf{x}) = \frac{1}{(4\pi\rho_0)^2}$$

$$\rho_0 = \sqrt{(x-\xi_{01})^2 + (y-\xi_{02})^2 + z^2}$$

$A_s(\mathbf{x})A_g(\mathbf{x})$ : offset Green's function amplitude

$$A_s(\mathbf{x})A_g(\mathbf{x}) = \frac{1}{(4\pi\rho_s)(4\pi\rho_g)}$$

$$\rho_s = \sqrt{(x-\xi_{s1})^2 + (y-\xi_{s2})^2 + z^2}$$

$$\rho_g = \sqrt{(x-\xi_{g1})^2 + (y-\xi_{g2})^2 + z^2}$$

$v_0$ : zero offset modeling velocity

$v_m$ : inversion velocity

$\phi_0(\mathbf{x}, \xi_0)$ : zero offset Green's function phase

$$\phi_0(\mathbf{x}, \xi_0) = \frac{2\rho_0}{v_0}$$

$\phi_s(\mathbf{x}, \xi)$ : offset Green's function phase

$$\phi_s(\mathbf{x}, \xi) = \frac{(\rho_s + \rho_g)}{v_m}$$

$|h(\mathbf{x}, \xi)|$ : determinant of the form:

$$h(\mathbf{x}, \xi) = \det \begin{vmatrix} \nabla \phi_s \\ \frac{\partial}{\partial \xi_1} \nabla \phi_s \\ \frac{\partial}{\partial \xi_2} \nabla \phi_s \end{vmatrix}$$

$D(\eta, \xi)$ : input data (Fourier transformed)

$F(\eta)$ : band limited prefilter (optional)

## BACKGROUND AND INTRODUCTION

This thesis is about dip moveout. The viewpoint is one which arises from seismic inversion theory.

In a more general context, this thesis is about the process of transforming seismic data to zero offset. Traditionally, this transformation to zero offset was accomplished by means of normal-moveout (NMO) applied to common-midpoint (CMP) gathers. Unfortunately, such a process has the effect of acting as a dip filter since NMO velocities are related to dip through the relationship (Levin, 1971):

$$v_{\text{nmo}} = \frac{v}{\cos\theta}$$

More recently, dip moveout has been introduced to properly position events for stacking. With dip moveout, the correct NMO velocity is the true velocity,  $v$ , which is dip independent. Together, the procedures NMO + DMO comprise current state-of-the-art in transforming seismic data to zero offset.

Although dip moveout is a fairly recent development in seismic data processing, the list of contributors is long, and their contributions are outstanding. The idea for dip moveout is generally credited to Judson, Schultz and Sherwood, who presented a paper at the 48th Annual SEG Meeting in San Francisco describing a technique they called

DEVILISH. This technique was never published in detail.

Yilmaz and Claerbout (1980) published "Prestack Partial Migration". There, they arrived at dip moveout through the double square root equation. Although, in hindsight, their methodology appears cumbersome, this paper was a landmark in defining the dip moveout problem and in illustrating many of the relevant concepts behind dip moveout.

Deregowski and Rocca (1981) gave a geometrical interpretation to dip moveout which serves as the foundation for much of this thesis. They described the transformation to zero offset as a two-stage process - full prestack migration followed by zero offset modeling.

Bolondi, Loinger and Rocca (1982) presented dip moveout in the context of finite differencing over offset (offset continuation). Introducing a differential equation for dip moveout, they show that the solution can be expressed by continuing the recorded data over offset until zero offset is reached. This differential equation was never derived. It can be derived by pure traveltime arguments, or by recognizing that dip moveout is equivalent to migration with a velocity  $h/t$ .

In a companion paper to Bolondi, et al., Salvador and Savelli (1982) discussed offset continuation in the context of seismic stacking. They made the observation that offset continuation offers the possibility of stacking along the way. This makes finite differencing particularly attractive from the perspective of computation time.

In his Ph.D. dissertation, Dave Hale (1983) treats dip moveout in

the context of the Fourier Transform. This work was published in **Geophysics** the following year. Hale shows a method for doing dip moveout by a simple substitution of variables in the  $(\omega, k)$  domain.

Berg (1984) derived a time domain implementation of the Hale algorithm. Starting with Hale's result, Berg transforms the dip moveout operator to the  $(x, t)$  domain. The algorithm derived in this thesis is also an  $(x, t)$  algorithm. Berg's results are used as the basis for comparison.

Biondi and Ronen (1986) presented a paper at the SEG Annual Meeting in Houston which discussed a substitution of variables which makes the dip moveout impulse response time invariant. By making the substitution  $t = e^{\tau}$ , both the Fourier methods and finite-difference methods for dip-moveout are made much faster. This is undoubtedly a trick which will soon become commonplace.

The above review is by no means comprehensive. It does, however, represent the major works which serve as a background for this thesis.

In Chapter 1 Hale's  $(\omega, k)$  algorithm is reviewed. This provides motivation for the inversion based algorithm which is the major result of this thesis. Chapter 1 will attempt to underscore the idea that the conventional approach to dip moveout is not based on the wave equation. It is a mapping based on travelttime considerations. Chapter 1 will introduce a wave-equation based approach, leaving the derivation for subsequent discussion.

The wave-equation approach suggested by Chapter 1 will rely heavily

on the mathematics of seismic inversion. To this end, Chapter 2 reviews some of this inversion machinery. Those uninterested in the mathematical details of the inversion algorithm are invited (and encouraged) to skip Chapter 2.

Chapter 3 will present the inversion-based algorithm for transforming data to zero offset. This algorithm is derived in the appendices. Chapter 3 will discuss many of the attributes of this algorithm. These include the relationship of this algorithm to dip-moveout, two- and three-dimensional applications, and the duality of the velocity field suggested by the algorithm.

Chapter 3 will also present two prestack applications of this wave-equation based dip moveout - velocity analysis and amplitude versus offset processing.

This thesis relies heavily on mathematical methods which are involved and unfamiliar to most geophysicists. In the final analysis the mathematics are irrelevant. They are a means to an end. Many of the mathematical details have been banished to the appendices.

## 1. WAVE EQUATION DIP MOVEOUT

### 1.1 Review of DMO by Fourier Transform

The constant velocity travelttime relationship for reflectors on a CMP gather is given by:

$$t^2 = t_0^2 + \frac{4h^2}{v_{nmo}^2} . \quad (1.1)$$

For horizontal reflectors this relationship is exact and the stacking velocity,  $v_{nmo}$ , is equal to the interval velocity,  $v$ . If the reflector is dipping, there still exists a  $v_{nmo}$  which aligns the reflectors on a CMP gather. The  $v_{nmo}$  which aligns the reflector is a function of the dip (Levin, 1971):

$$v_{nmo} = \frac{v}{\cos\theta} . \quad (1.2)$$

Using  $v_{nmo}$  as defined by Eq.(1.2), NMO can align events from reflectors of arbitrary dip. Unfortunately, the  $v_{nmo}$  which produces this alignment is a function of the dip. If two events cross one another on a time section the process of NMO + stacking has the effect of selecting one dip over another. Thus, stacking is a dip filter.

Furthermore, even though Eq.(1.1) can be used to align dipping events on CMP gather, the reflection points do not coincide (Fig. 1.1). That is, the reflection points come from a smear on the reflector. It

is only the horizontal reflector which contains reflections from the same subsurface point. Thus, the negative effects of dipping reflectors on CMP stacking are two-fold. Not only is the optimum stacking velocity dip dependent (and, therefore, dip selective), but the stack is over a smear in the subsurface.

Substituting Eq.(1.2) into Eq.(1.1), and using the trigonometric relationship  $\cos^2\theta = 1 - \sin^2\theta$  gives:

$$t^2 = t_0^2 + \frac{4h^2}{v^2} - \frac{4h^2}{v^2} \sin^2\theta \quad . \quad (1.3)$$

This suggests that there is a two-stage process. Defining a new traveltime variable,  $t_n$ , by:

$$t_n^2 = t_0^2 - \frac{4h^2}{v^2} \sin^2\theta \quad . \quad (1.4)$$

Equation 3 can be rewritten to look exactly like NMO using the true earth velocity,  $v$ :

$$t^2 = t_n^2 + \frac{4h^2}{v^2} \quad . \quad (1.5)$$

Equation 1.5 describes an NMO relationship. The output from this NMO is no longer  $t_0$ , but a new variable  $t_n$  as given by Eq.(1.4). Eq.(1.4) is dip moveout, though still cast in terms of the dip  $\theta$ . That

is, it is still dip selective. Furthermore, Eq.(1.4) describes a travelttime shift. Used by itself it will not reposition events such that the stack is over common subsurface reflection points. This repositioning (i.e., partial migration) comes for free once we express these relationships in the  $(\omega, k)$  domain.

The goal is to find a Fourier method to transform recorded data to zero offset. Zero offset data for a given offset  $h$  can be written in the Fourier domain as a transform over space and time:

$$D_0(\omega_0, k, h) = \int dt_0 e^{i\omega_0 t_0} D_0(t_0, k, h) \quad . \quad (1.6)$$

Equation (1.4) defines a relationship between offset recorded data and equivalent zero offset data. To use this relationship in a Fourier method, it must be expressed in terms of  $(\omega, k)$ . In terms of zero offset data:

$$\sin\theta = \frac{vk}{2\omega_0} \quad . \quad (1.7)$$

Equation (1.4) becomes:

$$t_n^2 = t_0^2 - \frac{h^2 k^2}{\omega_0^2} \quad . \quad (1.8)$$

Now the zero offset data,  $D_0(t_0, k, h)$ , can be expressed in terms of

the offset data,  $D(t_n, k, h)$ :

$$D_0(t_0, k, h) = D(t_n(t_0), k, h) \quad . \quad (1.9)$$

$D(t_n, k, h)$  is the recorded data after NMO with the earth velocity,  $v$ . Equation (1.9) suggests a substitution in the Fourier integral of Equation (1.6):

$$D_0(\omega_0, k, h) = \int dt_0 e^{i\omega_0 t_0} D(t_n(t_0), k, h) \quad . \quad (1.10)$$

This integral can be rewritten as an integral over  $t_n$  by a simple substitution of variables. The Jacobian of this substitution is commonly given the name  $A$ :

$$A = \frac{dt_n}{dt_0} = \sqrt{1 + \left[ \frac{hk}{\omega_0 t_n} \right]^2} \quad . \quad (1.11)$$

Then Eq.(1.10) becomes:

$$D_0(\omega_0, k, h) = \int dt_n A^{-1} e^{i\omega_0 A t_n} D(t_n, k, h) \quad . \quad (1.12)$$

This is dip moveout by Fourier transform. A serious problem with Eq.(1.12) is the  $A$  appearing in the exponent.  $A$  is a function of input time  $t_n$ . The net effect is that Eq.(1.12) as written cannot utilize

fast Fourier Transform algorithms. The  $t_n \rightarrow \omega_0$  transform must be done explicitly. However, Fabio Rocca has suggested a log-stretch transformation (Biondi and Ronen (1986)) which makes the Jacobian A time invariant and greatly enhances the practical applicability of Eq. (1.12).

Furthermore, note that A is not a function of the velocity, v. Thus, dip moveout is considered to be a process which is velocity independent. To be fair, we should note that this is only partially true. A truer statement is that dip moveout requires no more knowledge of the velocity field than that required by NMO, where NMO is taken to be NMO with the true earth velocities. Any error made in these velocities is passed on by dip moveout. The relevance of this remark will become clearer in Chapter 3.

Figure 1.2 shows an impulse response from dip moveout by Fourier Transform. The impulse response is an ellipse given by:

$$\left[ \begin{array}{c} t_o \\ t_n \end{array} \right]^2 + \left[ \begin{array}{c} x \\ h \end{array} \right]^2 = 1 \quad . \quad (1.13)$$

x is the distance from the midpoint.

The horizontal axis of the ellipse is equal to the offset (2h). The limbs of the operator near the surface are evanescent, corresponding to events with a travelttime slower than the travelttime of the media (i.e., the slope of the limbs is greater than 2/v). This evanescent energy is not a problem if one intends to migrate the output before

stacking over offset. Migration will naturally remove this energy by not migrating it. However, this evanescent energy may seriously degrade the signal to noise ratio if it is stacked along with the data enroute to post-stack migration. Limiting the integration of Eq.(1.12) in order to cancel the evanescent energy requires knowledge of the velocity field. This removes the velocity independence of dip-moveout processing (Hale, 1983).

### 1.2 Why a New Dip Moveout Formulation?

In the past decade dip moveout has established itself as a major tool in the processing of seismic data for complex structure. It is robust and fairly insensitive to velocity error. One might justifiably ask why we need consider a new algorithm. The answer, simply put, is that conventional dip moveout is not a wave-equation based algorithm. The goal is to formulate a wave-equation based dip moveout which might be an improvement over conventional dip moveout.

The derivation of dip moveout in the previous section does not reference the wave equation. Conventional dip moveout is based entirely on travelttime arguments. In particular, consider again the substitution given by Eq.(1.9) which is restated here for convenience:

$$D_0(t_0, k, h) = D(t_n(t_0), k, h) \quad . \quad (1.9)$$

This states that data recorded with source-geophone offset,  $D(t_n, k, h)$ , is equal to the corresponding zero offset data,  $D_0(t, k, h)$

given the appropriate travelttime relationship,  $t_n = t_n(t_0, \omega, k, h)$ . What is the basis for this equality? Among other things, the two wavefields have experienced different travelpaths and, therefore, exhibit different amplitude decay.

A fundamental assumption behind Eq.(1.9) is that  $D(t_n, k, h)$  has been corrected for spherical divergence. Spherical divergence corrections attempt to remove all wavefront decay. Therefore, Eq.(1.9) can only be true in the context that by  $D_0(t_0, k, h)$  we mean a  $D_0$  which has spherical divergence corrections applied. The bottom line is that the equality implied by Eq.(1.9) is a dubious equality with respect to the amplitude of the respective wavefields.

Let's step back from this discussion for a moment and review the goals of this procedure. The primary goal is to transform a recorded dataset to zero offset. That is, we would like to recover a wavefield which is equivalent to a wavefield we might have recorded if the shots and geophones had been together on the surface. Any tendency of the acquisition geometry to favor certain areas of the subsurface over others should not be mirrored in the zero offset data. This violates the requirement that the resultant zero offset data should be nearly equivalent to data which would have been recorded by a zero offset field procedure.

To illustrate this point, consider Fig. 1.3, which shows a sample shot and raypaths for two dipping layers. There is a marked difference in raypath density between the layer dipping toward the end of the cable

(dipping right) and the layer dipping toward the beginning of the cable (dipping left). The layer dipping to the right receives a higher density of subsurface coverage than the layer dipping to the left.

This example has significant repercussions with respect to transforming the recorded data to zero offset. The aperture of seismic recording geometries results in an uneven density of subsurface ray coverage. For a complete survey, this unevenness of ray density is more complex than the simple illustration of Fig. 1.3. An NMO + DMO algorithm which ignores this phenomenon will mirror it in the zero offset data.

So the driving question of "why a new dip-moveout formulation?" should be restated - "why not a new dip-moveout formulation?" Since conventional dip moveout is not wave-equation based, a wave equation procedure is worthy of consideration. The formulation proposed in this thesis addresses both major issues raised herein. The relationship between the offset ( $D(t_n, k, h)$ ) and zero offset ( $D(t_0, k, h)$ ) amplitudes are addressed rigorously, and the dip selectivity of the acquisition geometry is compensated for in transforming to zero offset.

### 1.3 Wave Equation Dip Moveout

Deregowski and Rocca (1981) gave a very elegant and simple interpretation to the process of transforming seismic data to zero offset. They showed that, geometrically, the process of taking offset recorded seismic data to zero offset can be viewed as a two-step

procedure - full prestack migration followed by a zero offset forward model. Schematically:

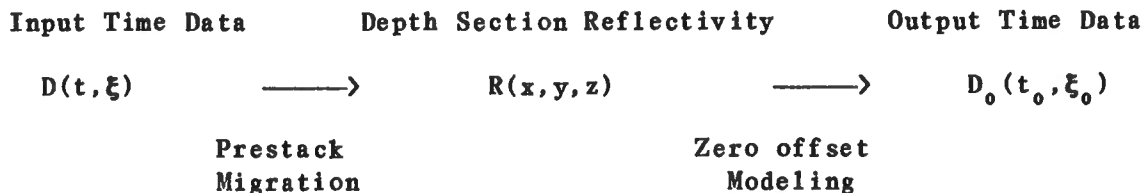


Figure 1.4 shows this process geometrically. An impulse on a recorded seismic trace corresponds to an elliptical mirror in the subsurface. All raypaths corresponding to reflections off the ellipse arrive at the geophone at the same time. The ellipse is simply the impulse response of prestack migration. It is a function of subsurface variables  $\mathbf{x} = (x, y, z)$ . The dimensions of the ellipse are a function of the source-geophone offset, media velocity, and input travelttime.

Once defined, the ellipse can be used to generate zero offset data. For zero offset modeling, each point on the ellipse becomes a source for a diffraction hyperbola. The superposition of these hyperbolas is the zero offset time section. The hyperbolas of Fig. 1.4 are parameterized by position along the ellipse and by the medium velocity. The envelope formed by the osculation of the hyperbolas is the net operator which transforms the input impulse to zero offset. The process of taking the input data and spreading it along this curve (also an ellipse) is geometrically equal to transforming the input data to zero offset (NMO + DMO). It is a remarkable fact that the net shape of the

resultant curve formed by the hyperbolas is not a function of the medium velocity. Although changing the velocity changes both the ellipse and the hyperbolas, the net osculation curve remains the same. In terms of NMO and DMO, the time difference between the input time sample and the base of the osculation curve is the NMO correction. The osculation ellipse is the DMO operator. Thus, since the shape of the DMO operator is not a function of velocity, dip moveout is said to be independent of velocity. This is, however, only strictly true for input data which has the correct NMO velocity applied.

This review of Deregowski and Rocca's geometrical interpretation sets the stage for the wave equation dip moveout which is the central theme of this thesis. These geometrical relationships can be restated in operator notation. First, consider an operator which transforms input seismic data to a model of the subsurface reflectivity:

$$R(\mathbf{x}) = L_I \left[ D(t, \xi) \right] . \quad (1.14)$$

Any operator which performs the indicated transformation is a valid candidate.  $L_I$  might be an operation involving finite differences, integrals, Fourier methods, etc. The only criterion is that  $L_I$  produce a reliable model of the subsurface,  $R(\mathbf{x})$ .

Now consider a zero offset modeling operator which produces zero offset data from a model of the subsurface:

$$D_0(t_0, \xi_0) = L_0 \left[ R(\mathbf{x}) \right] . \quad (1.15)$$

Again, any operator which produces zero offset data is a valid candidate. The operator  $L_0$  might be a ray tracer, a finite difference modeling program, an integral modeling algorithm, etc. The single criterion is that it produce reliable zero offset data from the input subsurface model.

Together, Eqs. (1.14) and (1.15) suggest a cascaded operation by which data might be transformed to zero offset:

$$D_0(t_0, \xi) = L_0 \left[ L_I \left[ D(t, \xi) \right] \right] . \quad (1.16)$$

Equation (1.16) suggests that  $D(t, \xi)$  can be transformed into  $D_0(t_0, \xi_0)$  by cascading the output of  $L_I$  into  $L_0$ .

Up until now the only criteria that has been placed on  $L_I$  and  $L_0$  is that they perform their respective operations "reliably". The "reliability" of these operators serves as the first criterion by which the specific form of  $L_I$  and  $L_0$  are selected. By "reliable", we mean that both  $L_I$  and  $L_0$  must honor the acoustic wave equation. By suggesting operators which honor the wave equation, the cascaded system is intrinsically a wave-equation based algorithm.

Secondly, the cascaded system must be solvable in a usable format. Many candidate operators perform the required wave-equation operations,

but not all operator types result in a cascaded system (1.16) which is tractable. The final result must be some explicit formalism which maps input data,  $D(t, \xi)$ , to zero offset data,  $D_0(t_0, \xi_0)$ . The particular choice for  $L_I$  and  $L_0$  must facilitate this goal.

Thirdly, the operators  $L_I$  and  $L_0$  must be three-dimensional in nature. The transformation to zero offset is properly a three-dimensional problem. All reflections recorded by a shot/geophone pair, whether from reflection points in-plane or out-of-plane, have equivalent zero offset locations which lie on the line connecting the shot and geophone (Fig. 1.5). In principle, two-dimensional assumptions are unnecessary and inappropriate when transforming data to zero offset. This point will be revisited in Sec. 3.7 (Two and Three Dimensions).

In order to have a reasonable chance at reducing Eq.(1.16) to a usable format, integral operators are utilized. The cascaded system Eq.(1.16) becomes a system of cascaded integrals. The reason for the choice of integral operators over other operator types is not irrefutable. A system of cascaded integrals is a more appealing system to solve than a system of cascaded finite differences or other more exotic operator types. (Undoubtedly, many would disagree with this statement. It is ultimately a function of the type of mathematics with which one is most familiar.)

An integral inversion operator is utilized for  $L_I$ . An inversion operator has the advantage over a migration operator in that it explicitly addresses the issue of what quantity is being imaged (i.e.,

velocity, density, etc.). Migration operators leave the interpretation of the output undefined, relying instead on an imaging condition which gives the wavefield at the reflection point. The forward modeling operator,  $L_0$ , requires a well-defined model of the subsurface on which to operate (i.e., Eq.(1.15) calls for reflectivity, not just a structural image). Hence the choice of a seismic inversion operator.

The particular operator utilized is one which was developed by Gregory Beylkin (1985) at Schlumberger and Cohen, Bleistein, and Hagin at the Center for Wave Phenomena at the Colorado School of Mines (Bleistein (1987), Cohen, Bleistein and Hagin (1986)). The inversion operates on recorded data to produce the perturbation in velocity,  $\alpha(\mathbf{x})$ . Perturbation is defined as the relationship of the total slowness of the medium to a background slowness:

$$\frac{1}{v^2(\mathbf{x})} = \frac{1}{v_m^2(\mathbf{x})} (1 + \alpha(\mathbf{x})) \quad . \quad (1.20)$$

In general, the background velocity  $v_m(\mathbf{x})$  can be any function (the subscript  $m$  refers to migration velocity). The theory is equipped to handle a background velocity of arbitrary  $(x,y,z)$  variation. However, the more complicated the function  $v_m(\mathbf{x})$ , the more complicated the resultant computations. For the development of this thesis,  $v_m(\mathbf{x})$  is taken to be a constant reference value,  $v_m$ . This is for computational ease at the expense of accuracy. Inversion and migration programs require that traveltimes from point to point in the subsurface are known. A constant background velocity makes the computations of these

traveltimes simple. More elaborate background velocities require more elaborate means to compute the traveltimes (ray tracing, finite differencing the eikonal equation, etc.). Such an extension of this theory to more complicated background velocities remains a ripe area for further research.

As will be demonstrated in Chapter 3, the assumption of a constant background velocity still offers the advantage of improving over existing algorithms. The processes NMO + DMO are also constant velocity algorithms. No cruder approximations to the velocity field are made than those made in standard processing.

The particular form of the inversion operator is (Bleistein (1987)):

$$\alpha(\mathbf{x}) = \frac{v_m^2}{(2\pi)^3} \iint d^2\xi \int d\eta \frac{|h(\mathbf{x}, \xi)|}{A_s(\mathbf{x}) A_g(\mathbf{x})} e^{-i\eta\phi(\mathbf{x}, \xi)} D(\eta, \xi) . \quad (1.21)$$

This operator is discussed in detail in Chapter 2. The operator is a threefold integral over the input data. The  $d\eta$  integral is over the input frequency,  $\eta$ . The  $d^2\xi$  integrals are over the recorded data. The output perturbation  $\alpha(\mathbf{x}) = \alpha(x, y, z)$  is a three-dimensional function. The generalization of this operator to lines of data is discussed in Chapter 3.

The various terms of the inversion kernel are defined in the glossary. The nature of the double integral  $d^2\xi$  changes depending upon the nature of the inversion. For example, if one is inverting common

shot records,  $\xi = (\xi_1, \xi_2)$  refers to the coordinates of the geophones for that shot. If the inversion is common geophone,  $\xi_1$  and  $\xi_2$  are the coordinates of the shots for that particular geophone. If the inversion is over common offset data,  $\xi_1$  and  $\xi_2$  are the coordinates of the midpoints on the acquisition surface.

The zero offset modeling operator,  $L_0$ , is chosen to be the Born approximation modeling operator (Bleistein (1984)):

$$D_0(\omega, \xi_0) = \omega^2 \int d^3 \mathbf{x} \frac{A_0^2(\mathbf{x}) e^{i\omega\phi_0(\mathbf{x}, \xi_0)} \alpha(\mathbf{x})}{v_0^2(\mathbf{x})} . \quad (1.22)$$

Again, all quantities are as defined in the glossary.  $v_0(\mathbf{x})$  is the background velocity for a forward perturbation problem:

$$\frac{1}{\tilde{v}^2(\mathbf{x})} = \frac{1}{v_0^2(\mathbf{x})} (1 + \alpha(\mathbf{x})) . \quad (1.23)$$

There are really three velocities in this problem. There is the actual earth velocity field  $v_e(\mathbf{x})$ . In the migration/inversion stage, we make an estimate of this velocity field in order to image the data. This estimate is  $v_m(\mathbf{x})$ . Whereas we hope that  $v_m(\mathbf{x})$  is nearly identical to  $v_e(\mathbf{x})$ , this is rarely the case. Once the perturbation,  $\alpha(\mathbf{x})$ , is known, the velocities  $v_m(\mathbf{x})$  and  $v_e(\mathbf{x})$  leave the problem. The format for the Born approximation modeling integral leaves the choice of  $v_0(\mathbf{x})$  at our discretion. In almost every case we would choose  $v_0(\mathbf{x})$  to be equal

to  $v_m(\mathbf{x})$ . Nevertheless, we are completely free to choose otherwise. This analysis leaves  $v_m(\mathbf{x})$  and  $v_0(\mathbf{x})$  uncoupled. This point will be revisited in Sec. 3.6.

Finally, substituting Eq.(1.22) into Eq.(1.21) gives the cascaded system by which we might transform  $D(\eta, \xi)$  to  $D_0(\omega, \xi_0)$ :

$$D_0(\omega, \xi_0) = \omega^2 \iiint d^3 \mathbf{x} \frac{A_0^2(\mathbf{x}) e^{i\omega\phi_0(\mathbf{x}, \xi_0)}}{v_0^2} \cdot \frac{v_m^2}{(2\pi)^3} \quad (1.24)$$

$$\cdot \iint d^2 \xi \int d\eta \frac{|h(\mathbf{x})|}{A_s(\mathbf{x}) A_g(\mathbf{x})} e^{-i\eta\phi(\mathbf{x}, \xi)} D(\eta, \xi) .$$

Counting the inverse transform over  $\omega$  to yield  $D_0(t, \xi_0)$ , Eq.(1.24) describes a seven-fold integral system. Since both the input and output data sets are functions of time (or, alternatively, frequency) and surface location, the variables  $\mathbf{x} = (x, y, z)$  pass through the process as dummy variables of integration. Before Eq.(1.24) is usable, these subsurface variables must be eliminated from the problem entirely.

Chapter 3 discusses the solution.

## 2. INVERSION BACKGROUND

### 2.1 The Beylkin Transformation

The inversion formula Eq.(1.21) has been presented without proof or extensive discussion. Since this inversion forms the core of the cascaded system Eq.(1.24), it deserves considerable discussion. This section will review the philosophy and concepts behind Eq.(1.21).

In 1985, Gregory Beylkin published a landmark paper (Beylkin, 1985) in which he described a general approach to seismic inversion based on the theory of pseudo-differential operators. In this paper, Beylkin proposed a change of variables motivated by the search for an inversion operator. This change of variables allows for the derivation of inversion formulas for a wide variety of data types and acquisition geometries. This change of variables was later justified on a more rigorous basis by Bleistein (1987).

The rigorous justification for this theory relies on asymptotic expansions. As such, it is a high frequency theory. For those purposes, data are considered to be high frequency if the wavelengths are small compared to the dimensions of the problem at hand. In terms of temporal quantities, high frequency means that (Bleistein, 1984)

$$2\pi fT \gg 1$$

where  $f$  is frequency in Hz and  $T$  is a typical time scale of the problem.

For our purposes  $2\pi fT > 3$  is sufficient. Thus, seismic data can be considered to be high frequency.

Consider a very general inversion formula for seismic data,  $D(\eta, \xi)$ . As before,  $\xi_1$  and  $\xi_2$  are taken to represent coordinates along the acquisition surface,  $\xi = (\xi_1, \xi_2)$ ;  $\eta$  is the frequency. For common shot data these coordinates represent geophone coordinates. For common geophone geometry the coordinates are shot coordinates. For common offset  $\xi_1$ , and  $\xi_2$  are the coordinates of the midpoint. Nevertheless, the inversion is performed by a double integral over surface coordinates,  $\xi$ , and a single integral over input frequency,  $\eta$ :

$$\alpha(\mathbf{x}) = \iiint d^2\xi \int d\eta B(\mathbf{x}, \xi, \eta) e^{-i\eta\phi(\mathbf{x}, \xi)} D(\eta, \xi) . \quad (2.1)$$

This inversion, given the appropriate kernel,  $B(\mathbf{x}, \xi, \eta)$ , recovers the perturbation in velocity,  $\alpha(\mathbf{x})$ . The task at hand, therefore, is to find the  $B(\mathbf{x}, \xi, \eta)$  which makes Eq.(2.1) a valid inversion (i.e., identity).

The determination of  $B(\mathbf{x}, \xi, \eta)$ , is based upon a suitable representation for the input data,  $D(\eta, \xi)$ . To this end, we represent  $D(\eta, \xi)$  as a Born approximation integral (Bleistein, 1984) over the input perturbation  $\alpha(\mathbf{x}')$ :

$$D(\eta, \xi) = \eta^2 \iiint d^3 \mathbf{x}' \frac{A_s(\mathbf{x}') A_g(\mathbf{x}')}{v_m^2} e^{i\eta \phi(\mathbf{x}', \xi)} \alpha(\mathbf{x}') \quad (2.2)$$

The Born approximation is but one of many choices at our disposal. The Born approximation is selected for Eq.(2.2) because it involves perturbation in velocity, which is the output of the inversion formula, Eq.(2.1). Had the inversion formula been selected to output reflectivity,  $R(\mathbf{x})$ , the Kirchhoff representation would have been a more suitable choice for Eq.(2.2). Either choice will lead to a similar end. Choosing the Born approximation makes the analysis self-consistent.

There is a close relationship between perturbation,  $\alpha(\mathbf{x})$ , and reflectivity,  $R(\mathbf{x})$ .  $R(\mathbf{x})$  is the normal derivative of the perturbation,  $\partial\alpha/\partial n$ . In this discussion the two quantities will often be used interchangeably.

Note that the subsurface variables in Eq.(2.1) are noted  $\mathbf{x} = (x, y, z)$ , whereas the subsurface variables in Eq.(2.2) are noted  $\mathbf{x}' = (x', y', z')$ . This is because they are not necessarily the same coordinates. The variables  $\mathbf{x}'$  in Eq.(2.2) are dummy variables of integration. The output is not a function of these variables. The variables  $\mathbf{x}$  in Eq.(2.1) are variables of the output perturbation  $\alpha(\mathbf{x})$ .

This point deserves some amplification. Migration/Inversion algorithms Eq. (2.1) attempt to solve for an unknown earth. To this end one builds this unknown earth by superposing the outputs from various

test points, or guesses (Fig. 2.1). Thus, in Eq.(2.1), the indicated integrals are performed for each test point  $\mathbf{x} = (x,y,z)$  without the a priori knowledge as to whether there is a reflector at  $\mathbf{x}$ . The analogue for downward continuation algorithms is the **imaging condition**. The imaging condition is drawn upon at each depth level without the a priori knowledge that the depth level contains actual reflectors. When there is no reflector at the output point, the output is of negligible amplitude. Where there are reflectors, the image is strong. The condition of an actual reflector occurring at the test point is the condition that  $\alpha(\mathbf{x}) = \alpha(\mathbf{x}')$ . (Here perturbation and reflectivity are being used interchangeably.)

Substituting the Born representation for  $D(\eta,\xi)$  into Eq.(2.1) gives:

$$\alpha(\mathbf{x}) = \iint d^2\xi \int d\eta B(\mathbf{x},\xi,\eta) \cdot \eta^2 \iiint d^3\mathbf{x}' \cdot \frac{A_s(\mathbf{x}')A_g(\mathbf{x}')}{v_m^2} e^{i\eta(\phi(\mathbf{x}',\xi) - \phi(\mathbf{x},\xi))} \alpha(\mathbf{x}') \quad (2.3)$$

All quantities in this equation are well-defined except the unknown kernel,  $B(\mathbf{x},\xi,\eta)$ . The problem becomes one of finding the  $B(\mathbf{x},\xi,\eta)$  which completes the equality. Since  $\alpha(\mathbf{x}')$  is the input and  $\alpha(\mathbf{x})$  is the output, one technique (Bleistein, Cohen, Hagin, 1985) is to recognize that the sum total of the amplitude and phase factors must be the

distribution  $\delta(\mathbf{x}' - \mathbf{x})$ , whose sifting property,

$$\iiint d\mathbf{x}'^3 \delta(\mathbf{x}' - \mathbf{x}) f(\mathbf{x}') = f(\mathbf{x}) \quad ,$$

recovers the desired output,  $a(\mathbf{x})$ . This approach was very successful. It does however, carry the inherent difficulty that it must be redone for every distinct inversion geometry (common shot, common geophone, common offset).

Beylkin argued that the essential throw-weight of the procedure defined by Eq.(2.3) must occur near the point  $\mathbf{x} = \mathbf{x}'$ . This was later justified rigorously by Bleistein (1987). Beylkin suggested linearizing the phase function  $\phi(\mathbf{x}', \xi)$  about the point  $\mathbf{x}' = \mathbf{x}$ :

$$\phi(\mathbf{x}', \xi) = \phi(\mathbf{x}, \xi) + \nabla\phi(\mathbf{x}, \xi) \cdot (\mathbf{x}' - \mathbf{x}) \quad . \quad (2.4)$$

Since the significant energy of the operation Eq.(2.3) occurs only very near those points where  $\mathbf{x} = \mathbf{x}'$ , we can make some preliminary observations about  $B(\mathbf{x}, \xi, \eta)$ . Certainly,  $B(\mathbf{x}, \xi, \eta)$  must cancel the other amplitude factors when  $\mathbf{x}$  and  $\mathbf{x}'$  coincide. Therefore, let  $B(\mathbf{x}, \xi, \eta)$  be given by:

$$B(\mathbf{x}, \xi, \eta) = \frac{v_m^2}{A_s(\mathbf{x}')A_g(\mathbf{x}')} b(\mathbf{x}, \xi, \eta) \quad . \quad (2.5)$$

Then inserting Eq.(2.4) and Eq.(2.5) into Eq.(2.3), the remaining

unknown becomes the amplitude factor  $b(\mathbf{x}, \xi, \eta)$ :

$$\alpha(\mathbf{x}) = \iint d^2 \xi \int d\eta \eta^2 b(\mathbf{x}, \xi, \eta) \cdot \iiint d^3 \mathbf{x}' e^{-i\eta \nabla \phi(\mathbf{x}', \xi) \cdot (\mathbf{x}' - \mathbf{x})} \alpha(\mathbf{x}') \quad (2.6)$$

Beylkin observed that Eq.(2.6) has the appearance of a forward and inverse Fourier-like operator. That is, we can consider a forward Fourier transform over the perturbation to have the form:

$$\alpha(\mathbf{k}) = \iiint d^3 \mathbf{x}' e^{-i\mathbf{k} \cdot \mathbf{x}'} \alpha(\mathbf{x}') \quad (2.7)$$

Then if we make the substitution,  $\eta \nabla \phi(\mathbf{x}, \xi) = \mathbf{k} = (k_1, k_2, k_3)$ , the integration over  $\mathbf{x}'$  looks exactly like Eq.(2.7). Under this substitution, Eq.(2.6) becomes:

$$\alpha(\mathbf{x}) = \iint d^2 \xi \int d\eta \eta^2 b(\mathbf{x}, \xi, \eta) e^{i\mathbf{k} \cdot \mathbf{x}} \alpha(\mathbf{k}) \quad (2.8)$$

If the integrals in Eq.(2.8) could be cast in terms of integrals over the wavenumber coordinates,  $\mathbf{k} = (k_1, k_2, k_3)$ , Eq.(2.8) would have the exact appearance of an inverse transform over wavenumber. ( $d^2 \xi d\eta \rightarrow d^3 \mathbf{k}$ ). Beylkin suggested a substitution of variables of integration from  $(\eta, \xi_1, \xi_2)$  to  $(k_1, k_2, k_3)$ . The Jacobian of this substitution is:

$$J \left[ \frac{\mathbf{k}}{\eta, \xi} \right] = \det \begin{vmatrix} \frac{\partial}{\partial \eta} \mathbf{k} \\ \frac{\partial}{\partial \xi_1} \mathbf{k} \\ \frac{\partial}{\partial \xi_2} \mathbf{k} \end{vmatrix} . \quad (2.9)$$

The change of variables of integration involves the substitution  $d^3 \mathbf{k} = J[\mathbf{k}/\eta, \xi] d^2 \xi d\eta$ . After changing the variables of integration from  $(\eta, \xi_1, \xi_2)$  to  $(k_1, k_2, k_3)$  and the insertion of appropriate  $2\pi$  scale factors, the forward/inverse inversion representation Eq.(2.3) has the exact form of a forward and inverse Fourier transform:

$$\alpha(\mathbf{x}) = \frac{1}{(2\pi)^3} \iiint d^3 \mathbf{k} e^{i\mathbf{k} \cdot \mathbf{x}} \iiint d^3 \mathbf{x}' e^{-i\mathbf{k} \cdot \mathbf{x}'} \alpha(\mathbf{x}') . \quad (2.10)$$

Following along with this argument, we can infer immediately that the unknown amplitude factor  $b(\mathbf{x}, \xi, \eta)$  must be the scaled determinant:

$$\eta^2 b(\mathbf{x}, \xi, \eta) = \frac{1}{(2\pi)^3} \det \begin{vmatrix} \frac{\partial}{\partial \eta} \mathbf{k} \\ \frac{\partial}{\partial \xi_1} \mathbf{k} \\ \frac{\partial}{\partial \xi_2} \mathbf{k} \end{vmatrix} = \frac{\eta^2}{(2\pi)^3} h(\mathbf{x}, \xi) . \quad (2.11)$$

$h(\mathbf{x}, \xi)$  can be expressed in terms of known quantities, since we have

defined  $(k_1, k_2, k_3)$  to be equal to  $(\eta \nabla \phi_1, \eta \nabla \phi_2, \eta \nabla \phi_3)$ .  $h$  is given by:

$$h = \det \begin{bmatrix} \nabla \phi \\ \frac{\partial}{\partial \xi_1} \nabla \phi \\ \frac{\partial}{\partial \xi_2} \nabla \phi \end{bmatrix} . \quad (2.12)$$

The inversion formula, Eq.(2.1), becomes:

$$\alpha(\mathbf{x}) = \frac{v_m^2}{(2\pi)^3} \iint d^2 \xi \int d\eta \frac{|h(\mathbf{x}, \xi)|}{A_s(\mathbf{x}) A_g(\mathbf{x})} e^{-i\eta \phi(\mathbf{x}, \xi)} D(\eta, \xi) . \quad (2.13)$$

This is a general inversion formula for any background velocity,  $v_m(\mathbf{x})$ . It is also a general inversion formula for any geometry (common shot, common geophone, common offset). The geometry has been left unspecified in the derivation.

## 2.2 The Inversion Geometry

The particular acquisition geometry has been left unspecified in the derivation of the previous section. It is implicit in the final form of the inversion formula. As previously stated, the variables  $\xi = (\xi_1, \xi_2)$  parameterize the acquisition surface. The particular inversion geometry is intimately related to the way  $\xi$  enters in the functional relationships of the various quantities.

For example, the phase function,  $\phi(\mathbf{x}, \xi)$ , is a sum of traveltimes from source to  $\mathbf{x}$  and from  $\mathbf{x}$  to receiver:

$$\phi(\mathbf{x}, \xi) = \tau_s(\mathbf{x}) + \tau_g(\mathbf{x}) \quad . \quad (2.14)$$

In a constant velocity earth, these reduce to simple distances divided by velocity. In a more general earth,  $\tau_s$  and  $\tau_g$  are found by more elaborate means. Nevertheless, the interpretation of  $\phi(\mathbf{x}, \xi)$  as a sum of traveltimes remains. The gradient  $\nabla\phi$  is given by a sum of vectors - one along the ray from  $\mathbf{x}$  to the source, the other along the ray from  $\mathbf{x}$  to the receiver.

The geometry of the input data reflects itself through the particular form of the determinant,  $h$ . For a common shot configuration the coordinates of the shot can be given by  $\xi_s = (\xi_{s1}, \xi_{s2})$ .  $\xi_s$  (and  $\tau_s$ ) is a constant with respect to the variables of the integration. The coordinates of the receivers are the variables of integration. They are given by the  $\xi_g = \xi = (\xi_1, \xi_2)$ . Therefore,  $h$  takes the form:

$$h = \det \begin{vmatrix} \nabla(\tau_s + \tau_g) \\ \frac{\partial}{\partial \xi_1} \nabla \tau_g \\ \frac{\partial}{\partial \xi_2} \nabla \tau_g \end{vmatrix} . \quad (2.15)$$

For common shot acquisition the derivatives of the second and third rows of this determinant depend on the geophone coordinates and output coordinates, but not on the source coordinates. Likewise, for a common receiver inversion the derivatives are with respect to the shot portion of  $\phi$  only. Similar relationships hold true for common offset and zero offset inversion. It is the form of  $h$  which compensates for the particular inversion geometry.

In hindsight, this should not surprise us. The derivation of Sec. 2.1 treated the forward problem as a Fourier transform. The particular geometry parameterizes the forward transform Eq.(2.7). If we view this as a transform from subsurface variables  $x$  to wavenumber variables  $k$ , then any areal configuration of sources and receivers which is consistent with this interpretation should be consistent with the derivation of Sec. 2.1. The Jacobian of the substitution in the inverse problem absorbs the specifics of the problem at hand. The self-consistency is guaranteed by the substitutions:

$$(\eta \partial_x \phi, \eta \partial_y \phi, \eta \partial_z \phi) = (k_1, k_2, k_3) \quad . \quad (2.16)$$

or, in terms of the variables of integration:

$$dk_1 dk_2 dk_3 = \eta^2 |h| d^2 \xi d\eta \quad . \quad (2.17)$$

The forward transform illuminates the subsurface (i.e., transforms it from space to wavenumber). The inversion recovers the illuminated portion. The geometry is accounted for as long as we are very careful in our specific definition of  $h$ . It must match the problem at hand.

### 2.3 Illuminating the Subsurface with Limited Aperture

Seismic imaging would be a simple task if the world were as cooperative as Sec. 2.1 suggests. With the forward problem seen as a forward Fourier transform, the inverse problem becomes an inverse Fourier transform and the problem is solved. We have recovered the model of the subsurface and can go on to solve new, more challenging problems. Or can we?

Before declaring total victory, perhaps we should revisit some of the assumptions made in Sec. 2.1 and consider their limitations. Consider Eq.(2.7) which defined the forward Fourier-like transform (repeated here for convenience):

$$\alpha(\mathbf{k}) = \iiint d^3 \mathbf{x}' e^{i\mathbf{k} \cdot \mathbf{x}'} \alpha(\mathbf{x}') \quad . \quad (2.18)$$

We defined the wavenumber,  $\mathbf{k}$  by:

$$\mathbf{k} = \eta \nabla \phi = \eta \nabla (\tau_s + \tau_g) \quad . \quad (2.19)$$

There are subtle, but significant, limits to the substitution of Eq.(2.19). Figure 2.2 is a graphical depiction of Eq.(2.19). The quantity  $\nabla(\tau_s + \tau_g)$  is a vector which is the sum of two vectors,  $\nabla\tau_s$  and  $\nabla\tau_g$ . As shown by Fig. 2.2,  $\nabla\tau_s$  is a vector along the ray from the source to the subsurface point. Likewise,  $\nabla\tau_g$  is a vector along the ray from the receiver to the subsurface point. Eq.(2.19) says that  $\mathbf{k}$  is a vector which lies between  $\nabla\tau_s$  and  $\nabla\tau_g$ .

We can make an estimate of the magnitude of  $\mathbf{k}$ . The eikonal equation is:

$$|\nabla\tau|^2 = \frac{1}{v^2} \quad . \quad (2.20)$$

Therefore, the magnitudes  $|\nabla\tau_s|$  and  $|\nabla\tau_g|$  are both equal to  $1/v$ . The bounds on  $|\mathbf{k}|$  can be deduced directly:

$$0 \leq |\mathbf{k}| \leq \frac{2|\eta|}{v} . \quad (2.21)$$

For a given  $\eta$ , the lower and upper bounds correspond to source/receiver offsets. The upper bound ( $|\mathbf{k}| = 2|\eta|/v$ ) corresponds to zero offset. the lower bound ( $|\mathbf{k}| = 0$ ) corresponds to infinite offset. Thus, there are reasonable bounds on the magnitude of  $|\mathbf{k}|$ .

A far more serious problem lies with limits on the direction of  $\mathbf{k}$ . Referring again to Figure 2.2, the direction of  $\mathbf{k}$  is the direction of the normal to the reflector. This is because  $\mathbf{k}$  bisects the angle between  $\nabla\tau_s$  and  $\nabla\tau_g$ . (At reflection points the angle of incidence equals the angle of reflection). A limit on the direction of  $\mathbf{k}$  is a limit on the range of dips which can be imaged. Real-life acquisition cannot recover all dips at every point in the subsurface. The limited aperture of practical recording limits the dips that can be recovered by a given experiment.

For an excellent discussion of these concepts, see Beylkin, Oristaglio and Miller (1985). This paper contains some excellent examples of the effect of limited aperture on seismic migration.

Eq.(2.7) would be an exact transformation if the recording frequency and aperture of the array were infinite. Limits on frequency introduce limits on the magnitude  $|\mathbf{k}|$ . Limits on the array introduce limits on the direction of  $\mathbf{k}$ . Thus, instead of  $\alpha(\mathbf{k})$ , the forward transform of Eq.(2.7) produces  $\tilde{\alpha}(\mathbf{k})$ , where  $\tilde{\alpha}(\mathbf{k})$  is a band-limited

version of  $\tilde{\alpha}(\mathbf{k})$ .

These concepts apply directly to the interpretation of the inverse Fourier-like transform Eq.(2.10). The output of the inversion is not  $\alpha(\mathbf{x})$ , but  $\tilde{\alpha}(\mathbf{x})$  - the inverse transform of the band-limited  $\tilde{\alpha}(\mathbf{k})$ . Fig. 2.3 illustrates how limits of the recording array can be translated into limits on recorded dips, and how these translate to limits on the direction of  $\mathbf{k}$ .

### 3. THE TRANSFORMATION TO ZERO OFFSET

#### 3.1. Overview

The process of transforming recorded seismic data to zero offset can be represented as a prestack inversion followed by a zero offset forward model. This was expressed in operator notation in Chapter 1. We would like this process to preserve amplitude information in the recorded data. For this reason, an inversion is utilized in lieu of a migration. The specifics of this inversion are the subject of Chapter 2. The forward model is the Born approximation integral for zero offset. Inserting the inversion operator into the forward modeling operator gives a cascaded operator which accomplishes the transformation to zero offset. This operator was given by Eq.(1.24), and is repeated here:

$$D_0(\omega, \xi_0) = \omega^2 \iiint d^3x \frac{A_o^2(\mathbf{x}) e^{i\omega\phi_0(\mathbf{x}, \xi_0)}}{v_o^2} \frac{v_m^2}{(2\pi)^3} \cdot \iint d^2\xi \int d\eta \frac{|h(\mathbf{x}, \xi)|}{A_s(\mathbf{x})A_g(\mathbf{x})} e^{-i\eta\phi(\mathbf{x}, \xi)} D(\eta, \xi) \quad (3.1)$$

The input to this integral system are the Fourier transformed recorded data  $D(\eta, \xi)$ , which are a function of frequency  $\eta$ , and surface coordinates  $\xi = (\xi_1, \xi_2)$ . The output is zero offset data  $D_0(\omega, \xi_0)$ , which are a function of frequency  $\omega$  and zero offset location  $\xi_0 = (\xi_{01}, \xi_{02})$ .

Counting the inverse Fourier transform over  $\omega$ , Eq.(3.1) is a seven-fold integral.

The goal is to reduce Eq.(3.1) to a format suitable for implementation on a digital computer. The integrals over surface coordinates  $\xi$  and input frequency  $\eta$  present no problem. These are variables for which the data are explicitly defined. The integrals over the subsurface variables  $x = (x,y,z)$  are a different matter. The subsurface variables arose from the formulation of the problem as a prestack inversion followed by a zero offset forward model. These subsurface variables are dummy variables of integration in Eq.(3.1). Before the cascaded system is implemented, the integrals over these variables can be eliminated by analytic means.

Alternative solutions to the cascaded inversion/modeling problem might, indeed, leave the subsurface variables in the solution path. The solution path described herein is for a constant velocity earth. For this simple earth model, calculating the subsurface integrals analytically is a tractable problem. More exotic velocity models might require that the subsurface remain a part of the problem. For example, the cascaded inversion/modeling problem in an arbitrarily varying velocity field might require tracing rays from the subsurface point  $x$  to the shot  $\xi_s$ , geophone  $\xi_g$ , and zero offset location  $\xi_o$ .

The inversion philosophy discussed in Chapter 2 is a prestack theory. Since reflectivity is a function of angle of incidence the best one can hope for from the theory of Chapter 2 is an estimate of the

angularly dependent reflection coefficients. Since a stack over offset is a stack over the angularly dependent reflection coefficients, the stacking process degrades much of the amplitude information that this theory is designed to preserve.

There are two issues involved here. First, we expect a stacking theory developed upon this cascaded inversion/modeling transformation to do a better job than standard NMO+DMO+STACK, primarily because the theory developed herein is wave equation based. Secondly, (and perhaps of greater significance), we expect that theory developed herein to offer some prestack analysis which is an improvement over conventional dip moveout processing. We have two applications in mind - shot domain velocity analysis and amplitude versus offset processing. The cascaded system of Eq.(3.1) offers the potential to do both processes in a wave equation consistent fashion.

### 3.2 The 2.5D Solution

Eq.(3.1) describes a full three-dimensional problem. The subsurface is allowed to vary arbitrarily as a function of  $\mathbf{x} = (x,y,z)$  (within the confines of a constant background velocity). The forward modeling operator introduced the three-fold integration over  $\mathbf{x}$  in Eq.(3.1) The inversion operator is three-dimensional problem. Thus, the inversion operator also introduced a three-fold integration - two surface variables  $\xi = (\xi_1, \xi_2)$  and frequency  $\eta$ . The six-fold integration of Eq.(3.1) describes the full three-dimensional transformation to zero

offset.

The solution path can be simplified if we assume that the line of recorded data is a dip line. We retain the three-dimensional nature of the wave propagation, but we assume that the earth is invariant in the cross-line direction. That is, parallel lines of recorded data would be identical. This assumption has been termed 2.5D in order to contrast it with approaches which utilize only the 2D wave equation. The geometry of the 2.5D problem is illustrated in Fig. 3.1.

A nice result from making a 2.5D assumption is that the out-of-plane receiver integral ( $\xi_2$ ) and the out-of-plane subsurface integral ( $y$ ) can be evaluated by the method of stationary phase. (See Appendix C for a brief review of the stationary phase formula). The mechanics of the 2.5D solution of Eq.(3.1) are given in Appendix A. The result is the mapping from finite offset to zero offset:

$$\begin{aligned}
 D_o(t_o, \xi_o) &= \frac{t_o v_m^{7/2}}{(2\pi)^{3/2} 16} \int d\eta F(\eta) |\eta|^{1/2} \exp\left[\frac{i\pi}{4} \text{sgn}\eta\right] \\
 &\cdot \int d\xi \frac{A_o^2(\mathbf{x}) |h(\mathbf{x}, \xi)|}{z_o A_s(\mathbf{x}) A_g(\mathbf{x})} \left[\frac{1}{\rho_s} + \frac{1}{\rho_g}\right]^{-1} \frac{\left[\frac{\partial\phi}{\partial t}\right]^2}{\left|\frac{\partial^2\phi}{\partial \mathbf{x}^2}\right|^{1/2}} \quad (3.2) \\
 &D(\eta, \xi) \exp\left[-i\eta\phi(\mathbf{x}, \xi)\right] .
 \end{aligned}$$

The various factors are defined in the glossary and Appendix A.

A very nice feature of the derivation of Appendix A, and of the resultant Eq.(3.2), is that it is very general in regard to the geometry (i.e., common shot data, common receiver data, or common offset data). As discussed in Chapter 2, the specifics of the problem geometry are accounted for by the specific form of the determinant  $|h(\mathbf{x},\xi)|$ . Thus, one would use a different  $|h(\mathbf{x},\xi)|$  depending upon whether the problem were cast in the common shot, common receiver, or common offset domain. The derivation and form for the common shot  $|h(\mathbf{x},\xi)|$  is given in Appendix H. The common receiver  $|h(\mathbf{x},\xi)|$  can be deduced from the common shot  $|h(\mathbf{x},\xi)|$  by simply reversing the roles of shot and receiver variables in that formula. The common offset  $|h(\mathbf{x},\xi)|$  is derived in Appendix I.

One must be very careful in formulating the geometry of the problem if Eq.(3.2) is to be used correctly. The phase function of Eq.(3.1),  $\phi(\mathbf{x},\xi)$  is a sum of shot and geophone traveltimes,  $\tau_s$  and  $\tau_g$ . In a constant velocity earth, these can be expressed by:

$$\tau_s(\mathbf{x}) = \frac{1}{v_m} \sqrt{(x-\xi_{s1})^2 + (y-\xi_{s2})^2 + z^2} \quad (3.3)$$

$$\tau_g(\mathbf{x}) = \frac{1}{v_m} \sqrt{(x-\xi_{g1})^2 + (y-\xi_{g2})^2 + z^2} .$$

Equation (3.3) is valid for all geometries. However, in

formulating the problem given by Eq.(3.1), one must be careful in defining what is meant by the double integral over receivers,  $\xi = (\xi_1, \xi_2)$ . The reason for this is because in deriving Eq.(3.2) the  $\xi_2$  integral is eliminated by stationary phase. The nature of the  $\xi_2$  integral changes with the geometry. Common shot geometry is defined to be one in which the source point is fixed and the receivers are distributed along the acquisition surface. Thus, the position of the source,  $\xi_s = (\xi_{s1}, \xi_{s2})$ , is held constant with respect to the  $\xi$  integration in Eq.(3.1). The variables of integration  $\xi = (\xi_1, \xi_2)$  become the geophone coordinates  $\xi_g = (\xi_{g1}, \xi_{g2})$ . Alternatively, one might envision parallel lines of common offset data. Thus, the shot coordinate,  $\xi_s$  in Eq.(3.3), could be expressed by  $\xi_s = (\xi_{s1}, \xi_{s2}) = (\xi_1 - h, \xi_2)$ , and the receiver position by  $\xi_g = (\xi_{g1}, \xi_{g2}) = (\xi_1 + h, \xi_2)$ . In the common offset formulation,  $\xi_1$  and  $\xi_2$  are the midpoints on the acquisition surface and  $h$  is the half offset. The derivation of Appendix A is valid for each of these cases so long as one is careful in defining the geometry of the problem.

### 3.3 The TZO Impulse Response

As we have said, a prestack inversion theory offers the greatest utility in prestack applications. Thus, one might apply Eq.(3.2) in a common shot, common receiver, or common offset configuration. Each of these applications represents a partial stack over the data. The goal of this partial stack is to generate the best estimate for zero offset

data from the domain of the partial stack. Thus, we might expect the operator to vary depending upon the geometry of the partial stack.

There are really four different operators involved. These are for common shot, common receiver, common offset, and stacking. The common shot operator tries to give the best estimate of zero offset data by processing only single shot records. Likewise, the common receiver implementation tries to produce the best zero offset data by considering only single common receiver records. The common offset implementation is a partial stack over both shots and receivers. There is an inherent geometrical bias in recording. For example, a shot record tends to favor dips inclined towards the geophones (thus, one attempts to "shoot into the dip"). The inversion theory of Chapter 2 attempts to compensate for this bias. The operators which result from Eq.(3.2) are different depending upon their domain of application. These differences are explained entirely by differences in the determinant  $|h(x,\xi)|$ .

How do these operators differ from conventional dip moveout? Before answering this question, perhaps we should define what we mean by conventional dip moveout. The application of Eq.(3.2) will be in the  $(x,t)$  domain. Therefore, to have a fair comparison we should use a conventional dip moveout algorithm which is an  $(x,t)$  domain application. Lars Berg (1984) presented an  $(x,t)$  domain implementation of Dave Hale's (1983)  $(\omega,k)$  dip moveout algorithm. Figure 3.2 shows an impulse response of this algorithm for an offset of 5,000 ft., and velocity of 8,000 ft./sec.

Figures 3.3a and 3.3b show a comparison of the Berg algorithm with the common shot operator of Eq.(3.2). In these figures the operator on the left is from the Berg algorithm, the operator on the right is the inversion-based operator. The comparisons are for seven impulses at offsets of 10,000 ft. and 5,000 feet. Note that the common shot operator has amplitudes which are asymmetric with respect to the midpoint. The Berg operator (and all conventional dip moveout operators) are symmetric with respect to the midpoint. This asymmetry is a direct consequence of the asymmetry of the inversion operator. It compensates for the geometrical bias of the recording geometry.

Figure 3.4 (a repeat of Fig. 1.3) shows a ray plot which might shed some light on the asymmetry of the common shot operator. Note that the ray density for the geometry shown is significantly higher for beds which dip into the geophone. The transformation to zero offset can be thought of as a procedure which projects this ray density onto an evenly sampled zero offset trace spacing. Figure 3.5 illustrates the zero offset geometry, and associated zero offset rays. The ray density of Figure 3.4 is mapped to the ray density of Figure 3.5. An uneven ray density in the original recording will evidence itself as a bias in the zero offset data. Therefore, the asymmetric operator tries to compensate for the inherent asymmetry of the original recording.

As previously discussed in Chapter 2, the determinant  $|h|$  has the form:

$$h(\mathbf{x}, \xi) = \det \begin{bmatrix} \nabla\phi_s \\ \frac{\partial}{\partial\xi_1} \nabla\phi_s \\ \frac{\partial}{\partial\xi_2} \nabla\phi_s \end{bmatrix} . \quad (3.4)$$

The magnitude of this determinant  $|h|$  is a function of the quantity  $\partial\nabla\phi/\partial\xi$ , which is simply the rate of change of traveltime with respect to change in the receiver position. Figure 3.6 graphs this rate of change for a common shot configuration. For several subsurface points, the change in the gradient of the phase with changing receiver coordinates is illustrated. With common shot data, the change in  $\nabla\phi$  is equal to the change in  $\tau_s$ . Comparing Fig. 3.6 with Fig. 3.4, we see that this rate of change of the ray with respect to the receiver position is directly related to the ray density. They are a measure of the same quantity - the density of subsurface coverage. At subsurface points where  $\partial\nabla\phi/\partial\xi$  is low (i.e., the ray position changes slowly with change in receiver position), the ray density is high. At subsurface points where  $\partial\nabla\phi/\partial\xi$  is high (i.e., the ray position changes rapidly with change in receiver position), the ray density is low. The determinant  $|h(\mathbf{x}, \xi)|$  attempts to compensate for this phenomenon such that the resultant inversion (or, equivalently, zero offset data) does not mirror this bias. Thus,  $|h(\mathbf{x}, \xi)|$  can be thought of as a wave-consistent "fold" compensator.

This is the reason for the asymmetry of the common shot operator. The common receiver operator has a similar asymmetry with amplitudes higher on the side of the shot.

One might wonder if the asymmetry of the operator violates reciprocity. Reciprocity states that there is no change in the data if we interchange source and receiver. The operators pictured in Fig. 3 do not violate reciprocity. Recall that this asymmetry is anticipating that there will be a sum over the data. Although viewed independently, reciprocity seems to be an issue, taken in the context of the sum over surface data, it is not violated.

The common shot operator is the operator which gives the best estimate of zero offset data from a given shot record. It is not the operator which would be appropriate in stacking the data. As stated above, the common receiver operator has equal but opposite asymmetry. Since a recorded seismic survey can be expressed as either common shot or common receiver data, to stack with either the common shot or common receiver operators is to use a different operator depending upon the sorting of the input data! We do not advocate such an approach.

Bleistein and Jordan (1987) give an inversion theory appropriate for stacking. There they develop a criteria for stacking which demands that a stack with a common shot operator must equal a comparable stack with a common geophone operator. The result is an averaged operator which is suitable for stacking. The operator is symmetric.

The raypath density discussion of the previous paragraphs also

applies to the common offset implementation of Eq.(3.2). In common offset geometry, the ray density changes as a function of the dip. As in the common shot case, the determinant  $|h(x,\xi)|$  compensates for the uneven ray density. However, in the common offset implementation the operator is symmetric but has amplitudes which vary with dip (i.e., which vary along the limbs of the operator).

Figures 3.7a and 3.7b compare the Berg operator with the common offset inversion-based operator. As expected, the inversion-based operator applies a higher relative weight to the limbs of the operator (the higher dips) than does the Berg algorithm. An impulse on a constant offset section could come from a reflector of arbitrary dip. The inversion-based operator tells us that, for a fixed common offset traveltime, the flat beds received a higher ray density than the dipping beds. Since the reflections from dipping beds originate at shallower depths than contemporaneous flat reflections, a review of Fig. 3.6 confirms this to be true. Once again, the determinant  $|h(x,\xi)|$  is acting as a wave-consistent "fold" compensator.

"Fold" as commonly defined is a zero-dip number (i.e., number of common midpoints). The inversion theory of Chapter 2 extends the concept of fold to more realistic geometries. The operators of Figs. 3.3 and 3.7 incorporate this "fold" compensation.

Note the behavior of the amplitudes at the edges of the limbs of the operator (the  $90^{\circ}$  point). The Berg algorithm truncates abruptly. To compensate for this phenomena, a tapering operator is often applied

to the impulse response. The TZO algorithm naturally tapers at the edge of the operator.

### 3.4 Processing Applications

Applications for the algorithm defined by Eq.(3.2) fall into two major categories - prestack and stacking. This section will discuss two prestack applications - velocity analysis and amplitude versus offset analysis.

As stated previously, the stacking process has the effect of summing over the angularly dependent (i.e., offset dependent) reflection coefficients. The result is a loss of meaningful amplitude information. Since stacked data has dubious amplitudes, the best measure for stack quality is the quality of the resultant image. Conversely, since prestack data has the potential of preserving amplitude information, the best measure for a prestack algorithm should be quality (and consistency) of the data, as well as the behavior of the amplitudes.

The operator of Eq.(3.2) (here and throughout we will occasionally refer to this operator as the TZO operator, TZO meaning Transformation to Zero Offset) can be cast in the time domain by inverse Fourier transforming over the frequency variable,  $\eta$  (Appendix A). The resultant operator has a complicated amplitude term, but a travelttime relationship which is equal to NMO + DMO when  $v_m$  equals  $v_0$  (see Appendix D for proof).

The operators displayed in the previous section were valid for dips

ranging from +/- 90 degrees. As a practical matter, it is often advantageous to limit the operator to a specified range of dips. This amounts to truncating the impulse response. Appendix E details the means by which the dip limits are defined.

Another practical matter in processing is the domain of application of the dip-moveout operator. An (x,t) domain algorithm offers the potential to read in each trace and map it to the domain of zero offset traces it affects. In this case, the domain of zero offset traces are those traces which lie between the surface locations of the shot and geophone. As each trace is read, it is spread along the impulse response corresponding to the geometry of that trace. The output data can be constructed from the input data one trace at a time, eliminating the need to sort.

#### 3.4.1 Velocity Analysis

Several goals guide the formulation of the velocity analysis application. First and foremost, we would like a velocity analysis which has the potential to estimate the dip-independent velocities. Secondly, we would like the data to be processed in shot order, eliminating the need to sort to common-midpoint. Thirdly, we would like the ability to display the velocity analysis in both a true amplitude fashion and a semblance display.

The stationary phase evaluation of Eq.(3.1) dictates that the output trace must lie between the location of the shot and geophone on

the line connecting them. This is nothing more than a restatement of the fact that the dip moveout impulse response is an ellipse with horizontal axis equal to the offset - all the output traces lie between the shot and geophone. This is the domain of influence of a given input trace. Likewise, one can define the domain of influence for a given shot record. A shot record (here we are considering off-end shooting) will contribute to zero offset traces which lie between the shot and the far offset.

Figure 3.8 shows the domains of influence of a set of shot records. Each shot contributes to the shaded zone of zero offset data. Figure 3.9 shows the same figure, but with a location  $x_0$  identified.  $x_0$  is a location for which we might wish to do velocity analysis. Note that each of the shots of Figs. 3.8 and 3.9 contributes to the zero offset location  $x_0$ . That is, for  $n$  input shots, there will be  $n$  different contributing traces to the location  $x_0$  - one from each shot. If the velocity is correct, each of the  $n$  traces should be identical, or nearly so. If the velocity is incorrect the  $n$  traces should differ.

In the shot domain velocity analysis, the transformation to zero offset is formulated using the common shot operator (Fig. 3.3). The correct velocity is that velocity for which the various traces (one from each shot) are identical.

Figure 3.10 shows a model on which this velocity analysis is demonstrated. The model contains six layers with crossing and conflicting dips. The modeling algorithm is a constant

Kirchhoff integral code, with a velocity of 8,000 ft./sec. Within the confines of the constant velocity assumption, the fact that the layers cross is a geometrical artifact (the rays do not bend at the interfaces). The modeling geometry consisted of 25 split spread shot records. There are 96 channels per shot, with a near offset of 100 ft. and a far offset of 4,800 ft. (receiver interval 100 ft.). The first shot was at the location marked "S1", the last shot is at the location marked "S2". The shot interval is 200 ft.

Figure 3.11 shows a velocity panel for a location midway between the first and last shot (marked  $x_0$  on Fig. 3.10). As velocity is varied, each of the 25 traces contributing to the given location (one trace for each of the 25 shots) are plotted side by side. Note that the best agreement between the contributions from different shots occurs at the model velocity of 8,000 ft/sec. This analysis estimated the same velocity for both the dipping and flat beds. It is a dip-independent velocity analysis which processes the data in shot order without sorting.

The data in the following examples are from a seismic line acquired in the vicinity of a Gulf of Mexico salt dome. These data were generously provided by Golden Geophysical and Anadarko Petroleum.

Figure 3.12 shows a near trace display. The offset is 1,056 ft. The data were shot from left to right, with a 120 channel cable and a receiver interval of 82 ft. The shot interval was also 82 ft., resulting in 60 fold data.

Because of the volume of data involved in this dataset, it was more efficient to scan over velocity functions rather than over constant velocity panels. Linear velocity functions were defined by an intercept and a slope (i.e.,  $v = v_0 + kt$ ). Both the intercept and the slope were incremented in the velocity scans. For each velocity function, the separate contributions to the zero offset location from each shot were saved and plotted side by side. Each trace, therefore, represents a sum over geophones for each shot record. The correct velocity was determined by agreement (i.e., horizontal alignment) of zero offset traces generated from different shots.

The velocity analyses in the following examples correspond to the location marked  $x_0$  on the near trace display of Fig. 3.12. Figure 3.13 shows a comparison between the Berg algorithm and the TZO algorithm for a sample velocity function ( $v = 5000 + 375t$ ). As before, the figure displays the various contributing traces from each shot plotted side by side. This velocity function was too slow for all but the most shallow data. The traces generated from the different shots do not agree - they 'smile up' toward those shots whose contributions are predominantly far offset traces.

Figures 3.14a through 3.14c show enlargements of the data in Fig. 3.13. The data for the TZO panel is superior, particularly in Figs. 3.14b and 3.14c. However, both algorithms have done a good job. Recall that the traveltimes of the algorithms is identical. The differences, therefore, will be in coherency and amplitude 'quality'.

Fig. 3.15 is a similar comparison for a faster velocity function ( $v = 5600 + 1050t$ ). As demonstrated by the horizontal alignment of events, this velocity function is quite good for much of the data (though too fast for the shallow data). Figs. 3.16a through 3.16c show an enlargement of the data in Fig. 3.15.

Fig. 3.17 is a comparison for a velocity function which is too fast for all but the deepest data ( $v = 6000 + 1500t$ ). The traces 'frown' towards the traces from shots which contributed predominantly far offsets. Figs. 3.18a through 3.18c are enlargements of the data in Fig. 3.17.

Finally, Fig. 3.19 shows a comparison of semblance displays from the velocity panels of the two algorithms. Both semblance panels give good definition of the velocity spectra (Cook and Taner (1969), Douze and Laster (1979), Garotta and Michon (1967), Neidell and Taner (1971), Taner and Koehler (1969)). The TZO semblance display is marginally better for the shallow data.

There is a peculiar packet of energy on the semblance displays at 2.1 seconds. This packet has a velocity slower than the general trend. This is energy off the flank of the dome. Even though this analysis is designed to estimate the dip independent velocities, it has somehow failed to give the same velocity for the dome reflection and contemporaneous flat reflections. This is due to a failure of the constant velocity algorithm to properly handle a layered earth. The slower velocity is, indeed, the dip independent velocity for the dome

reflection (RMS velocity), but it is occurring at a time much later than comparable RMS velocities. The angled raypaths off the dome have traveled through a slower velocity than the raypaths for flat events arriving at the same time. An algorithm designed for a depth dependent velocity field is required to properly handle the reflection off the dome.

Dip moveout is an offset dependent operation. Since a common shot formulation represents a stack over offset, common shot is a poor choice of domains in which to compare the performance of dip moveout algorithms. The natural domain of comparison is offset.

#### 3.4.2 Amplitude vs. offset.

Much attention has been paid in recent years to the variation of seismic amplitudes with offset. These variations have been used as a means for direct detection of hydrocarbons. In the presence of structure, one would like to be assured that the comparison of amplitudes is made for a common reflection point. This often requires dip moveout.

The role of dip moveout in an amplitude offset processing flow is ill-defined. In particular, since dip moveout is not wave equation based, and has amplitude factors derived solely from a travelttime Jacobian, one would be wise to be suspicious of the resultant amplitudes after dip moveout processing. This is not to say that the resultant amplitudes are unreliable, but rather to say that there is no basis upon

which to judge them.

The TZO algorithm of Eq.(3.2) addresses the question of amplitudes rigorously within the framework of the acoustic wave equation. We would, therefore, expect it to produce more reliable amplitudes than conventional dip moveout.

The following examples are from the location marked  $x_0$  on Fig. 3.12 (the same location as the velocity analysis of the previous section). The data affecting this location were processed to zero offset. The contributions from the various offsets were saved and plotted side by side for comparison.

This type of analysis suggests an advantage of an  $(x,t)$  domain algorithm. As stated previously, the data are processed in trace sequential order. Each trace is read and then spread over the domain of zero offset traces affected by that trace. For a given input trace, isolating a particular output trace makes the transformation to zero offset a one to one mapping. That is, instead of spreading the input trace over the entire impulse response, one can map the input trace only to that part of the impulse response corresponding to the desired output location. This is in stark contrast to an  $(f,k)$  algorithm, which would need to process all the common offset panels in order to generate the contributions from each offset at a particular point.

Figure 3.20 shows an offset comparison for the Berg and TZO algorithms. On this display the offset increases from left to right. The near offset is 1056 ft. The far offset is 10814 ft. Each trace is

the contribution to the location  $x_0$  from each offset. For the TZO displays, the common offset operator (Fig. 3.7) was used.

The velocity function at this location was picked from the semblance analysis. The extent to which events align is the extent to which the velocity is correct. Misalignment is caused by a combination of bad picking and the failure of a constant velocity algorithm to handle a variable velocity media. For example, the frowning events just below the 2.0 second timing line are reflections off the flank of the dome. These arrive at a slower velocity, as discussed in the previous section.

Figs. 3.21a through 3.21c are enlargements of Fig. 3.20. Note that the TZO algorithm has produced events which have overall better coherency. The amplitudes also show a slightly different distribution between the outputs of the two algorithms. It would be foolish to claim that one is unequivocally 'right'. The TZO algorithm, however, does address the question of amplitudes. Overall, it has produced superior results.

### 3.5 Stacking

Certainly no discussion on dip moveout would be complete without some attention paid to stacking. As we have seen previously, the inversion theory upon which this thesis is based is a pre-stack theory. The inversion estimates the angularly dependent reflection coefficients (or, equivalently, perturbation in velocity). A stack over offset is, therefore, a stack over these offset dependent reflection coefficients.

Therefore, the process of stacking degrades much of the amplitude information which this theory was designed to preserve.

Stacking is a necessity. The relevant question here is which is the appropriate stacking operator to use. We have seen operators derived for common shot (and , equivalently, common geophone) and for common offset. Neither of these derivations discusses the justification for summing over shots or summing over offsets.

Bleistein and Jordan (1987) discuss a theory for seismic stacking which is based upon a weighted average of the various inversions. That is, the common shot inversions and the common receiver inversions are weighted such that the net operator is symmetric and produces an averaged value of the reflectivity. A similar justification can be offered for using the common offset operator to stack. With the caution that the amplitudes of the output are numerically dubious, one can proceed with a stack over offsets. The resultant stack is an average of a wave-equation based procedure, though the numerical meaning of the average is now a weighted sum over angularly dependent reflection coefficients.

Figure 3.22 shows the near trace from the Gulf of Mexico data (near offset is 1056ft.). The zone of stacked data is indicated on the figure. (Practical limitations on computer time prohibited the stacking of the entire line).

Figure 3.23 shows a comparison of the stacks from the Berg algorithm and from the TZO common offset algorithm. The light

amplitudes in the shallow data are a result of the drop in fold. The stack routine did not compensate for the fold loss at the surface.

Figures 3.24a through 3.24c show enlargements of the data in Figure 3.23 for three time windows (0-1s, 1-2s, and 2-3s, respectively). A careful inspection of the coherency and overall quality of the events shows that the TZO algorithm has produced a superior stack. For example, note the horizontal (or nearly so) events in Figure 3.24c. The TZO stack is noticeably cleaner.

Arguably, the differences between the two algorithms are small. This is to be expected since the traveltimes of the mapping is the same for both algorithms. The differences are to be found in subtle amplitude and coherency variations. One is a wave equation based procedure, the other is not.

### 3.6 When $v_0$ Is Not Equal To $v_m$

The TZO formulation separates the two velocities,  $v_0$  and  $v_m$ . This is a constant background theory, formulated as a cascaded inversion/modeling procedure. The inversion produces an estimate of the perturbation in velocity. This is a perturbation within some background velocity field ( $v_m$ ). Alternatively, the algorithm could have been formulated about an inversion scheme which inverted for reflectivity. In this case, the output would be reflection coefficients in some constant velocity medium (again,  $v_m$ ). Once the perturbation or reflectivity is found, there is no a priori reason to demand that the

forward model be generated with the same  $v_m$ . One can choose a new velocity  $v_0$ . That is, from the same depth model (perturbation or reflectivity) one can generate any time model (zero offset data).

This degree of freedom is afforded because the algorithms are constant velocity algorithms. That is, the rays do not bend at changes in the reflectivity or perturbation. The effect of letting  $v_m$  be different from  $v_0$  is to produce an algorithm which not only transforms the recording geometry to zero offset, but also transforms the velocity field from  $v_m$  to  $v_0$ .

In general, one would like to keep  $v_0$  equal to  $v_m$ . There are, however, cases where it is useful to let them vary independently. One such case is in velocity analysis. Once velocities have been picked, they can be verified through a  $(v_0, v_m)$  analysis. By generating a zero offset section with  $v_0$  not equal to  $v_m$ , errors in velocity picks show up as radical changes in shape of reflectors. Comparing a zero offset section with  $v_0$  equal to  $v_m$  (i.e., NMO + DMO) to one where  $v_0$  differs from  $v_m$ , any error in velocity shows up as a change in shape of reflectors between the two sections. When the velocity is correct, reflectors are positioned at a different time, but retain the same relative shape.

Since the zero offset trace spacing is a parameter at the users discretion, these zero offset 'check-sections' can be generated with a greatly relaxed trace spacing. In this way errors in velocity can be flagged and the velocity spectrum repicked.

### 3.7 Two or Three Dimensions?

Much of the justification for the particular choices of the inversion and modeling operators hinged upon the fact that they needed to be three-dimensional operators. This was a consequence of the fact that dip moveout is a three-dimensional problem. All reflections recorded by a shot-geophone pair, whether in-plane or out-of-plane, have equivalent zero offset projections which lie between the shot and geophone. This suggests that by processing only lines of data, the full three-dimensional variation of the subsurface can be preserved.

The derivation for the algorithm of Eq.(3.2) was for a 2.5-dimensional earth. This was defined to be an earth which did not vary in the off-line direction (i.e., recording along true dip lines). Thus, the wave propagation is allowed to be three dimensional, but the reflection points all lie in-plane. The convenience of the 2.5D assumption is in computational simplicity. The computations of Appendix A become straightforward because the out-of-plane receiver integral,  $\xi_2$ , and the out-of-plane subsurface integral,  $y$ , can be done by stationary phase.

With full three-dimensional variations, the stationary phase analysis in  $\xi_2$  and  $y$  is not justifiable. There are no critical points in the off-line variables. One must search for alternative means to evaluate the cascaded system of Eq. 3.1.

Appendix B outlines a possible three-dimensional solution path.

The solution involves uniform expansions of integrals along the lines suggested by Bleistein and Handelsman (1967). This three-dimensional implementation is not carried to completion, and Appendix B is presented solely as a suggestion for further research.

The three-dimensional solution suggests that there are significant offline contributions from the dip-movement operator. That is, not only does a recorded trace affect zero offset traces lying between the shot and geophone, but it also has a nonnegligible contribution to nearby offline zero offset traces. In hindsight, perhaps this should not be surprising. Dip moveout maps a specular reflection to an equivalent zero offset specular reflection. When the offset and zero offset reflection points do not exactly coincide in the subsurface (but are near one another), the Fresnel zones might overlap in a geometrical arrangement which is more complicated than the Fresnel zone considerations of migration. We can consider an offset reflection point as having a contribution to a zero offset reflection point if their respective Fresnel zones overlap. Thus, the reflection points might be separated by two Fresnel zones and still have some significant interaction in the mapping from offset to zero offset (Fig. 3.25). The three-dimensional solution of Appendix B might, indeed, be revealing just this phenomena.

The mathematics of the enclosed methodology is involved and lengthy. However, if treated properly, the physics reveals itself through the mathematics in an elegant and logical fashion. Thus, in the

2.5D solution, the mathematics dictated that the offset trace lie between the shot and geophone. Likewise, the mathematics revealed the particular location of the reflection points corresponding to zero offset traces. These remarks are made solely as a motivation for pursuing the mathematics of the three-dimensional solution. Deviations between the mathematical principles and intuition (i.e., the presence of significant off-line contributions) might, indeed, require a readjustment of one's intuition.

### 3.8 Cost

In preparing the applications for this thesis, little attention has been given to optimization. Therefore, these remarks are to be taken as preliminary.

The applications shown herein were developed on a Gould 9750 computer which lacked virtual memory and an array processor. The inversion-based algorithm ran approximately twice as long as the Berg algorithm. However, this is an unfair comparison. The inversion-based algorithm has a much more complicated amplitude function than the Berg algorithm. Lacking virtual memory, these amplitude factors were calculated for each input trace. This involved a high degree of redundancy of calculations. On a virtual memory installation, these factors could be calculated once for the entire dataset and read from look-up tables. With virtual memory the execution times of the inversion-based and Berg algorithms should be approximately equal.

## CONCLUSIONS

Conventional dip moveout algorithms are derived from traveltime relationships between offset recorded data and their equivalent zero offset reflections. However, to consider only traveltime arguments is to leave a number of issues unaddressed. In particular, one would like an algorithm based on the wave equation, not solely on traveltime considerations.

A wave equation based algorithm has been derived by treating the process of transforming seismic data to zero offset as a cascaded inversion/modeling procedure. The output from a seismic inversion is cascaded as input to a forward modeling algorithm. The logic of this procedure demands an inversion rather than a migration, since the modeling algorithm requires particular estimates of the earth parameters. Furthermore, the richness of the inversion theory has been shown to offer a geometric versatility, as well as the ability to carefully address the issue of amplitude variations along the limbs of the operator.

Amplitude variations along the limbs of the dip moveout operator have traditionally been handled in a makeshift fashion. The operator derived in this thesis has amplitude distributions which differ markedly from those of conventional dip moveout. The process of transforming recorded data to zero offset is a process which projects an uneven ray density (finite offset) to an even ray density (zero offset). The

amplitudes along the limbs of the operator account for these variations. Heuristically, the resultant operator incorporates a wave-equation consistent "fold compensation." The result is amplitudes which are more reliable than those from conventional dip moveout.

Applications for a wave equation based dip moveout have been shown for velocity analysis and for amplitude offset processing. In both cases the results are similar to conventional dip moveout. The differences are in fine variations in data character and quality. This is not surprising since the traveltimes relationships of both algorithms are the same.

## REFERENCES

- Berg, L.A., 1984. Pre Stack Partial Migration, paper presented at the 1984 SEG Annual Meeting, Atlanta, Georgia.
- Berkhout, A.J., 1985. Seismic Migration (Vols. A and B): Elsevier.
- Beylkin, G., 1985. Imaging of discontinuities in the inverse scattering problem by inversion of a causal generalized Radon transform: J. Math Phys., 26, 99-108.
- Beylkin, G., Oristaglio, M., and Miller, D., 1985. Spatial Resolution of Migration Algorithms, in Acoustical Imaging, vol. 14, A.J. Berkhout, J. Ridd, and L.F. van der Wal, Eds., 155-168: Elsevier.
- Biondi, B., and Ronen, J., 1986. Dip Moveout in Shot Profiles, paper presented at the 51st Annual Meeting of the SEG, Houston, Texas.
- Bleistein, N., and Handelsman, R.A., 1967. Uniform Asymptotic Expansions of Certain Integrals, SIAM J. Appl. Math., 15, 1422-1433.
- Bleistein, N., and Handelsman, R.A. 1986. Asymptotic Expansions of Integrals: Dover.
- Bleistein, N., 1984. Mathematical Methods for Wave Phenomena: Academic Press, Inc.
- Bleistein, N., Cohen, J.K., and Hagin, F.G., 1985. Computational and asymptotic aspects of velocity inversion, Geophysics, 50, 1253-1265.
- Bleistein, N., and Gray, S.H., 1985. An extension of the Born inversion

- method to a depth dependent reference profile, *Geophys. Prosp.*, 33, 999-1022.
- Bleistein, N., 1986. Two-And-One-Half Dimensional In-Plane Wave Propagation, *Geophysical Prospecting*, 34, 686-703.
- Bleistein, N., Cohen, J.K., and Hagin, F.G., 1987. Two and one-half dimensional Born inversion with an arbitrary reference, *Geophysics*, 52, 26-36.
- Bleistein, N., and Jordan, T.E., 1987. Symmetric Pre-Stack Inversion Operator for Multi-Source, Multi-Geophone Data, paper presented at the 1987 Tulsa Spring Migration/Inversion Symposium.
- Bolondi, G., Loinger, E., and Rocca, F., 1981. Offset Continuation of Seismic Sections, presented at the 43rd Meeting of the European Association of Exploration Geophysicists.
- Bolondi, G., Loinger, E., and Rocca, F., 1984. Offset Continuation in Theory and Practice, *Geophysical Prospecting*, 32, 1045-1073.
- Claerbout, J.F., 1985. *Imaging the Earth's Interior*: Blackwell Scientific Publications.
- Cohen, J.K., and Hagin, F.G., 1985. Velocity inversion using a stratified reference, *Geophysics*, 50, 1689-1700.
- Cook, E.E., and Taner, M.T., 1969. Velocity Spectra and Their Use in Stratigraphic and Lithologic Differentiation, *Geophysical Prospecting*, 17, 433-448.
- Deregowski, S.M., and Rocca, F., 1981. Geometrical optics and wave theory of constant offset sections in layered media, *Geophysical*

- Prospecting, 29, 374-406.
- Deregowski, S.M., 1982. Dip-Moveout and Reflector Point Dispersal, Geophysical Prospecting, 30, 318-322.
- Deregowski, S.M., 1985. An Integral Implementation of Dip Moveout, paper presented at the 47th Annual Meeting of the EAEG, Budapest, Hungary.
- Deregowski, S.M., 1986. What is DMO?, First Break, 4, 7-24.
- Dinstel, W.L., 1971. Short Note: Velocity Spectra and Diffraction Patterns, Geophysics, 36, 415-417.
- Douze, J., and Laster, S.J., 1979. Short Note: Statistics of Semblance, Geophysics, 44, 1999-2003.
- Garotta, R., and Michon, D., 1967. Continuous Analysis of the Velocity function and of the Move Out Corrections, Geophysical Prospecting, 15, 584-597.
- Hale, I.D., 1983. Dip-Moveout by Fourier Transform, Ph.D. thesis, Stanford University.
- Jorden, T.E., 1986. The Transformation to Zero Offset, paper presented at the 51st Annual Meeting of the SEG, Houston, Texas.
- Levin, F.K., 1971. Apparent velocity from dipping interfaces. Geophysics, 36, 510-516.
- Neidell, N.S., and Taner, M.T., 1971. Semblance and Other Coherency Measures for Multichannel Data, Geophysics, 36, 482-497.
- Ronen, J.M., 1985. Multichannel Inversion in Reflection Seismology, Ph.D. Dissertation, Stanford University.

- Salvador, L., and Savelli, S., 1981. Offset Continuation for Seismic Stacking, presented at the 43rd Meeting of the European Association of Exploration Geophysicists.
- Schneider, W.A., 1971. Developments in Seismic Data Processing and Analysis (1968-1970), *Geophysics*, 36, 1043-1073.
- Schneider, W.A., 1978. Integral formulation for migration in two and three dimensions, *Geophysics*, 43, 49-76.
- Sullivan, M.F., and Cohen, J.K., 1987. Prestack Kirchhoff inversion of common offset data, *Geophysics*, to appear.
- Taner, M.T., and Koehler, F., 1969. Velocity Spectra - Digital Computer Derivation and Applications of Velocity functions, *Geophysics*, 34, 859-881.
- Yilmaz, O., and Claerbout, J.F., 1980. Prestack partial migration, *Geophysics*, 45, 1753-1779.

APPENDIX A:

2.5D TZO DERIVATION

This appendix will detail the 2.5-dimensional derivation of the transformation to zero offset (TZO). By 2.5-dimensional, we mean a three-dimensional subsurface which varies in only two dimensions. This would be equivalent to acquisition along a true dip line. Although the geology is invariant in the out-of-plane dimension (strike), the wave propagation is still three-dimensional and is treated as such. That is, we use the full three-dimensional wave equation for both inversion and forward modeling. The out-of-plane integrals are done analytically.

Equation (1.24) will serve as a starting point. It arose from cascading a three-dimensional inversion operator into a three-dimensional forward modeling operator:

$$D_0(\omega, \xi_0) = \omega^2 \iiint d^3 \mathbf{x} \frac{A_0^2(\mathbf{x}) e^{i\omega\phi_0(\mathbf{x}, \xi_0)}}{v_0^2} \cdot \frac{v_m^2}{(2\pi)^3} \quad (\text{A-1})$$

$$\cdot \iint d^2 \xi \int d\eta \frac{|h(\mathbf{x}, \xi)|}{A_s(\mathbf{x})A_g(\mathbf{x})} e^{-i\eta\phi_s(\mathbf{x}, \xi)} D(\eta, \xi) .$$

(See Glossary for definition of symbols.)

Before beginning with the solution, a few observations on Eq.(A-1) are in order. Counting the inverse Fourier transform over  $\omega$ , Eq.(A-1)

is a seven-fold integral system. The input to this integral system are the recorded data. The output is a zero offset trace at the specified location,  $\xi_0 = (\xi_{01}, \xi_{02})$ . Note that three of the integrals involve subsurface variables,  $\mathbf{x} = (x, y, z)$ . Since neither the input data nor the output data are explicit functions of these subsurface variables, these integrals must be reduced analytically before Eq.(A-1) can be cast in a usable format.

Furthermore, Eq.(A-1) contains a double integral over receivers,  $\xi = (\xi_1, \xi_2)$ . This double integral is a natural consequence of a three-dimensional inversion algorithm. However, since we are treating the subsurface as 2.5-dimensional, the out-of-plane receiver integral can be done analytically. The acquisition envisioned here is one where parallel lines of data are recorded. Since these parallel lines of data are all dip lines over a strike-invariant earth, adjacent lines of data are identical. This invariance of adjacent data will serve as the justification for doing the  $\xi_2$  (out-of-plane receivers) integral by stationary phase.

Stationary phase (Appendix C) is a high frequency approximation. By high frequency, we mean that the wavelengths are small compared to typical scales of the problem. Thus, if  $f$  is temporal frequency and  $T$  is time, the high frequency requirement is that (Bleistein, 1984):

$$2\pi fT \gg 1$$

In practice, a value of  $2\pi fT$  greater than 3 is more than adequate. In this context, seismic data may be considered high frequency and the stationary phase approximation is justified.

The solution begins by inverse Fourier transforming Eq.(A-1) with respect to the output frequency,  $\omega$ . Under this transformation, the  $\omega^2$  term becomes  $-\partial^2/\partial t^2$ . The  $\exp[i\omega\phi_0]$  becomes a delta function with respect to output time,  $t_0$ :

$$D_0(t_0, \xi_0) = - \frac{\partial^2}{(2\pi)^3} \left[ \frac{v_m}{v_0} \right]^2 \int d\eta F(\eta) \iint d^2\xi D_s(\eta, \xi) \quad (A-2)$$

$$\cdot \iiint d^3x \frac{A_0^2(\mathbf{x}) |h(\mathbf{x}, \xi)|}{A_s(\mathbf{x}) A_g(\mathbf{x})} \delta(t_0 - \phi_0(\mathbf{x}, \xi_0)) e^{-i\eta\phi(\mathbf{x}, \xi)} .$$

Here we have taken advantage of the fact that  $v_m$  and  $v_0$  are constants by pulling them out of the integrals.

Equation (A-2) expresses the output trace as a function of zero offset location,  $\xi_0$ , and zero offset output time,  $t_0$ . Eq.(A-2) can be rewritten in order to isolate the  $x$  dependency. Since the zero offset phase term,  $\phi_0$ , is a function of  $x$ , it too must be grouped along with the  $x$ -dependent terms:

$$D_0(t_0, \xi_0) = - \frac{\partial^2}{(2\pi)^3} \left[ \frac{v_m}{v_0} \right]^2 \int d\eta F(\eta) \iint d^2\xi D(\eta, \xi) \cdot I, \quad (A-3)$$

where  $I$  is given by

$$I = \iiint d^3x \frac{A_0^2(\mathbf{x}) |h(\mathbf{x}, \xi)|}{A_s(\mathbf{x}) A_g(\mathbf{x})} \delta(t_0 - \phi_0(\mathbf{x}, \xi_0)) e^{-i\eta\phi(\mathbf{x}, \xi)}. \quad (A-4)$$

The  $\delta(t_0 - \phi_0)$  factor can be used to do one of the subsurface integrals in  $I$  by taking advantage of the identity:

$$\delta(t_0 - \phi_0(\mathbf{x}, \xi_0)) = \frac{\delta(z - z_0)}{\left| \frac{\partial \phi_0}{\partial z} \right|_{z = z_0}}. \quad (A-5)$$

In order to use this identity, it must first be noted that the zero offset phase,  $\phi_0$ , is twice the distance (divided by velocity  $v_0$ ) from the zero offset location to the reflection point divided by the velocity,  $v_0$ . Given a zero offset velocity,  $v_0$ , and an output zero offset time,  $t_0$ , this distance can be expressed directly:

$$\phi_0(\mathbf{x}, \xi_0) = t_0 = \frac{2}{v_0} \sqrt{(x-\xi_{01})^2 + (y-\xi_{02})^2 + z_0^2}$$

or:

(A-6)

$$z_0^2 = \left[ \frac{v_0 t_0}{2} \right]^2 - (x-\xi_{01})^2 - (y-\xi_{02})^2 .$$

This allows the specific evaluation of the partial derivative required by Eq.(A-5):

$$\left. \frac{\partial \phi_0}{\partial z} \right|_{z = z_0} = \left[ \frac{2}{v_0} \right]^2 \frac{z_0}{t_0} . \quad (A-7)$$

The final form of the substitution suggested by Eq.(A-5) is:

$$\delta \left[ t_0 - \phi_0(\mathbf{x}, \xi_0) \right] = \delta(z - z_0) \left[ \frac{v_0}{2} \right]^2 \frac{t_0}{z_0} . \quad (A-8)$$

Under this substitution, the  $z$  integral of Eq.(A-4) can be evaluated directly. After this evaluation,  $I$  becomes:

$$I = \iint dx dy \frac{A_0^2(\mathbf{x}) |h(\mathbf{x}, \xi)|}{A_s(\mathbf{x}) A_g(\mathbf{x})} \left[ \frac{v_0}{2} \right]^2 \frac{t_0}{z_0} e^{-i\eta\phi(\mathbf{x}, \xi)} . \quad (A-9)$$

where it is understood that  $\mathbf{x} = (x, y, z_0)$ .

Here the  $z$  dependency in both the amplitude and phase terms of Eq.(A-9) are now expressed as functions of  $z_0$  as given above. This makes the resultant phase function  $\phi$  a great deal more complicated, for it is now a phase function which is a coupled version of the original zero offset phase,  $\phi_0$ , and the prestack inversion phase,  $\phi$ :

$$\begin{aligned} \phi(x, \xi) &= \frac{1}{v_m} \left[ \rho_s + \rho_g \right] \\ &= \frac{1}{v_m} \left[ \sqrt{\left[ \frac{v_0 t_0}{2} \right]^2 + (\xi_{s2} - \xi_{o2})(\xi_{s2} + \xi_{o2} - 2y) + (\xi_{s1} - \xi_{o1})(\xi_{s1} + \xi_{o1} - 2x)} \right. \\ &\quad \left. + \sqrt{\left[ \frac{v_0 t_0}{2} \right]^2 + (\xi_{g2} - \xi_{o2})(\xi_{g2} + \xi_{o2} - 2y) + (\xi_{g1} - \xi_{o1})(\xi_{g1} + \xi_{o1} - 2x)} \right] . \end{aligned} \quad (A-10)$$

The next integral to be evaluated will be the out-of-plane receiver integral,  $\xi_2$ . Recall that the 2.5D assumption justifies the evaluation of this integral by stationary phase. Isolating the receiver integrals, the zero offset formula can be written as:

$$D_0(t_0, \xi_0) = \frac{-\partial^2}{(2\pi)^3} \frac{t_0 v^2}{4} \int d\eta F(\eta) \iint dx dy \cdot \frac{1}{z_0} \cdot J \quad (A-11)$$

Here J is now the isolation of the  $\xi = (\xi_1, \xi_2)$  dependence:

$$J = \iint d^2\xi \frac{A_0^2(\mathbf{x}) |h(\mathbf{x}, \xi)|}{A_s(\mathbf{x}) A_g(\mathbf{x})} D(\eta, \xi) e^{-i\eta\phi(\mathbf{x}, \xi)} \quad (A-12)$$

The stationary point of this integral with respect to  $\xi_2$  is found by setting the derivative of the phase equal to zero (see Appendix C for a review of the stationary phase formalism):

$$\frac{\partial\phi_s}{\partial\xi_2} = \frac{1}{v_m} \left[ \frac{2\xi_2 - 2y}{\rho_s} + \frac{2\xi_2 - 2y}{\rho_g} \right] = 0 \quad (A-13)$$

The critical point is, therefore:

$$\xi_2 = y$$

The stationary point with respect to  $\xi_2$  are those receiver locations which lie directly in line with the reflection point  $y$ . This is consistent with the 2.5D assumption. The second derivative of the phase is also required, along with its sign ( $\text{sgn}\phi''$ ):

$$\frac{\partial^2 \phi_s}{\partial \xi_2^2} = \frac{1}{v_m} \left[ \frac{2}{\rho_s} - \frac{(2\xi_2 - 2y)^2}{\rho_s^3} + \frac{2}{\rho_g} - \frac{(2\xi_2 - 2y)^2}{\rho_g^3} \right] \quad (\text{A-14})$$

$$\left. \frac{\partial^2 \phi_s}{\partial \xi_2^2} \right|_{y=\xi_2} = \frac{2}{v_m} \left[ \frac{1}{\rho_s} + \frac{1}{\rho_g} \right] \quad \text{sgn} \frac{\partial^2 \phi_s}{\partial \xi_2^2} = +1 .$$

Using the stationary phase formula Eq.(C-3), J can be expressed asymptotically as:

$$J \sim \int d\xi_1 \frac{A_0^2(\mathbf{x}) |h(\mathbf{x}, \xi)|}{A_s(\mathbf{x}) A_g(\mathbf{x})} D(\eta, \xi) \left[ \frac{2\pi v_m}{\left| 2\eta \left[ \frac{1}{\rho_s} + \frac{1}{\rho_g} \right] \right|} \right]^{1/2} \cdot \exp \left[ -i\eta\phi(\mathbf{x}, \xi) - \frac{i\pi}{4} \text{sgn}\eta \right] . \quad (\text{A-15})$$

Now the full formula can be expressed as:

$$D_0(t_0, \xi_0) = -\frac{\partial_t^2}{(2\pi)^{5/2}} t_0 \left[ \frac{v_m}{2} \right]^{5/2} \int d\eta \frac{F(\eta)}{|\eta|^{1/2}} \exp \left[ -\frac{i\pi}{4} \text{sgn}\eta \right] \cdot \int d\xi_1 D_s(\eta, \xi) \cdot L . \quad (\text{A-16})$$

Here L isolates the  $\mathbf{x} = (x, y)$  dependency:

$$L = \iint dx dy \cdot \frac{1}{z_0} \frac{A_0^2(\mathbf{x}) |h(\mathbf{x}, \xi)|}{A_s(\mathbf{x}) A_g(\mathbf{x})} \left[ \frac{1}{\rho_s} + \frac{1}{\rho_g} \right]^{-1/2} \cdot \exp \left[ -i\eta\phi(\mathbf{x}, \xi) \right] . \quad (\text{A-17})$$

The 2.5D assumption also justifies the evaluation of the y-integral by stationary phase. Since the subsurface is slowly varying (i.e., invariant with respect to y), the stationary phase treatment is reasonable. This will involve the evaluation of derivatives similar to those above (Eq. A-13 and A-14). After the  $\xi_2$  stationary phase,  $\phi$  is given by

$$\begin{aligned} \phi(\mathbf{x}, \xi) &= \frac{1}{v_m} (\rho_s + \rho_g) \\ &= \frac{1}{v_m} \left[ \sqrt{\left[ \frac{v_0 t_0}{2} \right]^2 - \left[ y - \xi_{02} \right]^2 + \left[ \xi_{s1} - \xi_{01} \right] \left[ \xi_{s1} + \xi_{01} - 2x \right]} \right. \\ &\quad \left. + \sqrt{\left[ \frac{v_0 t_0}{2} \right]^2 - \left[ y - \xi_{02} \right]^2 + \left[ \xi_{g1} - \xi_{01} \right] \left[ \xi_{g1} + \xi_{01} - 2x \right]} \right] . \end{aligned} \quad (\text{A-18})$$

The y-critical point is found by differentiating this phase with respect to y:

$$\frac{\partial \phi}{\partial y} = \frac{1}{v_m} \left[ \frac{2(\xi_{02} - y)}{\rho_s} + \frac{2(\xi_{02} - y)}{\rho_g} \right] = 0 \quad . \quad (\text{A-19})$$

The critical point is, therefore:

$$y_c = \xi_{02} \quad .$$

Together with Eq.(A-13), the stationary points dictate that, for a given  $\xi_{02}$  output coordinate, the leading order contribution comes from those receivers inline with  $\xi_{02}$ , with all reflection points also in-line.

Again, the second derivative and its sign are also required:

$$\frac{\partial^2 \phi}{\partial y^2} = - \frac{1}{v_m} \left[ - \frac{2}{\rho_s} + \frac{4(\xi_{02} - y)^2}{\rho_s^3} - \frac{2}{\rho_g} + \frac{4(\xi_{02} - y)^2}{\rho_g^3} \right] \quad (\text{A-20})$$

$$\left. \frac{\partial^2 \phi}{\partial y^2} \right|_{y=\xi_{02}} = - \frac{2}{v_m} \left[ \frac{1}{\rho_s} + \frac{1}{\rho_g} \right] \quad \text{sgn} \frac{\partial^2 \phi}{\partial y^2} = - 1 \quad .$$

Upon stationary phase evaluation of the y integral, L becomes

$$L \sim \int dx \frac{1}{z_0} \frac{A_0^2(\mathbf{x}) |h(\mathbf{x}, \xi)|}{A_s(\mathbf{x}) A_g(\mathbf{x})} \left[ \frac{1}{\rho_s} + \frac{1}{\rho_g} \right]^{-1/2} \left[ \frac{2\pi v_m}{|2\eta \left[ \frac{1}{\rho_s} + \frac{1}{\rho_g} \right]} \right]^{1/2} \cdot \exp \left[ -i\eta\phi(\mathbf{x}, \xi) + \frac{i\pi}{4} \operatorname{sgn} \eta \right] . \quad (\text{A-21})$$

The reader is reminded that  $\mathbf{x}$  is taken to mean  $\mathbf{x} = (x, y_C, z_0)$ .

This remaining  $\mathbf{x}$  integral is also a candidate for stationary phase. However, in this case the meaning of the stationary point is somewhat different. The justification of the  $y$  and  $\xi_2$  stationary phase calculations relied upon the 2.5D assumptions. Here, however, the subsurface varies as a function of  $\mathbf{x}$ . The  $\mathbf{x}$  stationary phase calculation finds the specular reflection point. Given a particular output location,  $\xi_0$ , and an output time,  $t_0$ , there exists a unique specular reflection from a shot and geophone pair which has an equivalent zero offset reflection at the point  $\mathbf{x}_0$ . (Appendix E proves this by actually finding the coordinates of this specular reflection for any given  $\xi_s, \xi_g, \xi_0$ , and  $t_0$ .)

As before, the critical point is found by setting the  $\mathbf{x}$  derivative of the phase  $\phi$  to zero. The particular form of the phase at this point is given by:

$$\begin{aligned}
\phi(x, \xi) &= \frac{1}{v_m} \left[ \rho_s + \rho_g \right] \\
&= \frac{1}{v_m} \left[ \sqrt{\left[ \frac{v_o t_o}{2} \right]^2 + \left[ \xi_{s1} - \xi_{o1} \right] \left[ \xi_{s1} + \xi_{o1} - 2x \right]} \right. \\
&\quad \left. + \sqrt{\left[ \frac{v_o t_o}{2} \right]^2 + \left[ \xi_{g1} - \xi_{o1} \right] \left[ \xi_{g1} + \xi_{o1} - 2x \right]} \right] . \tag{A-22}
\end{aligned}$$

Taking a derivative with respect to  $x$  gives:

$$\frac{\partial \phi}{\partial x} = \frac{1}{v_m} \left[ - \frac{2(\xi_{s1} - \xi_{o1})}{\rho_s} - \frac{2(\xi_{g1} - \xi_{o1})}{\rho_g} \right] = 0 . \tag{A-23}$$

Before proceeding with the evaluation of Eq.(A-23), note that since the denominator of each term is intrinsically a positive quantity, the sign of the numerators must be opposite

$$\text{sgn} (\xi_{s1} - \xi_{o1}) = - \text{sgn} (\xi_{g1} - \xi_{o1}) . \tag{A-24}$$

This relationship states that the zero offset output point must lie between the shot and geophone in order for the stationary phase condition to be satisfied. Thus, all reflections from a given input

trace map to zero offset traces which lie between the shot and geophone (Fig. A-1). This is a restatement of the dip-moveout impulse response geometry. The DMO impulse response is an ellipse with a horizontal axis equal to the offset (i.e., the DMO impulse response maps a given trace to zero offset traces which all lie between the shot and geophone).

The algebra of solving Eq.(A-23) for the stationary point,  $x_c$ , is straightforward but lengthy. The result is:

$$x_c = \xi_0 + \frac{\left[ \frac{v_0 t_0}{2} \right]^2 (\xi_g + \xi_s - 2\xi_0)}{2(\xi_s - \xi_0)(\xi_g - \xi_0)} . \quad (A-25)$$

The subscripts have been dropped with the understanding that  $\xi_s$ ,  $\xi_g$ , and  $\xi_0$  are all in-line.

The second derivative of  $\phi$  with respect to  $x$  is:

$$\frac{\partial^2 \phi}{\partial x^2} = - \frac{4}{v_m} \left[ \frac{(\xi_0 - \xi_s)^2}{\rho_s^3} + \frac{(\xi_0 - \xi_g)^2}{\rho_g^3} \right] \quad (A-26)$$

$$\text{sgn} \frac{\partial^2 \phi}{\partial x^2} = - 1 .$$

The subsurface integral  $L$  is asymptotically equal to:

$$L \sim \frac{1}{v_m} \frac{A_0^2(\mathbf{x}) |h(\mathbf{x}, \xi)|}{A_s(\mathbf{x}) A_g(\mathbf{x})} \left[ \frac{1}{\rho_s} + \frac{1}{\rho_g} \right]^{-1} \left[ \frac{\pi v_m}{\sqrt{2} |\eta|} \right]$$

(A-27)

$$\cdot \left[ \left| \frac{\partial^2 \phi}{\partial x^2} \right| \right]^{-1/2} \cdot \exp \left[ -i\eta\phi(\mathbf{x}, \xi) + \frac{i\pi}{2} \operatorname{sgn} \eta \right] .$$

As before,  $\mathbf{x} = (x_c, y_c, z_0)$ . Putting all this together gives the transformation to zero offset as a single integral over the recorded shot records:

$$D_0(t_0, \xi_0) = - \frac{\partial^2}{\partial t^2} t_0 \frac{v_m^{7/2}}{16} \int \frac{d\eta F(\eta) \exp \left[ \frac{i\pi}{4} \operatorname{sgn} \eta \right]}{|\eta|^{3/2}}$$

$$\cdot \int d\xi_g \frac{A_0^2(\mathbf{x}) |h(\mathbf{x}, \xi)|}{z_0 A_s(\mathbf{x}) A_g(\mathbf{x})} \left[ \frac{1}{\rho_s} + \frac{1}{\rho_g} \right]^{-1} \left| \frac{\partial^2 \phi}{\partial x^2} \right|^{-1/2}$$

(A-28)

$$D(\eta, \xi) \cdot \exp \left[ -i\eta\phi(\mathbf{x}, \xi) \right] .$$

The evaluation of the second time derivative,  $\partial^2 \phi / \partial t^2$ , is done by

considering only the leading order term. That is, since the phase,  $\phi$ , is a function of time, the evaluation of the time derivative will give rise to several terms which can be expressed a power series in the input frequency variable,  $\eta$  To leading order:

$$-\partial_t^2 \longleftrightarrow \eta^2 \left[ \frac{\partial \phi}{\partial t} \right]^2 . \quad (\text{A-29})$$

Therefore, the transformation to zero offset is given by:

$$D_o(t_o, \xi_o) = \frac{t_o}{(2\pi)^{3/2}} \frac{v_m^{7/2}}{16} \int d\eta F(\eta) |\eta|^{1/2} \exp \left[ \frac{i\pi}{4} \text{sgn}\eta \right]$$

$$\cdot \int d\xi_g \frac{A_o^2(\mathbf{x}) |h(\mathbf{x}, \xi)|}{A_s(\mathbf{x}) A_g(\mathbf{x})} \left[ \frac{1}{\rho_s} + \frac{1}{\rho_g} \right]^{-1} \frac{\left[ \frac{\partial \phi}{\partial t} \right]^2}{\left| \frac{\partial^2 \phi_s}{\partial \mathbf{x}^2} \right|^{1/2}} \quad (\text{A-30})$$

$$D(\eta, \xi) \exp \left[ -i\eta\phi(\mathbf{x}, \xi) \right] .$$

The specific form of the various factors is:

$$\rho_s = \left| \xi_s - \xi_0 \right| P^{1/2}$$

$$\rho_g = \left| \xi_g - \xi_0 \right| P^{1/2}$$

$$\varphi(x, \xi) = \frac{1}{v_m} (\rho_s + \rho_g) = \frac{|\xi_g - \xi_s|}{v_m} P^{1/2}$$

$$P = 1 + \frac{\left[ \frac{v_0 t_0}{2} \right]^2}{(\xi_0 - \xi_s)(\xi_g - \xi_0)}$$

$$\frac{\partial \varphi}{\partial t} = \frac{v_0^2 t_0}{4v_m} \left[ \frac{1}{\rho_s} + \frac{1}{\rho_g} \right]$$

$$\frac{\partial^2 \phi}{\partial x^2} = -\frac{1}{v_m} \left[ \frac{(\xi_0 - \xi_s)^2}{\rho_s^3} + \frac{(\xi_0 - \xi_g)^2}{\rho_g^3} \right]$$

The specific form of  $|h(x, \xi)|$  depends upon the geometry. Appendix G gives  $|h|$  for common shot. Appendix H gives  $|h|$  for common offset. In these formulations  $\beta$ , the angle between  $\rho_s$  and  $\rho_g$ , appears.  $\cos\beta$  is given by:

$$\cos\beta = \frac{1}{\rho_s \rho_g} \left[ \frac{v_o t_o}{2} \right]^2 \left[ 1 + \frac{(\xi_g + \xi_s - 2\xi_0)^2}{2(\xi_s - \xi_0)(\xi_g - \xi_0)} + (\xi_s - \xi_0)(\xi_g - \xi_0) \right]$$

$$A_o^2(x) = \frac{1}{(4\pi\rho_o)} = \frac{1}{\left[ 4\pi \left[ \frac{v_o t_o}{2} \right]^2 \right]}$$

$$A_s(x) A_g(x) = \frac{1}{(4\pi\rho_s)(4\pi\rho_g)}$$

In practice the data are processed as follows. The input shot records are read one trace at a time, Fourier transformed, then filtered with the filter:

$$D_{1/2}(t) = |\eta|^{1/2} \exp \left[ \frac{i\pi}{4} \operatorname{sgn}\eta \right] .$$

Those familiar with dip moveout will recognize this as the square-root differentiator which shows up in many time domain DMO algorithms. After filtering, traces are inverse Fourier transformed. Each trace is then spread out along its impulse response defined by the phase function,  $\phi$ . As expressed in Eq.(A-30), the output is an integral over the input shot records. Equivalently, each input trace can be spread over the time varying impulse response as given by  $\phi$ , with the amplitude factor dictated by Eq.(A-30). In this fashion, data can be processed in trace sequential format. Once each trace has been spread along its impulse response (i.e., mapped to all zero offset locations to which it contributes) the trace is no longer needed. Sorting and tape rewinding are eliminated.

APPENDIX B:  
3D TZO DERIVATION

This appendix will outline the full three-dimensional derivation of the transformation to zero offset (TZO). The derivation is not carried to completion (i.e., an implementable form). This remains a ripe area for further research. The solution path presented here differs markedly from the 2.5D solution of Appendix A.

Transforming data to zero offset is fully a three-dimensional problem. By processing only lines of data, the full three-dimensional variations on the subsurface can be maintained. Thus, two-dimensional assumptions are unnecessary in taking recorded data to zero offset. These assumptions are best left for when they are appropriate - after stack.

Figure B-1 illustrates the three-dimensional nature of dip-moveout. Two reflected raypaths, are shown. Note that, although the reflection points are out-of-plane, the zero offset mapping for these reflections lies at a surface point in-line. All reflections, whether in-plane or out-of-plane, have equivalent zero offset locations which are between the shot and the geophone.

This is, of course, a ray approximation. In practice there is a finite contribution from receivers which are offline. Often this offline contribution is assumed to be a sinc-like weighting function. The full three-dimensional solution of this appendix offers the

possibility of defining the offline contribution explicitly.

In Appendix A, the system of cascaded integrals could be reduced utilizing the stationary phase approximation. This is equivalent to assuming that parallel lines of recorded data would be identical, and that the subsurface did not vary in the out-of-plane direction. This is consistent with acquisition along true dip lines. However, the previous arguments render this assumption invalid. Alternative techniques must be found to evaluate the out-of-plane  $\xi_2$  and  $y$  integrals. As will be shown, the in-plane  $x$  integration is still properly handled by stationary phase.

This derivation will be for a 3D common shot acquisition geometry. 3D common shot is defined by a fixed source point with receivers distributed over the acquisition surface (Fig. B-2). Thus, the shot coordinates  $\xi_s = (\xi_{s1}, \xi_{s2})$  are constant. The receiver coordinates  $\xi_g = (\xi_{g1}, \xi_{g2})$  are the variables of integration. 3D common receiver would be defined in a similar fashion.

3D common offset could be defined by a recording geometry involving parallel lines of data. These data may then be written as parallel lines of common offsets. The shot coordinate would be  $\xi_s = (\xi_1 - h, \xi_2)$ . The receiver coordinate would be  $\xi_g = (\xi_1 + h, \xi_2)$ . The  $d^2\xi$  integration would then be over a midpoint coordinate  $\xi = (\xi_1, \xi_2)$ .

These remarks are intended to illustrate the generality of the theory used herein. The specifics of the geometry are accounted for by the form of the determinant  $|h(x, \xi)|$ . Thus, one could handle more

realistic 3D marine data by defining an offset vector  $\mathbf{h} = (h_1, h_2)$  and defining  $\xi_s$  and  $\xi_g$  in terms of midpoint and offset vectors. The theory is developed for any geometry.

The 3D common shot  $|\mathbf{h}(\mathbf{x}, \xi)|$  is given in Appendix I. It is anticipated that the solution path for other geometries (i.e., common offset) is very similar to the 3D common shot derivation given here.

Equation (1.24) will once again serve as a starting point. It is the cascaded inversion/modeling system by which recorded data is transformed to zero offset:

$$D_o(\omega, \xi_o) = \omega^2 \iiint d^3 \mathbf{x} \frac{A_o^2(\mathbf{x}) e^{i\omega\phi_o(\mathbf{x}, \xi_o)}}{v_o^2} \cdot \frac{v_m^2}{(2\pi)^3} \quad (B-1)$$

$$\cdot \iint d^2 \xi \int d\eta \frac{|\mathbf{h}(\mathbf{x}, \xi)|}{A_s(\mathbf{x}) A_g(\mathbf{x})} e^{-i\eta\phi(\mathbf{x}, \xi)} D(\eta, \xi) \quad .$$

(See Glossary for definition of terms.)

The solution begins along a path identical to Appendix A. Inverse Fourier transforming with respect to  $\omega$ , the  $\omega^2$  becomes  $-\partial_t^2$ . The  $\exp(i\omega\phi_o)$  becomes a delta function with respect to output time,  $t_o$ :

$$D_0(t_0, \xi_0) = - \frac{\partial^2}{\partial t^2} \left[ \frac{v_m}{v_0} \right]^2 \int d\eta F(\eta) \iint d^2\xi D_s(\eta, \xi) \quad (B-2)$$

$$\cdot \iiint d^3x \frac{A_0^2(\mathbf{x}) |h(\mathbf{x}, \xi)|}{A_s(\mathbf{x}) A_g(\mathbf{x})} \delta(t_0 - \phi_0(\mathbf{x}, \xi_0)) e^{-i\eta\phi(\mathbf{x}, \xi)} .$$

Here we have assumed that  $v_m$  and  $v_0$  are constant.

Equation (B-2) expresses the output trace,  $D_0(t_0, \xi_0)$ , as a function of the zero offset time,  $t_0$ , and zero offset location,  $\xi_0$  (as well as the variables under the integration). Regrouping Eq.(B-2) in order to isolate the  $\mathbf{x}$  dependency yields:

$$D_0(t_0, \xi_0) = - \frac{\partial^2}{\partial t^2} \left[ \frac{v_m}{v_0} \right]^2 \int d\eta F(\eta) \iint d^2\xi D(\eta, \xi) \cdot I \quad , \quad (B-3)$$

where  $I$  contains the integration involving the subsurface,  $\mathbf{x}$ :

$$I = \iiint d^3x \frac{A_0^2(\mathbf{x}) |h(\mathbf{x}, \xi)|}{A_s(\mathbf{x}) A_g(\mathbf{x})} \delta(t_0 - \phi_0(\mathbf{x}, \xi_0)) e^{-i\eta\phi(\mathbf{x}, \xi)} . \quad (B-4)$$

As in Appendix A, the delta function,  $\delta(t_0 - \phi_0)$ , can be used to evaluate the  $z$  integration by first taking advantage of the distributional identity:

$$\delta(t_0 - \phi_0(\mathbf{x}, \xi_0)) = \frac{\delta(z - z_0)}{\left| \frac{\partial \phi_0}{\partial z} \right|_{z = z_0}} \quad . \quad (\text{B-5})$$

The zero offset phase,  $\phi_0$ , is simply two-way traveltime from the zero offset surface location  $\xi_0$  to the subsurface reflection point  $\mathbf{x} = (x, y, z)$ . This two-way traveltime is  $t_0$ , the output time. This traveltime is equal to twice the distance divided by the velocity  $v_0$ :

$$\phi_0(\mathbf{x}, \xi_0) = t_0 = \frac{2}{v_0} \sqrt{(x - \xi_{01})^2 + (y - \xi_{02})^2 + z_0^2}$$

or:

(B-6)

$$z_0^2 = \left[ \frac{v_0 t_0}{2} \right]^2 - (x - \xi_{01})^2 - (y - \xi_{02})^2 \quad .$$

This allows the specific evaluation of the partial derivative required by Eq.(B-5):

$$\left| \frac{\partial \phi_0}{\partial z} \right|_{z = z_0} = \left[ \frac{2}{v_0} \right]^2 \frac{z_0}{t_0} \quad . \quad (\text{B-7})$$

Again, as in Appendix A, the final form of the substitution

suggested by Eq. (B-5) is:

$$\delta \left[ t_0 - \phi_0(\mathbf{x}, \xi_0) \right] = \delta(z - z_0) \left[ \frac{v_0}{2} \right]^2 \frac{t_0}{z_0} . \quad (\text{B-8})$$

Once this substitution is made, the  $z$  integral can be evaluated by means of the delta function. After this evaluation,  $I$  becomes:

$$I = \iiint dx dy \frac{A_0^2(\mathbf{x}) |h(\mathbf{x}, \xi)|}{A_s(\mathbf{x}) A_g(\mathbf{x})} \left[ \frac{v_0}{2} \right]^2 \frac{t}{z_0} e^{-i\eta\phi_s(\mathbf{x}, \xi)} . \quad (\text{B-9})$$

Here it is understood that  $\mathbf{x} = (x, y, z_0)$ ;  $z_0$  is as given by Eq.(B-6).

The phase functions,  $\phi_0$  and  $\phi$ , are now coupled through the variable  $z_0$ . After the substitution  $z = z_0$ , the resultant phase function is described by:

$$\phi(x, \xi) = \frac{1}{v_m} \left[ \rho_s + \rho_g \right]$$

$$\rho_s = \left[ \sqrt{\left[ \frac{v_0 t_0}{2} \right]^2 + (\xi_{s2} - \xi_{o2})(\xi_{s2} + \xi_{o2} - 2y) + (\xi_{s1} - \xi_{o1})(\xi_{s1} + \xi_{o1} - 2x)} \right] \quad (B-10)$$

$$\rho_g = \left[ \sqrt{\left[ \frac{v_0 t_0}{2} \right]^2 + (\xi_{g2} - \xi_{o2})(\xi_{g2} + \xi_{o2} - 2y) + (\xi_{g1} - \xi_{o1})(\xi_{g1} + \xi_{o1} - 2x)} \right] .$$

In Appendix A the next step was to evaluate the  $y$  and  $\xi_2$  integrals by stationary phase. This was equivalent to assuming that the data were acquired by parallel dip lines. All reflection points originated from the plane of the recorded data. For the three-dimensional derivation, this is an incorrect assumption. We must allow the subsurface to vary arbitrarily. We would, therefore, expect parallel lines of data to vary in an unpredictable fashion. Alternative means must be found to evaluate the  $y$  and  $\xi_2$  integrals.

Note that the form of the phase  $\phi$  is such that when  $\xi_{s2} = \xi_{g2} = \xi_{o2}$ , the phase is no longer a function of  $y$ . This was expressed graphically by Figure B-1. Figure B-1 shows two out-of-plane reflection points, as well as their equivalent zero offset rays. The

rays from the shot to reflection point, reflection point to geophone, and reflection point to zero offset location all lie in a common plane - the plane formed by the vectors  $\rho_s$  and  $\rho_g$ . The relationship between these vectors is preserved as they are rotated in or out of the plane of recording. As long as the output point  $\xi_0$  lies between the shot and geophone the mapping from finite offset to zero offset is not a function of  $y$ . The geometry of Figure B-1 can be rotated in- or out-of-plane at will without altering the geometrical relationships.

This is a geometrical description of what is indicated by the form of the coupled phase function,  $\phi$ , in Eq.(B-10). As long as the zero offset location lies in-line with the shot and geophone (i.e.,  $\xi_{02} = \xi_{s2} = \xi_{g2}$ ) the phase is not a function of  $y$ . This suggests that there is some pathology regarding the condition  $\xi_2 - \xi_{02}$  that we might exploit in the solution.

At this point one might wonder why we do not simply choose  $\xi_2 = \xi_{02}$  and take advantage of the resultant simplifications. The zero offset location,  $\xi_0 = (\xi_{01}, \xi_{02})$  is a parameter we are free to choose. For this 3D case, the  $\xi_2$  integration is over a range of  $\xi_{g2}$  values. We cannot fix the condition  $\xi_2 = \xi_{02}$ . The stationary phase analysis of the  $y$  and  $\xi_2$  integrals in Appendix A was essentially equivalent to specifying  $\xi_2 = \xi_{02}$ . However, because of our 2.5D assumptions, this analysis was justified on physical principles. Here in the general 3D case, no such arguments are at our disposal.

This is not just an exercise in abstract mathematics. The complications of the 3D solution arise from the physics of the problem. For 3D Geometry Fig. B-1 might, indeed be an over simplification. In transforming to zero offset the Fresnel zones of the offset and zero offset reflections might interact in such a way as to make off-line contributions to the integral (i.e.,  $\xi_2 \neq \xi_{02}$ ) non-negligible.

We will attempt to expand the kernel of the integral about the point  $\xi_2 = \xi_{02}$ . For convenience, consider a new variable  $\Theta$  which measures the offline distance of the zero offset point:

$$\Theta = \xi_2 - \xi_{02} = \xi_{g2} - \xi_{02} \quad . \quad (B-11)$$

For common shot geometry the variables of integration are  $\xi = (\xi_1, \xi_2) = (\xi_{g1}, \xi_{g2})$ . So choosing  $\xi_2 = \xi_{02}$  is equivalent to choosing  $\xi_{g2} = \xi_{02}$ .

Since  $\xi_g$  is the integration variable, the expansion about  $\xi_{g2} = \xi_{02}$  does nothing to facilitate the simplification of the  $(\xi_{s2} - \xi_{02})$  term in  $\rho_s$  of Eq.(B-10). That is,  $\rho_s$  is still a function of  $y$ . However, we are free to choose the coordinate system. Without loss of generality, we can select a coordinate system such that  $\xi_{s2} = \xi_{02}$ . With this choice the  $y$ -dependence of  $\rho_s$  vanishes. Therefore, the only  $y$ -dependence in  $\phi$  is the  $y$ -dependence in  $\rho_g$ .

So, when  $\Theta = 0$ , the function  $\phi$  has no  $y$  dependence. In fact, when  $\Theta = 0$  the entire amplitude term of the integral in Eq.(B-9) has no  $y$  dependence. Consider an expansion about the point  $\Theta = 0$ :

$$\phi(y, \theta) - \phi(y, 0) = \theta \Omega \quad . \quad (\text{B-12})$$

Although  $\phi$  is a function of more than  $\theta$  and  $y$ , for notational convenience let  $\phi$  be written as  $\phi(y, \theta)$ . Eq.(B-12) is an exact expansion. The  $\Omega$  of the right hand side is left undefined in order that the expansion be exact. Thus, one might think of  $\Omega$  to be all terms of the Taylor series for the expansion about  $\theta = 0$ . The expansion of Eq.(B-12) is exact.

As we have said, the function  $\phi(y, 0)$  has no  $y$  dependence because of the particular form of Eq.(B-10). We can rewrite Eq.(B-9) using the substitution of Eq.(B-12) (with the choice of coordinates  $\xi_{s_2} = \xi_{o_2}$ ):

$$\phi(x, \xi) = \phi(y, \theta) = \frac{1}{v_m} (\rho_s + \rho_g)$$

$$\rho_s = \sqrt{\left[ \frac{v_o t_o}{2} \right]^2 + (\xi_{s_1} - \xi_{o_1})(\xi_{s_1} + \xi_{o_1} - 2x)} \quad (\text{B-13})$$

$$\rho_g = \sqrt{\left[ \frac{v_o t_o}{2} \right]^2 + \theta(\theta + 2\xi_{o_2} - 2y) + (\xi_{g_1} - \xi_{o_1})(\xi_{g_1} + \xi_{o_1} - 2x)} \quad .$$

Now consider a substitution of variables from  $y$  to  $\Omega$ . The Jacobian of this substitution is given  $\partial y / \partial \Omega$ . From Eq.(B-12), it is easier to solve for  $\partial \Omega / \partial y$ . This is given by:

$$\frac{\partial \Omega}{\partial y} = \frac{\partial}{\partial y} \left[ \frac{\phi(y, \theta) - \phi(y, 0)}{\theta} \right] \quad (\text{B-14})$$

$$= \frac{1}{\theta} \frac{\partial}{\partial y} (\phi(y, \theta)) = \frac{1}{\theta} \frac{\partial \rho_g}{\partial y} .$$

Or, in terms of the explicit form of  $\rho_g$ ,  $\partial \Omega / \partial y$  is:

$$\frac{1}{\theta} \left[ - \frac{2\theta}{\rho_g} \right] \quad (\text{B-15})$$

or

$$\frac{\partial y}{\partial \Omega} = - \frac{\rho_g}{2}$$

It is critical to note that this Jacobian is non-singular at the point  $\theta = 0$ . This was guaranteed by the form of the expansion about the point  $\theta = 0$ .

In recasting the  $y$  integration in terms of a  $\Omega$  integration, we must address the question of limits of integration. The original problem (Eq.(B-1)) was in terms of infinite limits on the subsurface variables  $\mathbf{x} = (x, y, z)$ . However, specifying a zero offset output time naturally suggests finite limits to these integrals. Interpreting the original zero offset phase as twice the zero offset one-way traveltime (Eq.(B-6))

suggests that for a fixed output time  $t_0$  the limits cannot be infinite. The limits must be such that the distance from the subsurface point  $\mathbf{x}$  to the output location conforms to the two-way zero offset traveltime  $t_0$ . For a given time  $t_0$  the maximum offline distance  $y$  occurs when the reflection point is on the surface ( $z_0 = 0$ ). Referring to Eq.(B-6), these limits are given by:

$$y_{\max} = \xi_{02} + \sqrt{\left[\frac{v_0 t_0}{2}\right]^2 - (x - \xi_{01})^2} \quad . \quad (\text{B-16})$$

For notational convenience, let the amplitude terms of the integrand be given by:

$$f(\mathbf{x}, \xi, \xi_0) = \frac{A_0^2(\mathbf{x}) |h(\mathbf{x}, \xi)|}{A_s(\mathbf{x}) A_g(\mathbf{x})} \left[\frac{v_0}{2}\right] \frac{t_0^2}{z_0} \quad (\text{B-17})$$

$$F(\mathbf{x}, \xi, \xi_0) = f(\mathbf{x}, \xi, \xi_0) \frac{\partial y}{\partial \Omega} \quad .$$

Since we will be changing the  $y$  integration to an  $\Omega$  integration,  $F(\mathbf{x}, \xi, \xi_0)$  has been written to include the Jacobian,  $\partial y / \partial \Omega$ .

It can also be shown that this amplitude term is an explicit function of  $\theta$ , and that it, too, has no  $y$  dependence when  $\theta = 0$ . Therefore, we can perform a similar expansion of the amplitude (again, we will use  $F(y, \theta)$  as notation for  $F(\mathbf{x}, \xi, \xi_0)$ ):

$$F(y,\theta) - F(y,0) = \theta F_1 \quad . \quad (B-18)$$

As before, this is an exact expansion. No approximations have been made. We can rewrite the integral I of Eq.(B-9) in terms of these expansions:

$$I = \iint dx dy f(x,\xi,\xi_0) e^{-i\eta(\phi(y,0)+\theta\Omega)} \quad . \quad (B-19)$$

Since  $\phi(y,0)$  has no explicit  $y$ -dependence, it can be taken outside the  $y$ -integral:

$$I = \int dx e^{-i\eta\phi(y,0)} \int dy f(x,\xi,\xi_0) e^{-i\eta\theta\Omega} \quad . \quad (B-20)$$

Admittedly, the notation is a little sloppy here. In particular, it is somewhat confusing to use the notation  $\phi(y,0)$  and  $F(y,0)$  for quantities which have no  $y$ -dependence.

Changing the variable of integration to  $\Omega$  we now use  $F(x,\xi,\xi_0)$  (written as  $F(y,\theta)$ ).  $F(y,\theta)$  includes the Jacobian of the substitution. Here we utilize the expansion of Eq.(B-18):

$$I = \int dx e^{-i\eta\phi(y,0)} \int d\omega (F(y,0) + \Theta F_1) e^{-\eta\theta\Omega} . \quad (B-21)$$

There are really two integrals to evaluate here. Eq.(B-20) can be rewritten to isolate the two integrals:

$$I = \int dx e^{-i\eta\phi(y,0)} (J_1 + J_2) . \quad (B-22)$$

$J_1$  is given by:

$$\begin{aligned} J_1 &= \int d\Omega F(y,0) e^{-i\eta\theta\Omega} . \\ &= F(y,0) \int d\Omega e^{-i\eta\theta\Omega} . \end{aligned} \quad (B-23)$$

$F(y,0)$  can be taken out of the integral since it has no  $y$  (nor  $\Omega$ ) dependence.

$J_2$  is given by:

$$J_2 = \int d\Omega \Theta F_1 e^{-i\eta\theta\Omega} . \quad (B-24)$$

We will first evaluate  $J_1$ .  $J_1$  produces a band-limited delta function (a sinc function) in the offline variable  $\theta$ :

$$\begin{aligned}
J_1 &= 2\pi F(y,0) \operatorname{sinc}(\eta\theta\Omega) \\
&= 2\pi \frac{F(y,0) \operatorname{sinc} \theta}{|\eta \Omega_{\max}|} .
\end{aligned}
\tag{B-25}$$

$\Omega_{\max}$  is defined by Eq.(B-12) at the point  $y = y_{\max}$ . In order to evaluate the behaviour of  $\Omega_{\max}$  as  $\theta = 0$ , L'Hopital's rule must be used. The result shows that it is nonsingular at  $\theta = 0$ .

$J_2$  can be evaluated by parts. Integrating Eq.(B-24) by parts leads to two terms:

$$J_2 = \frac{\theta F_1 e^{-i\eta\theta\Omega}}{-i\eta\theta} \left[ \begin{array}{c} \Omega_{\max} \\ -\Omega_{\max} \end{array} \right] + \frac{1}{i\eta} \int d\Omega \left[ \frac{\partial F_1}{\partial \Omega} \right] e^{-i\eta\theta\Omega} .
\tag{B-26}$$

Note that the second term is of the form of the original  $J_2$  integral (Eq.(B-24)), but with a  $1/i\eta$  multiplier. Evaluation of this integral gives rise to terms that are of the same form of the two terms of Eq.(B-25). However, the  $1/i\eta$  multiplier insures that those terms will be of lower order, since the evaluation will lead to terms of order  $1/\eta^2$ . We can, therefore, neglect the second term of (Eq.B-26). For a more rigorous justification of this logic, see Bleistein and Handelsman (1967).

With these expressions for  $J_1$  and  $J_2$  Eq.(B-22) becomes:

$$I = \int dx e^{-i\eta\phi(y,0)} \left[ \frac{2\pi F(y,0) \operatorname{sinc}\theta}{\eta |\Omega_{\max}|} + \frac{F_1 e^{-i\eta\theta\Omega}}{-i\eta} \right]. \quad (27)$$

Eq.(B-27) can be evaluated by stationary phase. The result is an explicit functional relationship for the offline contributions in 3D dip moveout.

A detailed study of the offline contributions suggested by Eq.(B-27) is a ripe area for further research.

APPENDIX C:  
STATIONARY PHASE FORMULA

For a derivation of the method of stationary phase see Bleistein (1984) or Bleistein and Handelsman (1986). The method is outlined here. Consider an integral of the form:

$$I(\lambda) = \int_a^b f(x) e^{i\lambda\phi(x)} dx \quad . \quad (C-1)$$

For large  $\lambda$ , the dominant contribution to the integral is at certain critical points ( $x_c$ ) at which the phase,  $\phi(x)$ , is stationary. The condition of stationarity is:

$$\phi'(x_c) = 0 \quad . \quad (C-2)$$

By setting the derivative of the phase equal to zero, critical points ( $x_c$ ) can be found. Then the integral Eq.(C-1) can be approximated by:

$$I_c(\lambda) \sim e^{(i\lambda\phi(x_c) + i\mu\pi/4)} f(x_c) \left[ \frac{2\pi}{\lambda |\phi''(x_c)|} \right]^{1/2} \quad . \quad (C-3)$$

where  $\mu = \text{sgn}(\phi''(x_c))$ .



APPENDIX D:

$$TZO \stackrel{?}{=} NMO + DMO$$

This appendix will prove that the travelttime relationship of Eq.(A-31) is equal to NMO + DMO when  $v_o = v_m$ . The TZO travelttime is:

$$t_{tzo} = \frac{|\xi_g - \xi_s|}{v_m} \left[ 1 + \frac{\left[ \frac{v_o t_o}{2} \right]^2}{(\xi_o - \xi_s)(\xi_g - \xi_o)} \right]^{1/2} \quad (D-1)$$

The NMO + DMO travelttime relationship is commonly expressed in terms of travelttime squared. It is:

$$t_{dmo}^2 = t_o'^2 + \frac{4h^2}{v_m^2} - \frac{4h^2 \sin^2 \theta}{v_m^2} \quad (D-2)$$

Here  $t_{dmo}$  is taken to be the NMO + DMO travelttime. Note that the zero offset travelttime in Eq.(D-1) is  $t_o$ , whereas the zero offset travelttime in Eq.(D-2) is termed  $t_o'$ . They are not the same travelttimes. Eq.(D-1) maps a reflection point to its zero offset equivalent (Fig. D-1).  $t_o$  is the zero offset travelttime at the reflection point. Equation (D-2) also maps reflection points to their zero offset equivalent, but the frame of reference is the midpoint.  $t_o'$  is the zero offset travelttime at the midpoint.

Since NMO + DMO makes no distinction between the migration velocity and zero offset velocity, the single velocity  $v_m$  appears in Eq.(D-2).

In order to reconcile Eq.(D-1) and Eq.(D-2), they must be expressed in common variables. The shot and geophone coordinates ( $\xi_s$  and  $\xi_g$ ) can be expressed in midpoint, half-offset coordinates:

$$\begin{aligned}\xi_s &= m - h \\ \xi_g &= m + h\end{aligned}\quad (D-3)$$

Here the origin is taken to be the intercept of the dipping horizon in Fig. D-1.

Substituting Eq.(D-3) into Eq.(D-1) and squaring gives:

$$t_{tzo}^2 = \frac{4h^2}{v_m^2} \left[ 1 + \frac{\left[ \frac{v_o t_o}{2} \right]^2}{h^2 - (\xi_o - m)^2} \right] \quad (D-4)$$

Appendix E shows that the zero offset point,  $\xi_o$ , is equal to:

$$\xi_o = \frac{\xi_s \xi_g}{m} = \frac{m^2 - h^2}{m} \quad (D-5)$$

Then, referring to Fig. D-1,  $(v_o t_o / 2)$  can be given in terms of  $\sin\theta$ ,  $m$ , and  $h$ :

$$\rho_o = \xi_o \sin\theta \quad (D-6)$$

or

$$\left[ \frac{v_o t_o}{2} \right] = \left[ \frac{m^2 - h^2}{m} \right] \sin\theta \quad (D-7)$$

With these substitutions, Eq.(D-4) becomes:

$$t_{tzo}^2 = \frac{4h^2}{v_m^2} + \frac{4\sin^2\theta}{v_m^2} (m^2 - h^2) \quad (D-8)$$

Now the quantities  $t_{dmo}^2$  and  $t_{tzo}^2$  are expressed in terms of common variables.

Comparing Eq. D-8 to D-2, we see that  $t_{tzo}^2$  and  $t_{dmo}^2$  are equal if:

$$t_o'^2 = \frac{4m^2 \sin^2\theta}{v_m^2} \quad (D-9)$$

Referring again to Fig. D-2,  $\sin\theta$  can be expressed in terms of  $t_o'$ :

$$\sin\theta = \frac{v_o t_o'}{2m} \quad (D-10)$$

With this substitution, Eq.(D-9) becomes:

$$t_0'^2 = \left[ \frac{v_0}{v_m} \right]^2 t_0'^2 . \quad (D-11)$$

Thus,  $t_{dm0}$  equals  $t_{tz0}$  only when  $v_0$  equals  $v_m$ . For any other choice of  $v_0$  the mappings do not agree.

## APPENDIX E:

### DIP MOVEOUT AS INTERCEPT MAPPING

The TZO procedure maps offset specular reflections to zero offset specular reflections. This is a combination of NMO and DMO which maps directly to zero offset. Fig. E-1 shows the geometry of the mapping for a dipping layer which intercepts the surface at a location  $\xi_i$ . For many applications, it becomes necessary to find the exact location of the specular reflection point,  $\mathbf{x}_s = (x_s, z_s)$ . In particular, in reconciling the TZO phase to the DMO phase (Appendix D), finding this point as an explicit function of  $\xi_s$ ,  $\xi_g$ , and  $\xi_o$  is essential.

To solve for  $\mathbf{x}_s$ , consider a coordinate system with the origin at the intercept of the dipping layer of Fig. E-2. In such a coordinate system, we can express the dipping layer as:

$$z = x \tan\theta \quad . \quad (E-1)$$

Next we drop an image source,  $s = (s_x, s_z)$  by extending a perpendicular line segment across the dipping layer (Fig. E-2). The coordinates of the image source point can be expressed in terms of the surface variables and the dip  $\theta$ :

$$s_x = \xi_s - 2(\xi_s \sin\theta) = \xi_s (1 - 2\sin^2\theta) \quad (E-2)$$

$$s_z = 2\xi_s \sin\theta \cos\theta \quad .$$

The line from the image source,  $s$ , to the receiver  $\xi_g$  is given by:

$$z = s_z - (x - s_x) \tan\gamma \quad . \quad (E-3)$$

$\gamma$  is the dip of the line connecting the image source  $s$  with the receiver  $\xi_g$ :

$$\tan\gamma = \frac{s_z}{\xi_g - s_x} \quad . \quad (E-4)$$

Now we know that the two lines intersect at the specular reflection point  $x$ . That is, the  $z$  values from the equations for each line are equal:

$$s_z - (x - s_x) \tan\gamma = x \tan\theta \quad . \quad (E-5)$$

Solving for  $x$  gives

$$x_s = \frac{s_z + s_x \tan\gamma}{\tan\theta + \tan\gamma} \quad . \quad (E-6)$$

Then eliminating  $\tan\gamma$  from the above equation and substituting the relationships (Eq.(E-2)) for the points  $s_x$  and  $s_z$  leads to the desired end:

$$x_s = \frac{\xi_s \xi_g \cos^2 \theta}{h + \xi_s} \tag{E-7}$$

$$z_s = \frac{\xi_s \xi_g \sin \theta \cos \theta}{h + \xi_s}$$

where  $h$  is defined to be the half offset:

$$h = \frac{\xi_g - \xi_s}{2} . \tag{E-8}$$

Now we have the coordinates of the specular expressed in terms of the shot and receiver positions,  $\xi_s$  and  $\xi_g$ , and the dip  $\theta$ . It is peculiar that the coordinates of the specular point are not expressed as functions of the zero offset point  $\xi_0$ . Referring again to Fig. E-2 we can use the above relationships to solve for  $\xi_0$ :

$$\xi_0 = \frac{\xi_s \xi_g}{m} . \tag{E-9}$$

Here  $m$  is the midpoint between  $\xi_s$  and  $\xi_g$ . Equation (E-9) tells us that specular reflections from every bed (all dips  $\theta$ ) intersecting the surface at a given location have a zero offset mapping to the same surface point.

We can turn this problem on its head by taking Eq.(E-9) and transforming to a more general coordinate frame not centered at the intercept of the beds. That is, we let the (now unknown) intercept be

given by  $\xi_i$  and transform Eq.(E-9) to become:

$$(\xi_0 - \xi_i) = \frac{\xi_s - \xi_i)(\xi_g - \xi_i)}{(m - \xi_i)} . \quad (E-10)$$

Then solving for the intercept  $\xi_i$  we have:

$$\xi_i = m + \frac{h^2}{\Delta x} . \quad (E-11)$$

Here  $h$  is the half offset,  $m$  is the midpoint, and  $\Delta x$  is the distance from the midpoint,  $m - \xi_0$ . Now note that the intercept as given by Eq.(E-11) is not a function of the dip  $\theta$ . All dips map to the same intercept for a given output location  $\xi_0$  and given  $\xi_s$  and  $\xi_g$ .

The impulse response of TZO and DMO is an intercept mapping. The position along the impulse response determines the intercept of the reflector, and all reflectors with a common intercept map to the same trace on the TZO and DMO impulse responses.

This result is useful in reconciling the phases of TZO and DMO in order to demonstrate that TZO is, indeed, NMO + DMO (Appendix D).

APPENDIX F:  
LIMITS TO INTEGRATION

As a practical matter, one might occasionally wish to limit the TZO integration range to correspond to a known dip limitation in the recorded data. The mapping as defined by the TZO formula (i.e., Eq. (A-30) defines an integral over receivers,  $\xi_g$ , corresponding to a particular output location  $\xi_o$ . This integral will map all dips from +90 degrees to -90 degrees.

To limit the integration to a finite dip range consider Fig. F-1, which shows a particular zero offset location and a candidate shot/receiver pair. The length of the one way zero offset vector is  $\rho_o = v_o t_o / 2$ . This vector will be perpendicular to the reflecting bed. Referring to the figure, one can see that the sine of the dip angle is given by:

$$\sin \theta = \frac{(\xi_o - x_c)}{\rho_o} = \frac{(\xi_o - x_c)}{(v_o t_o / 2)} \quad . \quad (F-1)$$

Appendix A, Eq.(A-25) gives an expression for the location of the reflection point,  $x_c$ :

$$x_c = \xi_0 + \frac{\left[ \frac{v_0 t_0}{2} \right]^2 \left[ \xi_g + \xi_s - 2\xi_0 \right]}{2 \left[ \xi_s - \xi_0 \right] \left[ \xi_g - \xi_0 \right]} \quad (F-2)$$

Therefore, substituting Eq. (F-2) into Eq. (F-1) gives an expression for  $\sin\theta$ :

$$\sin \theta = \frac{\left[ \frac{v_0 t_0}{2} \right]^2 \left[ \xi_g + \xi_s - 2\xi_0 \right]}{2 \left[ \xi_s - \xi_0 \right] \left[ \xi_g - \xi_0 \right]} \quad (F-3)$$

Equation (F-3) states that for a fixed  $\xi_0$ ,  $\xi_s$ , and  $\xi_g$ , as time increases the quantity  $\sin\theta$  increases. In other words, reflecting horizons with increasing dips (i.e., increasing  $\sin\theta$ ) are mapped to that location. Fixing the maximum dip angle limits the maximum output time which need be processed at that particular zero offset location (again with  $\xi_s$  and  $\xi_g$  held fixed).

This maximum output time is given by

$$t_{\max} = - \frac{4(\xi_s - \xi_0) (\xi_0 - \xi_g) \sin \theta}{v_0 (\xi_g + \xi_s - 2\xi_0)} \quad (F-4)$$

Equation (F-4) defines the limits of the integration. As each trace is reading (i.e., each trace corresponds to a fixed  $\xi_s$  and  $\xi_g$ ) it

is mapped to all the zero offset traces to which it contributes. At each zero offset location  $\xi_0$ , Eq.(F-4) defines the maximum output time as a function of the given dip limitations.

Note that in order to be consistent with the sign notation of Eq. (F-1), dips to the left of the midpoint (i.e., beds dipping down to the right in Fig. F-1 are defined to be positive angles. Dips to the right of the midpoint (beds dipping down to the left are defined to be negative angles. This convention insures that  $t_{\max}$  is always a positive quantity.



APPENDIX G:

CALCULATION OF DETERMINANT h - 2.5D COMMON SHOT

The 2.5D derivation of the TZO formula (i.e., Appendix A and B) involves the evaluation of the determinant h. This determinant arises from the Jacobian of a change of variables originally suggested by Gregory Beylkin (see Beylkin, 1985, for details). For the purposes herein, it suffices to note that this determinant allows one to develop inversion formulas for a variety of acquisition geometries. The form of h is:

$$h(x, \xi) = \det \begin{bmatrix} \nabla\tau_s + \nabla\tau_g \\ \frac{\partial}{\partial \xi_1} (\nabla\tau_s + \nabla\tau_g) \\ \frac{\partial}{\partial \xi_2} (\nabla\tau_s + \nabla\tau_g) \end{bmatrix} . \quad (G-1)$$

In the notation, the lower case h will represent the determinant. The upper case H will represent the matrix.

This appendix deals with 2.5D common shot geometry. That is, the acquisition is along parallel lines of data. Only the  $\xi_1$  coordinate of the source is fixed. The  $\xi_2$  shot coordinate varies together with the  $\xi_2$  receiver coordinate, consistent with the geometry of parallel lines of recorded data. In this scenario,  $\tau_s$  and  $\tau_g$  in a constant velocity earth are given by:

$$\tau_s = \frac{\rho_s}{v_m} = \frac{1}{v_m} \sqrt{(x-\xi_{s1})^2 + (y-\xi_2)^2 + z^2} \quad (G-2)$$

$$\tau_g = \frac{\rho_s}{v_m} = \frac{1}{v_m} \sqrt{(x-\xi_1)^2 + (y-\xi_2)^2 + z^2}$$

Note that  $\xi_1$  and  $\xi_2$  ( $\xi_1 = \xi_{g1}$ ;  $\xi_2 = \xi_{s2} = \xi_{g2}$ ) are variables in this equation. The inline source coordinate,  $\xi_{s1}$ , is held fixed. A consequence of this is that the second row of Eq.(G-1) contains only derivatives of  $\tau_g$ .

For the general case the evaluation of Eq.(G-1) is quite complicated. However, since it is assumed that the earth is 2.5D, the evaluation is made much simpler. Recall that 2.5D implies that, though the earth is three-dimensional, the geology itself is invariant in the  $\xi_2$  direction. Parallel lines of data are identical. This is consistent with recording true dip lines.

This determinant will be evaluated at particular locations for which  $y = \xi_2$ . This arises out of the 2.5D stationary phase evaluation of Appendix A. Knowing this a priori will greatly simplify the analysis of Eq.(G-1).

The  $3 \times 3$  determinant  $h$  can be reduced to a more tractable determinant by multiplying the matrix  $H$  by an auxiliary matrix  $B$ . This is a trick suggested by Norm Bleistein. It takes advantage of the matrix property:

$$\det H \det B = \det(HB)$$

or:

(G-3)

$$\det H = \frac{\det(HB)}{\det B}$$

Thus, one hopes to find a matrix (having a simple determinant) such that the determinant of the product HB is easy to evaluate. Consider the matrix:

$$B = \begin{bmatrix} 1 & 0 & \partial_x \tau_g \\ 0 & 1 & \partial_y \tau_g \\ 0 & 0 & \partial_z \tau_g \end{bmatrix} \quad (G-4)$$

Clearly  $\det B$  is simple. The product HB is:

$$HB = \begin{bmatrix} \partial_x (\tau_s + \tau_g) & \partial_y (\tau_s + \tau_g) & \nabla \tau_g \cdot \nabla \tau_g + \nabla \tau_g \cdot \nabla \tau_s \\ \frac{\partial}{\partial \xi_1} (\partial_x \tau_g) & \frac{\partial}{\partial \xi_1} (\partial_y \tau_g) & \frac{\partial}{\partial \xi_1} (\nabla \tau_s \cdot \nabla \tau_g) \\ \frac{\partial}{\partial \xi_2} \partial_x (\tau_s + \tau_g) & \frac{\partial}{\partial \xi_2} \partial_y (\tau_s + \tau_g) & \frac{\partial}{\partial \xi_2} (\nabla \tau_g \cdot \nabla \tau_g + \nabla \tau_s \cdot \nabla \tau_s) \end{bmatrix} \cdot \quad (G-5)$$

Simplification of the matrix HB comes from recalling the eikonal equation:

$$\nabla\tau \cdot \nabla\tau = \frac{1}{v^2} \quad (G-6)$$

Therefore, Eq.(G-5) can be rewritten with the eikonal equation identity. The dot product,  $\nabla\tau_s \cdot \nabla\tau_g$ , is equal to  $\cos\beta/v^2$ , where  $\cos\beta$  is the angle between the shot and geophone vectors,  $\rho_s$  and  $\rho_g$ .

$$HB = \begin{bmatrix} \frac{\partial}{\partial x} (\tau_s + \tau_g) & \frac{\partial}{\partial y} (\tau_s + \tau_g) & \frac{1}{v^2} (1 + \cos \beta) \\ \frac{\partial}{\partial \xi_1} (\frac{\partial}{\partial x} \tau_g) & \frac{\partial}{\partial \xi_1} (\frac{\partial}{\partial y} \tau_g) & \frac{\partial}{\partial \xi_1} \left[ \frac{1}{v_m^2} \right] \\ \frac{\partial}{\partial \xi_2} \frac{\partial}{\partial x} (\tau_s + \tau_g) & \frac{\partial}{\partial \xi_2} \frac{\partial}{\partial y} (\tau_s + \tau_g) & \frac{\partial}{\partial \xi_2} \left[ \frac{1}{v_m^2} (1 + \cos\beta) \right] \end{bmatrix} \quad (G-7)$$

Clearly the subsurface velocity is not a function of the receiver coordinates,  $\xi_1$  and  $\xi_2$ . The derivatives of velocity with respect to surface location in the third column must be identically zero. Furthermore, in formulating the 2.5D problem, we have assumed that parallel lines of data are identical (i.e., dip lines). Under this assumption,  $\cos \beta$  must also be invariant with respect to the offline source and receiver position,  $\xi_2$ , since the sources and receivers vary together. Then taking advantage of these 2.5D observations, Eq.(G-7) becomes:

$$\text{HB} = \begin{bmatrix} \frac{\partial (\tau_s + \tau_g)}{\partial x} & \frac{\partial (\tau_s + \tau_g)}{\partial y} & \frac{1}{v_m} (1 + \cos \beta) \\ \frac{\partial}{\partial \xi_1} \frac{\partial \tau_g}{\partial x} & \frac{\partial}{\partial \xi_1} \frac{\partial \tau_g}{\partial y} & 0 \\ \frac{\partial}{\partial \xi_2} \frac{\partial (\tau_s + \tau_g)}{\partial x} & \frac{\partial}{\partial \xi_2} \frac{\partial (\tau_s + \tau_g)}{\partial y} & 0 \end{bmatrix} \quad (\text{G-8})$$

dethB has been reduced to the evaluation of a  $2 \times 2$  determinant.

This determinant is given by:

$$\det(\text{HB}) = \frac{1}{v_{ms}} (1 + \cos \beta) \left[ \left[ \frac{\partial}{\partial \xi_1} \frac{\partial \tau_g}{\partial x} \right] \left[ \frac{\partial}{\partial \xi_2} \frac{\partial (\tau_s + \tau_g)}{\partial y} \right] \right. \\
\left. - \left[ \frac{\partial}{\partial \xi_1} \frac{\partial \tau_g}{\partial y} \right] \left[ \frac{\partial}{\partial \xi_2} \frac{\partial (\tau_s + \tau_g)}{\partial x} \right] \right] \quad (\text{G-9})$$

Referring to Eq.(G-2), the particular forms of these partial derivatives are:

$$\frac{\partial}{\partial \xi_1} \partial_x \tau_g = \frac{1}{v_m} \left[ -\frac{1}{\rho_g} + \frac{(x - \xi_1)^2}{\rho_g^3} \right]$$

$$\frac{\partial}{\partial \xi_2} \partial_y (\tau_s + \tau_g) = \frac{1}{v_m} \left[ -\frac{1}{\rho_s} + \frac{(y - \xi_2)^2}{\rho_s^3} - \frac{1}{\rho_g} + \frac{(y - \xi_2)^2}{\rho_g^3} \right]$$

(G-10)

$$\frac{\partial}{\partial \xi_1} \partial_y \tau_g = \frac{1}{v_m} \left[ \frac{(y - \xi_2)(x - \xi_1)}{\rho_g^3} \right]$$

$$\frac{\partial}{\partial \xi_2} \partial_x (\tau_s + \tau_g) = \frac{1}{v_m} \left[ \frac{(x - \xi_{s1})(y - \xi_2)}{\rho_g^3} \right]$$

Again, the 2.5D geometry can simplify the analysis. The stationary phase condition for the 2.5D analysis dictates that  $y = \xi_2$  (see Appendix A). So all terms involving  $y - \xi_2$  vanish. Eq.(G-10) becomes:

$$\det(\text{HB}) = \frac{1}{v_m^4} (1 + \cos\beta) \left[ \left[ -\frac{1}{\rho_g} + \frac{(x - \xi_1)^2}{\rho_g^3} \right] \right. \\ \left. \left[ -\frac{1}{\rho_s} - \frac{1}{\rho_g} \right] \right] . \quad (\text{G-11})$$

Finally, recognizing that for the 2.5D case:

$$(x - \xi_1)^2 = \rho_g^2 - z^2 \quad (\text{G-12})$$

Equation (G-11) can be factored further:

$$\det(\text{HB}) = -\frac{1}{v_m^4} (1 + \cos\beta) \left[ \frac{1}{\rho_s} + \frac{1}{\rho_g} \right] \\ \left[ -\frac{\rho_g^2}{\rho_g^3} + \frac{\rho_g^2 - z^2}{\rho_g^3} \right] \quad (\text{G-13})$$

or:

$$\det(\text{HB}) = -\frac{z^2}{v_m^4 \rho_g^3} (1 + \cos\beta) \left[ \frac{1}{\rho_s} + \frac{1}{\rho_g} \right] . \quad (\text{G-14})$$

Now all that remains is to divide  $\det(\text{HB})$  to give  $\det H$ .  $\det B$  is trivial:

$$\det B = \partial_z \tau_g = \frac{1}{v_m} \frac{z}{\rho_g} . \quad (\text{G-15})$$

Therefore, the detH consistent with the 2.5D geometry is given by:

$$h(\mathbf{x}, \xi) = - \frac{z}{v_m^3 \rho_g^2} (1 + \cos \beta) \left[ \frac{1}{\rho_s} + \frac{1}{\rho_g} \right] . \quad (\text{G-16})$$

This is the particular form of the determinant appropriate to the derivations of Appendix A.

APPENDIX H:

CALCULATION OF DETERMINANT h - 3D COMMON SHOT

In order to evaluate the integrand for the 3D derivation of Appendix B, a determinant (h) must be evaluated. h arises from a general inversion derivation first suggested by Gregory Beylkin of Schlumberger Research (Beylkin, 1985). h has the form:

$$h(x, \xi) = \det \begin{bmatrix} \nabla\tau_s + \nabla\tau_g \\ \frac{\partial}{\partial \xi_1} (\nabla\tau_s + \nabla\tau_g) \\ \frac{\partial}{\partial \xi_2} (\nabla\tau_s + \nabla\tau_g) \end{bmatrix} . \quad (H-1)$$

The notation here will be to use the lowercase h to represent the determinant and the uppercase H to represent the matrix. Here  $\tau_s$  and  $\tau_g$  in a constant velocity earth are given by:

$$\tau_s = \frac{\rho_s}{v_m} = \frac{1}{v_m} \sqrt{(x-\xi_{s1})^2 + (y-\xi_{s2})^2 + z^2} \quad (H-2)$$

$$\tau_g = \frac{\rho_s}{v_m} = \frac{1}{v_m} \sqrt{(x-\xi_1)^2 + (y-\xi_2)^2 + z^2} .$$

For the general 3D case, h is the determinant of a  $3 \times 3$  matrix. Each column of the matrix contains the respective (x,y,z) spatial components of the indicated quantities. The partial derivatives of the

second and third rows,  $\partial/\partial\xi_1$  and  $\partial/\partial\xi_2$ , are derivatives with respect to the variables of integration of the inversion (Eq.(B-1)). Thus, for common shot inversion,  $\xi_1$  and  $\xi_2$  represent the receiver coordinates on the surface. For common receiver inversion,  $\xi_1$  and  $\xi_2$  represent the source coordinates on the surface. For common offset inversion,  $\xi_1$  and  $\xi_2$  would be the midpoint coordinates on the acquisition surface. In this fashion, a very general inversion formalism can be developed with the specifics of the inversion geometry imbedded in the particular form of the determinant  $h$ .

For the 3D common shot geometry the coordinates  $\xi_1$  and  $\xi_2$  will be the two receiver coordinates on the acquisition surface. By definition, a 3D common shot geometry assumes that the source position is fixed. The partial derivatives of the second and third rows will involve only the receiver traveltime (i.e., for a given point  $\mathbf{x} = (x,y,z)$  the traveltime from source to  $\mathbf{x}$  is neither a function of  $\xi_1$  nor  $\xi_2$ ).

The particular common shot form of  $h_s$  is:

$$h = \det \begin{bmatrix} \nabla\tau_s + \nabla\tau_g \\ \frac{\partial}{\partial\xi_1} (\nabla\tau_g) \\ \frac{\partial}{\partial\xi_2} (\nabla\tau_g) \end{bmatrix} . \quad (H-3)$$

The evaluation of this  $3 \times 3$  determinant is, in general, quite complicated. However, by taking advantage of a trick suggested by

Norman Bleistein, the evaluation can be greatly simplified. That is, using the same method as in Appendix G, the trick is to find an auxiliary matrix B, which when multiplied by H produces a matrix HB whose determinant is more easily evaluated. In this way one can take advantage of the matrix property:

$$\det (HB) = \det H \det B$$

or:

(H-4)

$$\det H = \frac{\det (HB)}{\det B} .$$

The task, therefore, is to find a matrix B for which the product HB has a determinant which is easily evaluated. Of course, since solving Eq.(H-4) will also involve evaluation of detB, one might hope that detB is simple. Consider the matrix

$$B = \begin{bmatrix} 1 & 0 & \partial_x \tau_g \\ 0 & 1 & \partial_y \tau_g \\ 0 & 0 & \partial_z \tau_g \end{bmatrix} . \quad (H-5)$$

The product HB is:

$$\text{HB} = \begin{bmatrix} \partial_x (\tau_s + t_g) & \partial_y (\tau_s + \tau_g) & \nabla\tau_g \cdot \nabla\tau_g + \nabla\tau_g \cdot \nabla\tau_s \\ \frac{\partial}{\partial \xi_1} (\partial_x \tau_g) & \frac{\partial}{\partial \xi_1} (\partial_y \tau_g) & \frac{\partial}{\partial \xi_1} (\nabla\tau_g \cdot \nabla\tau_g) \\ \frac{\partial}{\partial \xi_2} (\partial_x \tau_g) & \frac{\partial}{\partial \xi_2} (\partial_y \tau_g) & \frac{\partial}{\partial \xi_2} (\nabla\tau_g \cdot \nabla\tau_g) \end{bmatrix} \quad . \quad (\text{H-6})$$

The eikonal equation states that:

$$|\nabla\tau|^2 = \nabla\tau \cdot \nabla\tau = \frac{1}{v_m^2} \quad (\text{H-7})$$

Clearly the sound speed,  $v_m$ , is not a function of the receiver coordinates  $\xi_1$  and  $\xi_2$ . Thus, the partial derivatives in the third column must be zero. Furthermore, the dot products in the first row of the third column can be described as

$$\nabla\tau_g \cdot \nabla\tau_g + \nabla\tau_g \cdot \nabla\tau_s = \frac{1}{v_m^2} (1 + \cos\beta) \quad (\text{H-8})$$

Here,  $\beta$  is taken to be the angle between the shot vector and the receiver vector. Therefore, the matrix product HB can be written as:

$$\text{HB} = \begin{bmatrix} \frac{\partial}{\partial x} (\tau_s + \tau_g) & \frac{\partial}{\partial y} (\tau_s + \tau_g) & \frac{1}{v_m} (1 + \cos \beta) \\ \frac{\partial}{\partial \xi_1} (\frac{\partial}{\partial x} \tau_g) & \frac{\partial}{\partial \xi_1} (\frac{\partial}{\partial y} \tau_g) & 0 \\ \frac{\partial}{\partial \xi_2} (\frac{\partial}{\partial x} \tau_g) & \frac{\partial}{\partial \xi_2} (\frac{\partial}{\partial y} \tau_g) & 0 \end{bmatrix} . \quad (\text{H-9})$$

Although the evaluation of  $\text{dethB}$  is somewhat complicated, the zeros in the third column reduce the problem to the evaluation of a  $2 \times 2$  determinant. This is certainly preferable to the original  $3 \times 3$  determinant.  $\text{dethB}$  has the form:

$$\text{dethB} = \frac{1}{v_m^2} (1 + \cos \beta) \left[ \frac{\partial}{\partial \xi_1} (\frac{\partial}{\partial x} \tau_g) \frac{\partial}{\partial \xi_2} (\frac{\partial}{\partial y} \tau_g) - \frac{\partial}{\partial \xi_1} (\frac{\partial}{\partial y} \tau_g) \frac{\partial}{\partial \xi_2} (\frac{\partial}{\partial x} \tau_g) \right] . \quad (\text{H-10})$$

Referring to Eq.(H-2), the particular form of the derivatives in Eq. (H-10) becomes:

$$\frac{\partial}{\partial \xi_1} \frac{\partial \tau}{\partial x} = \frac{\partial^2 \tau}{\partial \xi_1 \partial x} = -\frac{1}{v_m \rho_g} + \frac{(x-\xi_1)^2}{v_m \rho_g^3}$$

$$\frac{\partial}{\partial \xi_2} \frac{\partial \tau}{\partial x} = \frac{\partial^2 \tau}{\partial \xi_1 \partial x} = +\frac{(x-\xi_1)(y-\xi_2)}{v_m \rho_g^3}$$

(H-11)

$$\frac{\partial}{\partial \xi_1} \frac{\partial \tau}{\partial y} = \frac{\partial^2 \tau}{\partial \xi_1 \partial y} = +\frac{(x-\xi_1)(y-\xi_2)}{v_m \rho_g^3}$$

$$\frac{\partial}{\partial \xi_2} \frac{\partial \tau}{\partial y} = \frac{\partial^2 \tau}{\partial \xi_2 \partial y} = -\frac{1}{v_m \rho_g} + \frac{(y-\xi_2)^2}{v_m \rho_g^3} .$$

Substituting these expressions into Eq. (H-10) gives:

$$\det HB = \frac{1}{v_m^2} (1 + \cos B) \left[ \left[ -\frac{1}{v_m \rho_g} + \frac{(x-\xi_1)^2}{v_m \rho_g^3} \right] \left[ -\frac{1}{v_m \rho_g} + \frac{(y-\xi_2)^2}{v_m \rho_g^3} \right] - \frac{(x-\xi_1)^2 (y-\xi_2)^2}{(v_m \rho_g^3)^2} \right] \quad (H-12)$$

$$= \frac{1}{v_m^2} (1 + \cos \beta) \left[ \frac{1}{v_m^2 \rho_g^2} - \frac{1}{v_m \rho_g} \left[ \frac{(x-\xi_1)^2 + (y-\xi_2)^2}{v_m \rho_g^3} \right] \right],$$

but:

$$(x-\xi_1)^2 + (y-\xi_2)^2 = \rho_g^2 - z^2, \quad (H-13)$$

then:

$$\begin{aligned}
\det HB &= \frac{1}{v_m^2} (1 + \cos \beta) \left[ \frac{1}{v_m^2 \rho_g^2} - \frac{1}{v_m \rho_g} \left[ \frac{\rho_g^2 - z^2}{v_m \rho_g^3} \right] \right] \\
&= \frac{1}{v_m^2} (1 + \cos \beta) \left[ \frac{1}{v_m^2 \rho_g^2} - \frac{\rho_g^2}{v_m \rho_g} \left[ \frac{1 - z^2/\rho_g^2}{v_m \rho_g^3} \right] \right] \quad (H-14) \\
&= \frac{1}{v_m^2} (1 + \cos \beta) \left[ \frac{1}{v_m^2 \rho_g^2} - \frac{1}{v_m^2 \rho_g^2} + \frac{z^2}{v_m^2 \rho_g^4} \right] = \frac{(1 + \cos \beta) z^2}{v_m^4 \rho_g^4} .
\end{aligned}$$

Returning to Eq.(H-6), h can be solved for directly:

$$h = \frac{\det HB}{\det B} \quad (H-15)$$

detB is trivial. It is given by:

$$\det B = \partial_z \tau_g = \frac{z}{v_m \rho_g} (1 + \cos \beta) . \quad (H-16)$$

Therefore, h is:

$$h = \frac{z}{v_m^3 \rho_g^3} (1 + \cos \beta) \quad (H-17)$$

Without the detHB trick, the calculation of h would have been much more involved. A similar trick exists for the calculation of h in the common receiver case. Unfortunately, no such trick exists for calculating h in common offset geometry.

APPENDIX I:

CALCULATION OF DETERMINANT  $h$  - 2.5D COMMON OFFSET

The transformation to zero offset operator (Eq.A-30) may be easily modified to operate in the common offset domain. The only significant modification is the calculation of the determinant  $h$  for common offset. This appendix will detail this calculation for 2.5D geometry.

As before,  $h$  has the form:

$$h = \det \begin{bmatrix} & V(\tau_s + \tau_g) \\ \frac{\partial}{\partial \xi_1} & V(\tau_s + \tau_g) \\ \frac{\partial}{\partial \xi_2} & V(\tau_s + \tau_g) \end{bmatrix} . \quad (I-1)$$

The 2.5D geometry envisioned is one where parallel lines of data are recorded over a subsurface which does not vary in the cross-line direction. Thus, parallel lines of data are identical. The variables  $\xi_1$  and  $\xi_2$  parameterize the midpoints of the common offset data. Since the acquisition is along parallel lines of data, each midpoint coordinate  $\xi = (\xi_1, \xi_2)$  is associated with a shot/geophone pair which share a common  $\xi_2$  coordinate:

$$\begin{aligned}\xi_s &= (\xi_1 - h, \xi_2) \\ \xi_g &= (\xi_1 + h, \xi_2) .\end{aligned}\tag{I-2}$$

With this convention the quantities  $\tau_s$  and  $\tau_g$  are given by:

$$\begin{aligned}\tau_s &= \frac{\rho_s}{v_m} = \frac{1}{v_m} \sqrt{(x-\xi_1+h)^2 + (y-\xi_2)^2 + z^2} \\ \tau_g &= \frac{\rho_g}{v_m} = \frac{1}{v_m} \sqrt{(x-\xi_1-h)^2 + (y-\xi_2)^2 + z^2} .\end{aligned}\tag{I-3}$$

The results of Appendix A tell us that the 2.5D condition of the TZO derivation is that  $y = \xi_2$ . This condition, which is a result of the stationary phase calculations, must be imposed after the evaluation of the various derivatives involved in  $h$ . To impose this condition before evaluating the derivatives would be equivalent to assuming that the condition  $y = \xi_2$  implies that all derivatives with respect to  $y$  and  $\xi_2$  are zero. This is not true.

We will evaluate the derivatives of  $h$  one row at a time. The derivatives of the first row are the components of the gradient:

$$\begin{aligned} \frac{\partial}{\partial x} (\tau_s + \tau_g) &= \frac{1}{v_m} \left[ \frac{x - \xi_1 + h}{\rho_s} + \frac{x - \xi_1 - h}{\rho_g} \right] \\ \frac{\partial}{\partial y} (\tau_s + \tau_g) &= \frac{(y - \xi_2)}{v_m} \left[ \frac{1}{\rho_s} + \frac{1}{\rho_g} \right] \\ \frac{\partial}{\partial z} (\tau_s + \tau_g) &= \frac{z}{v_m} \left[ \frac{1}{\rho_s} + \frac{1}{\rho_g} \right] . \end{aligned} \tag{I-4}$$

The derivatives of the second row are the derivatives of the gradient with respect to  $\xi_1$ :

$$\begin{aligned} \frac{\partial^2}{\partial \xi_1 \partial x} (\tau_s + \tau_g) &= \frac{1}{v_m} \left[ -\frac{1}{\rho_s} + \frac{(x - \xi_1 + h)^2}{\rho_s^3} - \frac{1}{\rho_g} + \frac{(x - \xi_1 - h)^2}{\rho_g^3} \right] \\ \frac{\partial^2}{\partial \xi_1 \partial y} (\tau_s + \tau_g) &= \frac{(y - \xi_2)}{v_m} \left[ \frac{x - \xi_1 + h}{\rho_s^3} + \frac{x - \xi_1 - h}{\rho_g^3} \right] \\ \frac{\partial^2}{\partial \xi_1 \partial z} (\tau_s + \tau_g) &= \frac{z}{v_m} \left[ \frac{x - \xi_1 + h}{\rho_s^3} + \frac{x - \xi_1 - h}{\rho_g^3} \right] . \end{aligned} \tag{I-5}$$

The derivatives of the third row are the derivatives of the gradient with respect to  $\xi_2$ :

$$\frac{\partial^2}{\partial \xi_2 \partial x} (\tau_s + \tau_g) = \frac{(y - \xi_2)}{v_m} \left[ \frac{x - \xi_1 + h}{\rho_s^3} + \frac{x - \xi_1 - h}{\rho_g^3} \right]$$

$$\frac{\partial^2}{\partial \xi_2 \partial y} (\tau_s + \tau_g) = \frac{1}{v_m} \left[ -\frac{1}{\rho_s} + \frac{(y - \xi_2)^2}{\rho_s^3} - \frac{1}{\rho_g} + \frac{(y - \xi_2)^2}{\rho_g^3} \right] \quad (I-6)$$

$$\frac{\partial^2}{\partial \xi_2 \partial z} (\tau_s + \tau_g) = \frac{z}{v_m} \left[ \frac{y - \xi_2}{\rho_s^3} + \frac{y - \xi_2}{\rho_g^3} \right] .$$

Now is the appropriate time to use the 2.5D condition,  $y = \xi_2$ . All terms involving the quantity  $(y - \xi_2)$  vanish. Under this condition  $h$  becomes:

$$h = \det \begin{vmatrix} \frac{\partial}{\partial x} (\tau_s + \tau_g) & 0 & \frac{\partial}{\partial z} (\tau_s + \tau_g) \\ \frac{\partial}{\partial \xi_1} \frac{\partial}{\partial x} (\tau_s + \tau_g) & 0 & \frac{\partial}{\partial \xi_1} \frac{\partial}{\partial z} (\tau_s + \tau_g) \\ 0 & \frac{\partial}{\partial \xi_2} \frac{\partial}{\partial y} (\tau_s + \tau_g) & 0 \end{vmatrix} . \quad (I-7)$$

Now the determinant can be evaluated directly:

$$h = \frac{\partial}{\partial \xi_2} \frac{\partial (\tau_s + \tau_g)}{y} \left[ \frac{\partial (\tau_s + \tau_g)}{z} \frac{\partial (\tau_s + \tau_g)}{\partial \xi_1} \frac{\partial (\tau_s + \tau_g)}{\partial x} - \frac{\partial (\tau_s + \tau_g)}{x} \frac{\partial (\tau_s + \tau_g)}{\partial \xi_1} \frac{\partial (\tau_s + \tau_g)}{z} \right] \quad (I-8)$$

Then calling upon the specific form of the derivatives as given by Eq.(I-4) through Eq.(I-6) with  $(y = \xi_2)$ , h is:

$$h = - \frac{1}{v_m} \left[ \frac{1}{\rho_s} + \frac{1}{\rho_g} \right] \left[ \frac{z}{v_m} \left[ \frac{1}{\rho_s} + \frac{1}{\rho_g} \right] \frac{1}{v_m} \left[ - \frac{1}{\rho_s} + \frac{(x-\xi_1+h)^2}{\rho_s^3} - \frac{1}{\rho_g} + \frac{(x-\xi_1-h)^2}{\rho_g^3} \right] - \frac{1}{v_m} \left[ \frac{x-\xi_1+h}{\rho_s} + \frac{x-\xi_1-h}{\rho_g} \right] \cdot \frac{z}{v_m} \left[ \frac{x-\xi_1+h}{\rho_s^3} + \frac{x-\xi_1-h}{\rho_g^3} \right] \right] \quad (I-9)$$

This expression can be simplified to become:

$$h = - \frac{z}{v_m^3} \left[ \frac{1}{\rho_s} + \frac{1}{\rho_g} \right] \left[ \frac{1}{\rho_s^2} + \frac{1}{\rho_g^2} \right] (1 + \cos\beta) \quad (I-10)$$

$\beta$  is the angle between  $\tau_s$  and  $\tau_g$ . It is twice the angle of incidence for a specular reflection.  $\cos\beta$  is given by:

$$\cos\beta = \frac{(x-\xi_1+h)(x-\xi_1-h) + z^2}{\rho_s \rho_g} \quad . \quad (\text{I-11})$$

The amplitudes of the resultant common offset operator are symmetric about the midpoint.

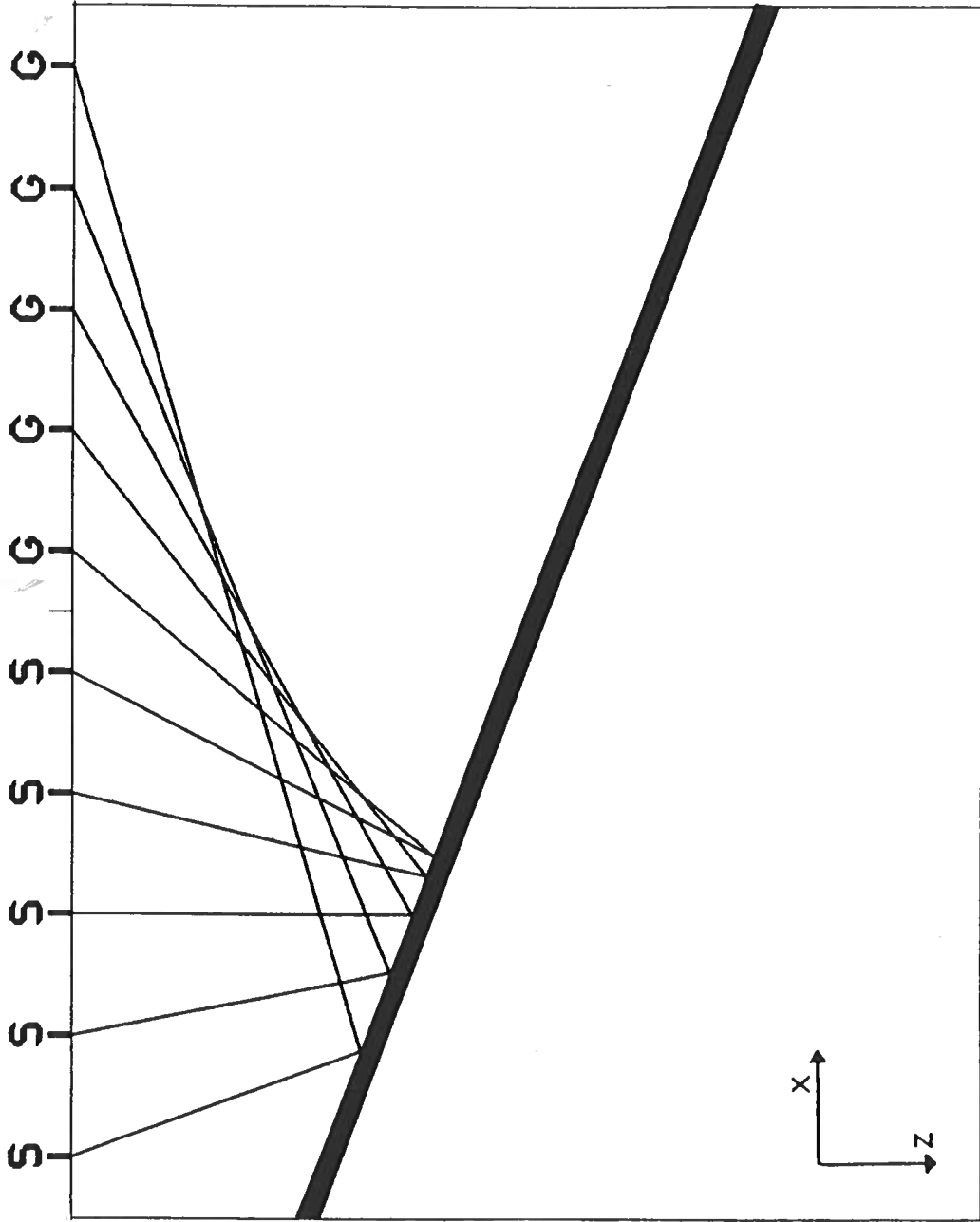
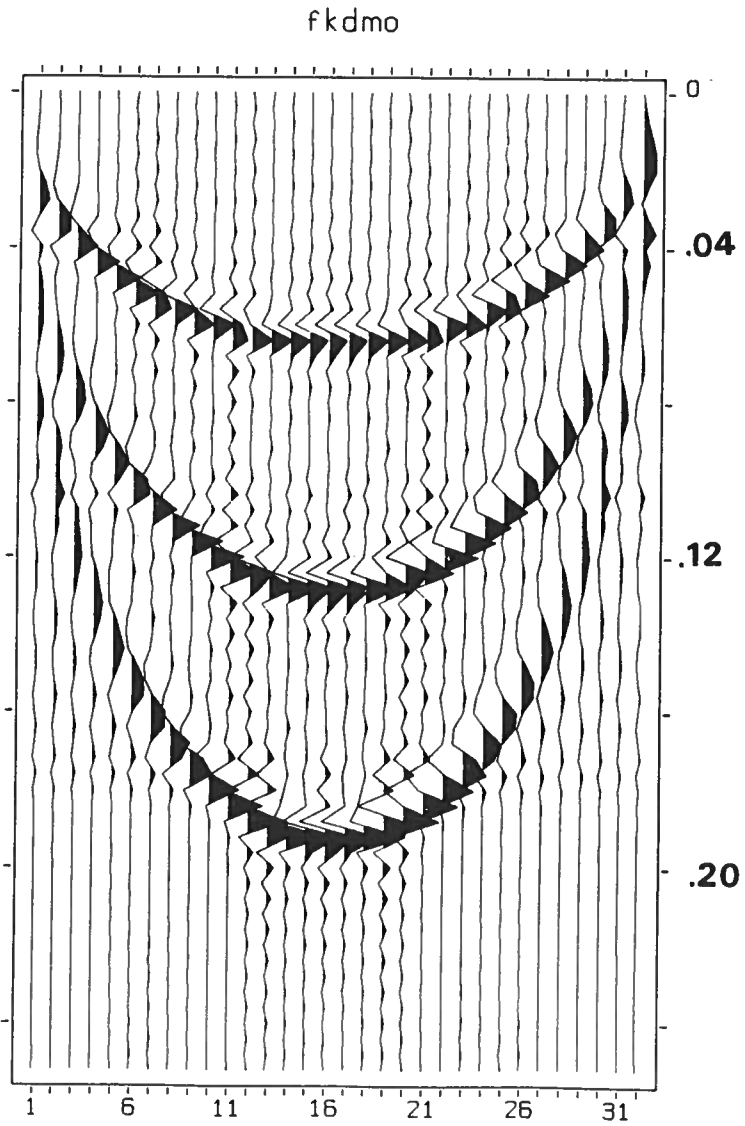


Figure 1.1: Reflector Point Dispersal. Common Midpoint Gather aligns data with different reflection points.



**Figure 1.2: FK DMO Impulse Response. Offset=800ft. Trace Spacing is 25 ft.**

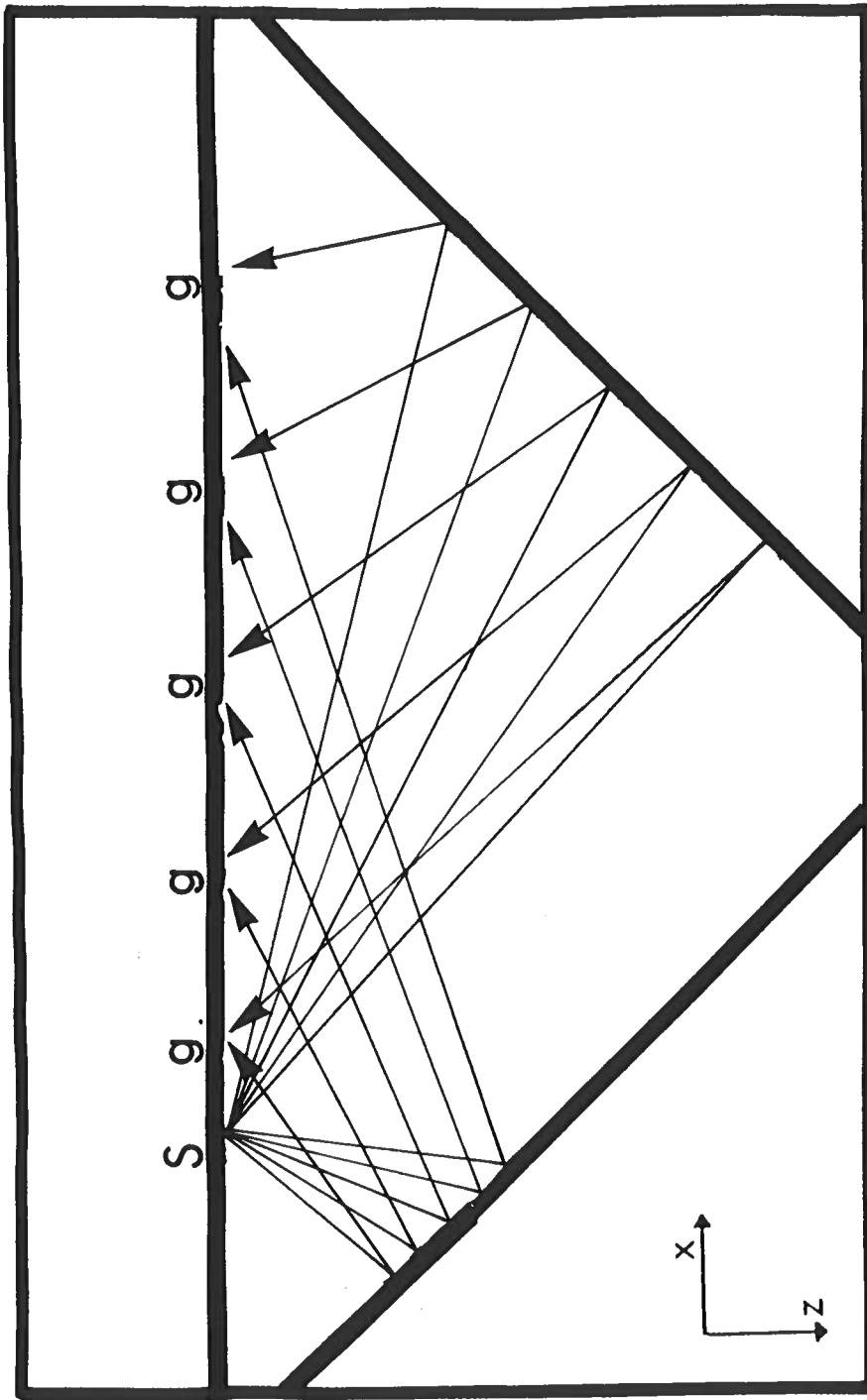
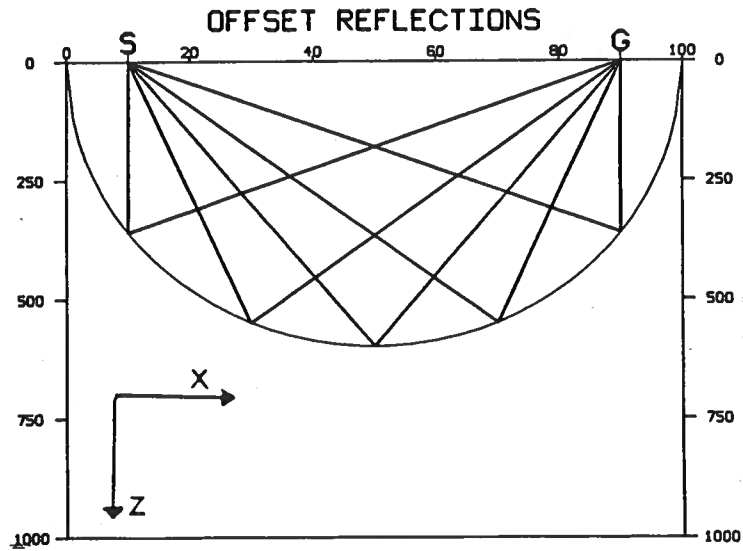
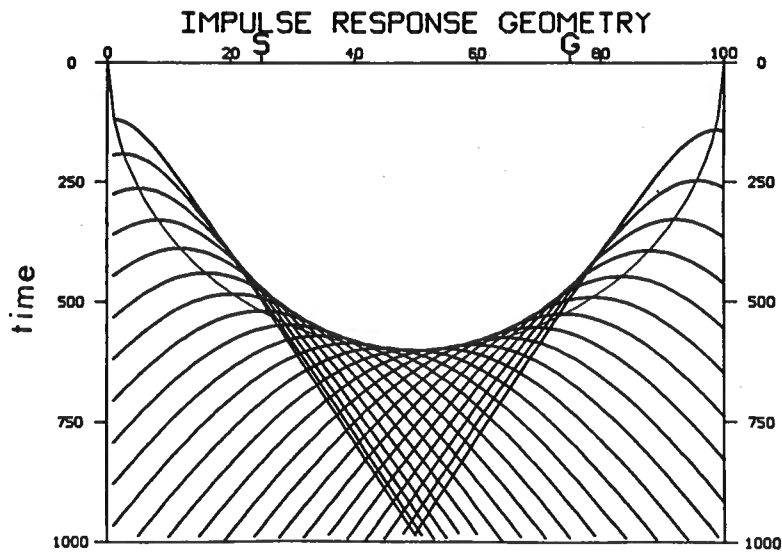


Figure 1.3: Shot Record Raypath Density. The bed dipping to the right receives a higher density of ray coverage than a comparable bed dipping to the left. If this were the only input to an NMO+DMO process, this bias would be mirrored in the zero offset data.



**Figure 1.4: Prestack Migration Ellipse. Every impulse on a seismic trace emanates from a point on an elliptical mirror in the subsurface. Each raypath shown has equal travelttime.**



**Figure 1.4b: Rocca's Smile. The process of transforming data to zero offset is equivalent to a prestack migration followed by a zero offset forward model. Thus, each point of the ellipse becomes a point diffractor. Net curve is the DNO impulse response.**

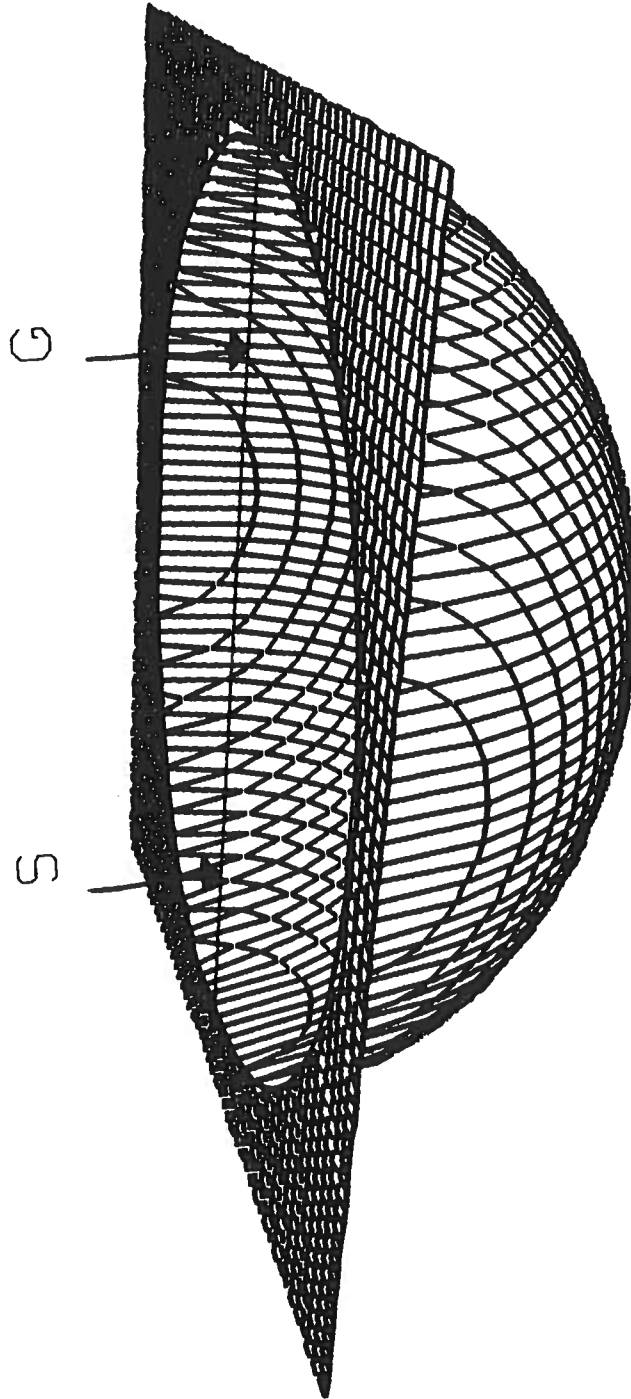
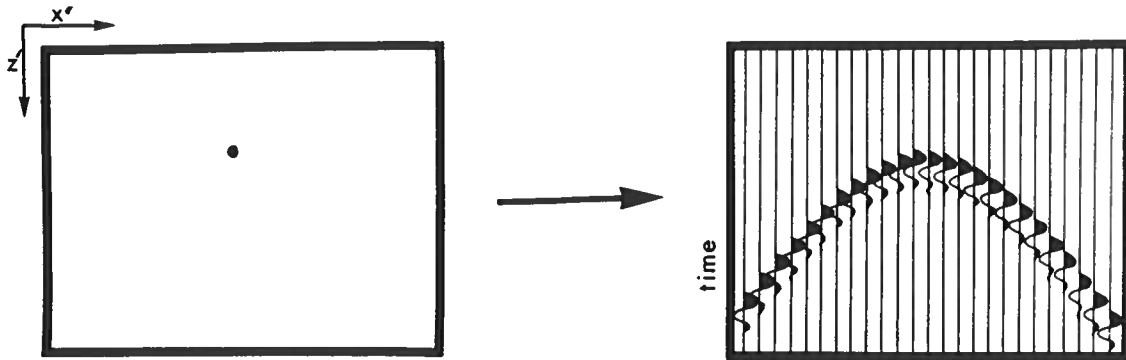
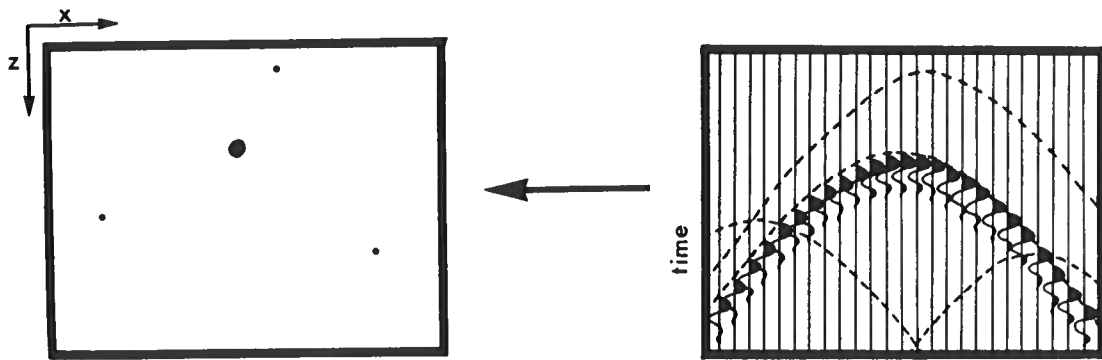


Figure 1.5: 3D Nature of DMO. In three dimensions the prestack migration impulse response is an ellipsoid of revolution. All zero offset reflections from this ellipsoid project to surface locations which lie on the line connecting the shot and geophone.



**Figure 2.1a:** A point diffractor in  $x'$  domain generates a diffraction on a recorded time section.



**Figure 2.1b:** In building the migrated section, each point on the output section  $x$  is assumed to be a source of a point diffractor. Each guess point  $x$  defines a diffraction curve on the time section. With no a priori knowledge of where the actual diffractors are, each guess point is used to define a sum over a test diffraction curve. Only when the guess point  $x$  corresponds to the actual diffraction point  $x'$  is the output of significant amplitude.

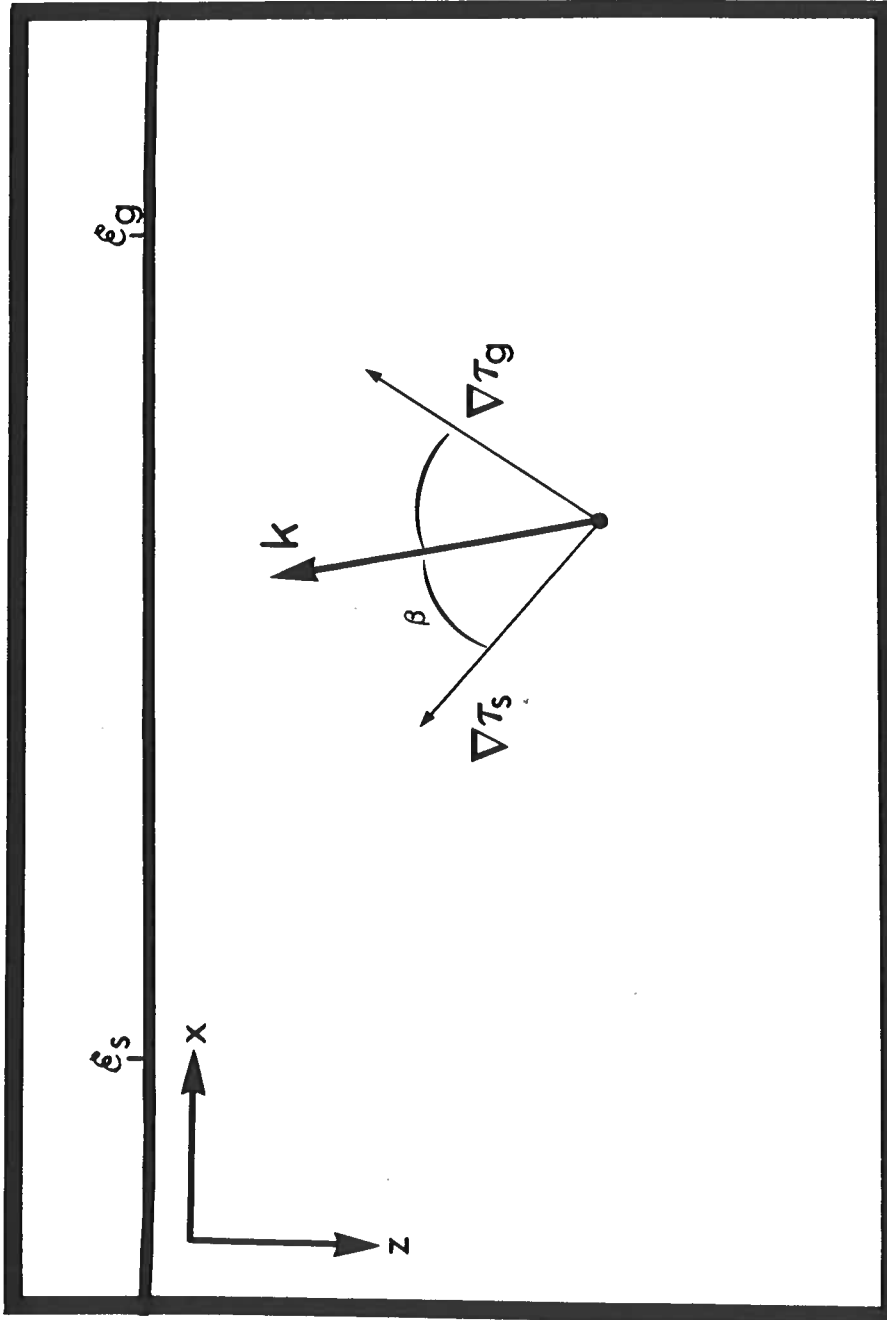


Figure 2.2: The wavevector  $k$  is the scaled sum of the gradient of the phase.  $k = \eta \nabla \phi = \eta (\nabla \tau_s + \nabla \tau_g)$ . The magnitude of  $k$  is a function of the frequency,  $\eta$ , the velocity,  $v$  (since  $|\nabla \tau| = 1/v$ ), and  $\beta$ , the angle between  $\tau_s$  and  $\tau_g$ . (Actual directions of  $\nabla \tau_s$  and  $\nabla \tau_g$  are opposite to those shown - pointing away from the source and receiver. Direction of  $k$  depends on the sign of  $\eta$ ).

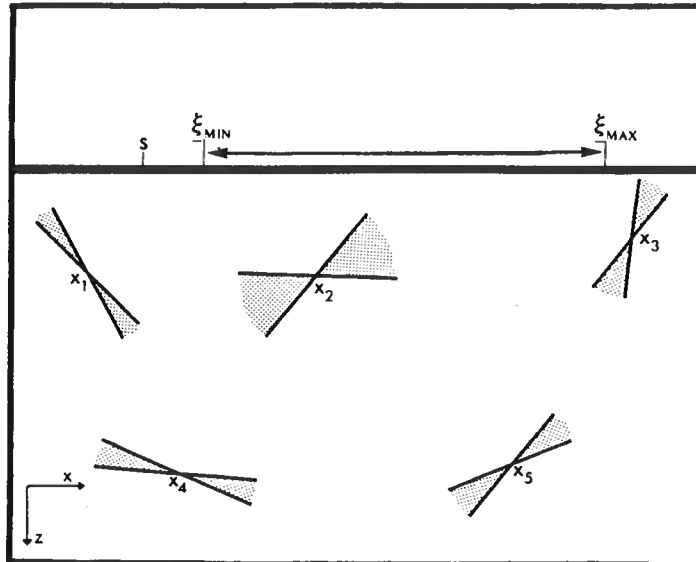


Figure 2.3a: A fixed source,  $s$ , and a receiver spread ( $\xi_{min}$  to  $\xi_{max}$ ) defines a range of dips which can be imaged by the recording aperture. Thus, the shaded regions are the possible dip limits for which the recording geometry can receive reflections.

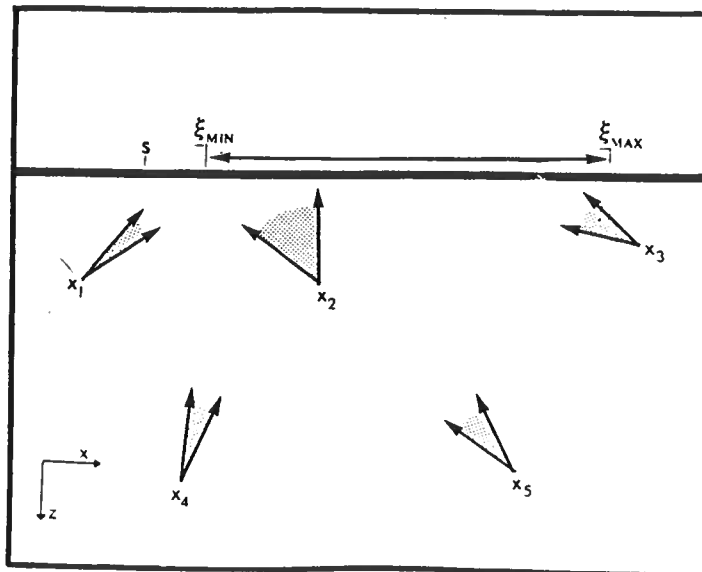


Figure 2.3b: The dip limits in (a) can be translated into limits upon the direction of the wavevector,  $k$ . Since  $k$  bisects the angle between the shot and geophone rays, it is normal to reflecting beds. Thus, the  $k$  coverage shown for various subsurface points is a graphical description of the filtering effect of the recording aperture (after Beylkin, Oristaglio, and Miller (1986)).

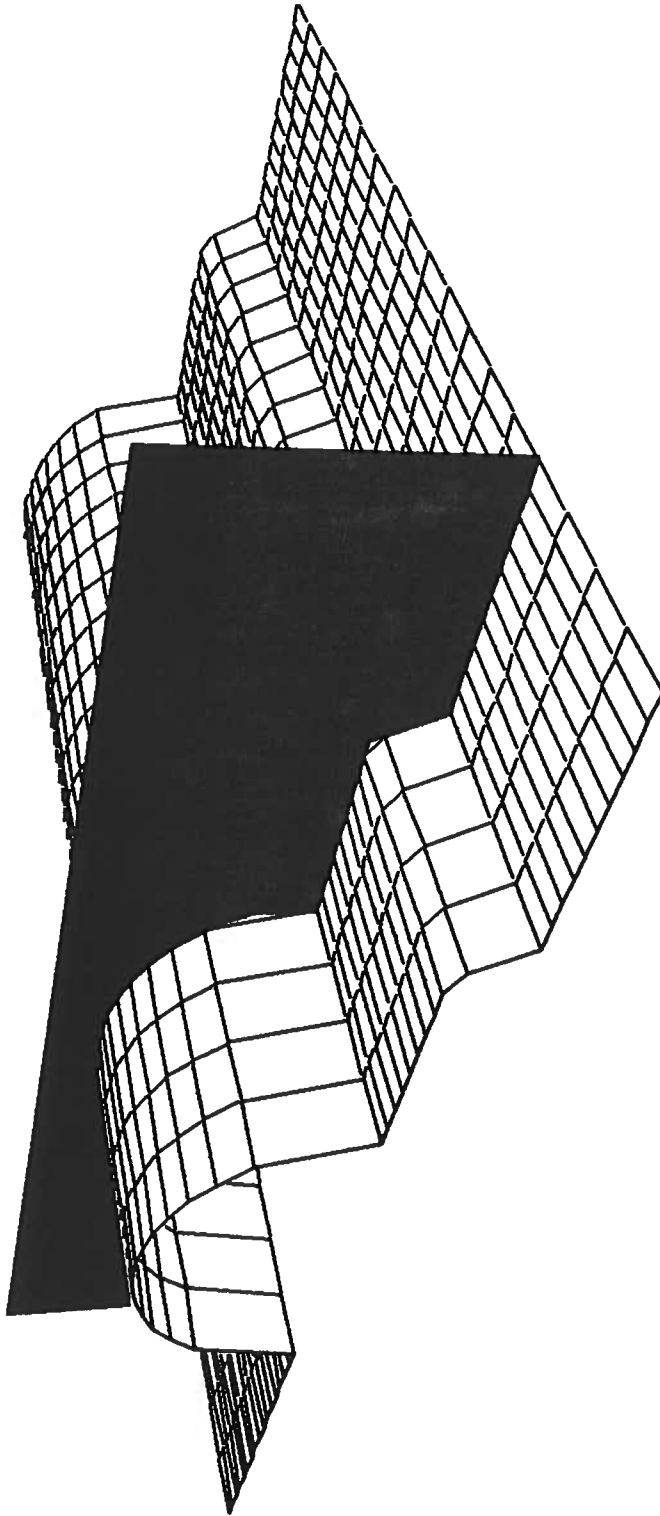
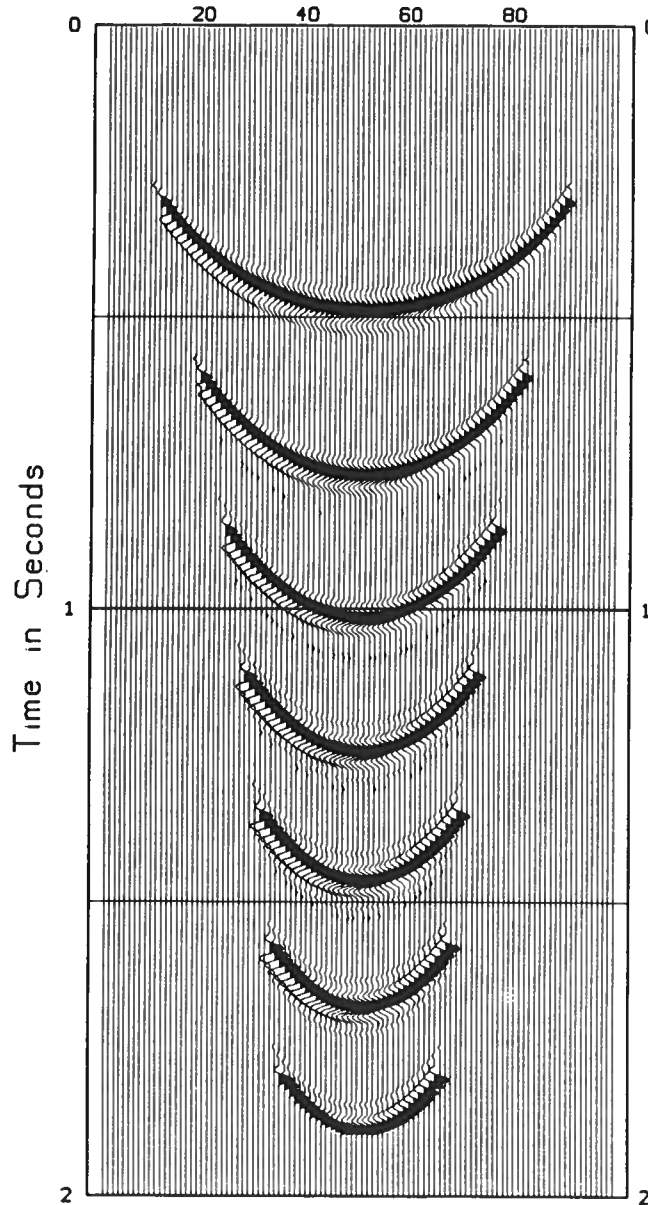
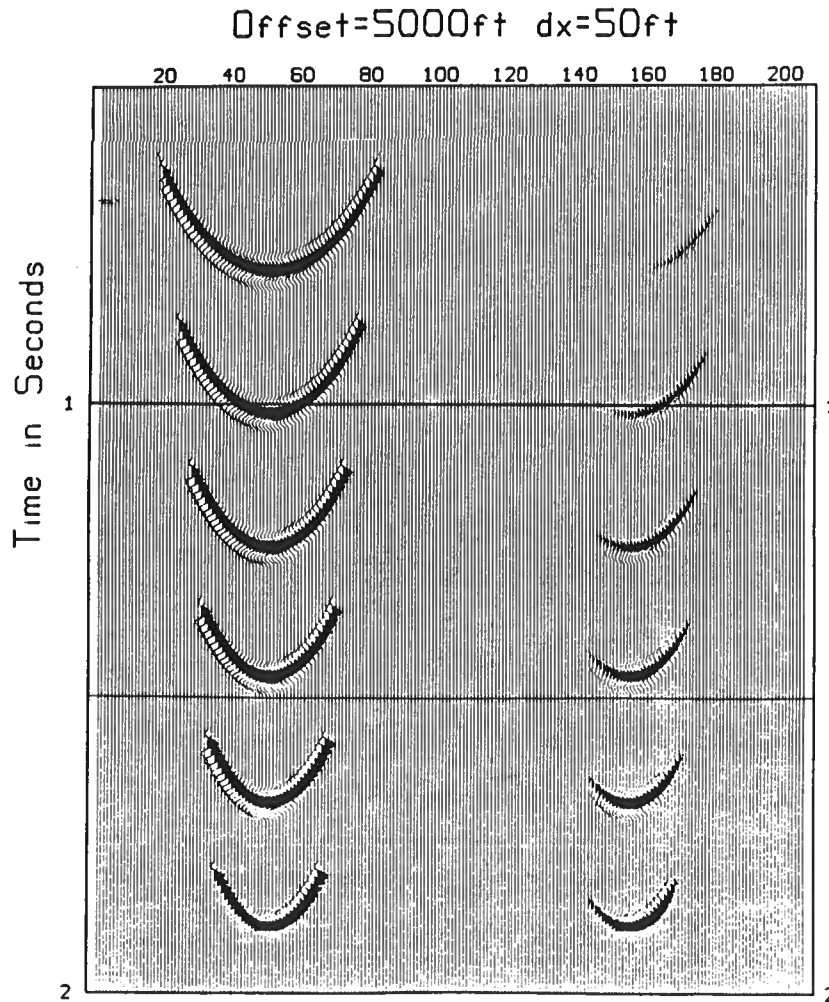


Figure 3.1: 2.5D Geometry. The earth is assumed to be invariant in the off-line direction. Acquisition is along a true dip line. Thus, the wave propagation is three-dimensional in an earth which varies in only two dimensions. The source is a true point source (not a line source). (Figure courtesy of M.F. Sullivan.)

BERG Offset=5000ft dx=50ft



**Figure 3.2:** Berg DMO Impulse Response. The input was seven isolated spikes. The offset is 5000ft, with a trace spacing of 50ft. The velocity is 8000 ft/sec. The velocity is used to truncate the evanescent part of the operator.



**Figure 3.3a: Berg DMO vs TZO Common Shot Operator. The offset equals 5000ft, trace spacing is 50ft, with a velocity of 8000 ft/sec.**

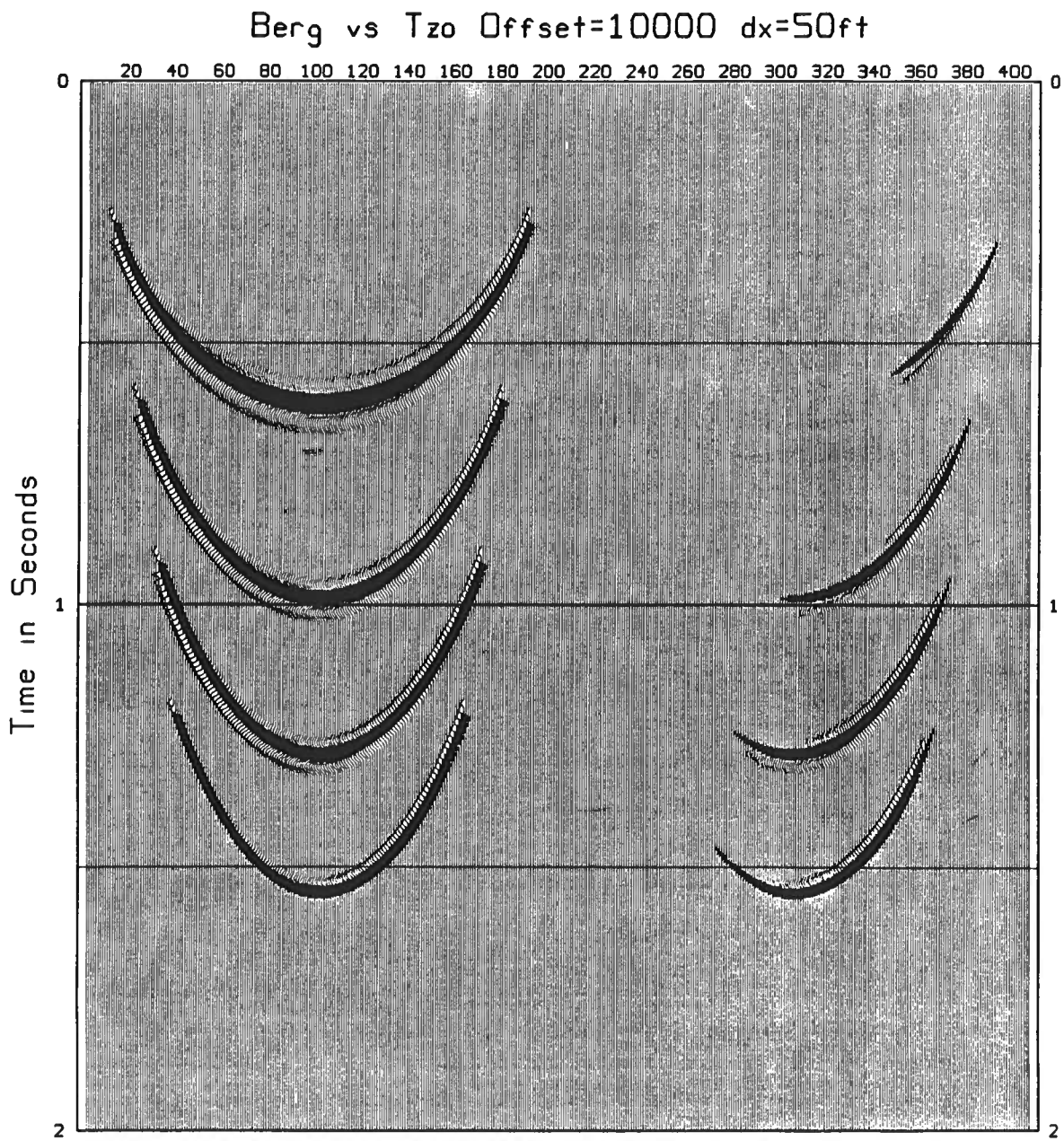


**Figure 3.3b: Berg DND vs TZO Common Shot Operator. The offset equals 10000ft, trace spacing is 50ft, with a velocity of 8000ft/sec.**

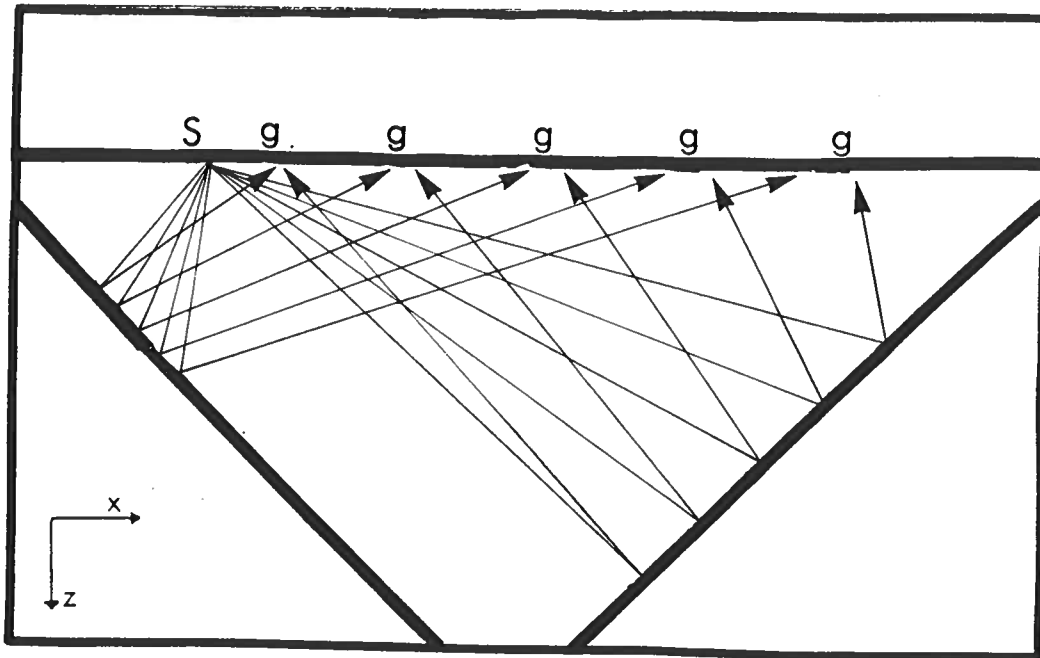


**Figure 3.4:** Shot record showing uneven ray coverage.

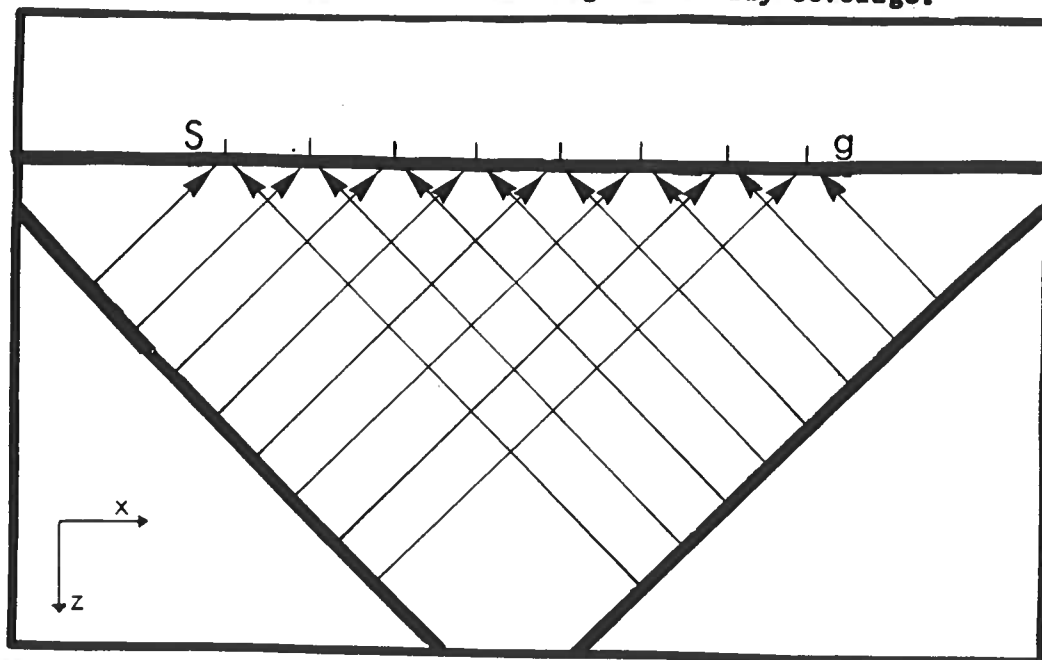


**Figure 3.5:** The process of transforming the data in 3.4 to equivalent zero offset data is a projection of the ray coverage in 3.4 to the zero offset ray coverage. Uneven ray coverage in 3.4 results in zero offset data with higher amplitudes for the bed dipping to the right.

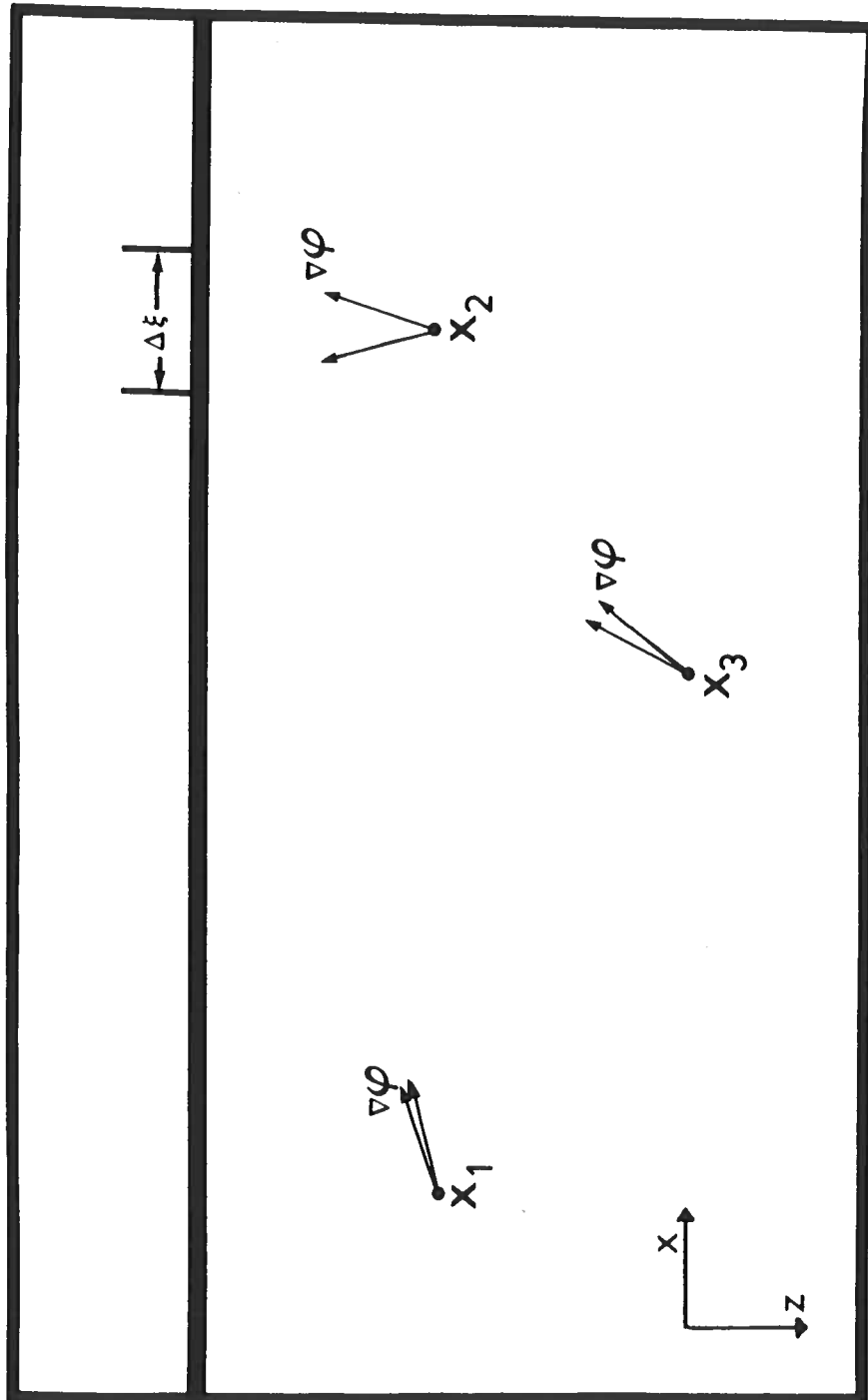
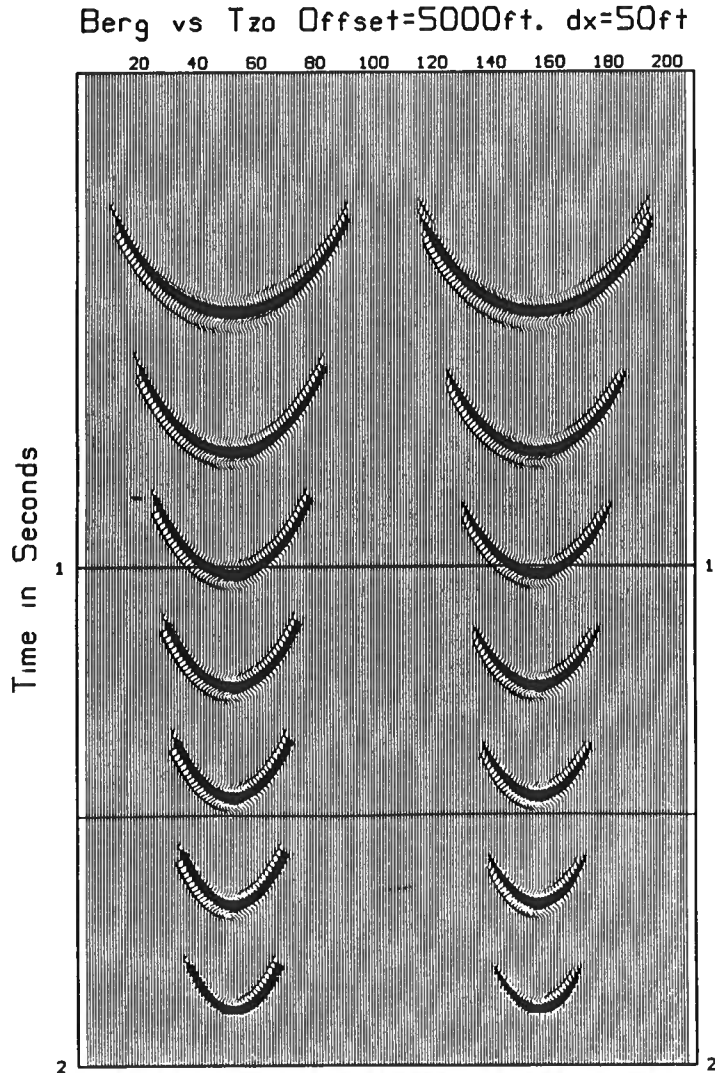


Figure 3.6:  $\partial \nabla \phi / \partial \xi$  as subsurface varies. The determinant  $|h(x, \xi)|$  has magnitude dependent upon the change in the gradient of the phase ( $\nabla \phi$ ) with changing receiver position,  $\xi$ . For a common shot configuration the change in the gradient is shown graphically for several subsurface points. The change in  $\nabla \phi$  is directly related to the ray density. (Actual direction of  $\nabla \phi$  is opposite to that shown - pointing away from the receiver)



**Figure 3.7a: Berg vs TZO Common Offset Impulse Response. Offset is 5000ft, receiver spacing 50ft, and velocity 8000ft. Note that Berg operator truncates abruptly at the edges of the operator (+/- 90 degrees). The TZO operator tapers smoothly to zero. Amplitudes along the limbs are distributed differently (this is clearer in Fig. 3.7b).**

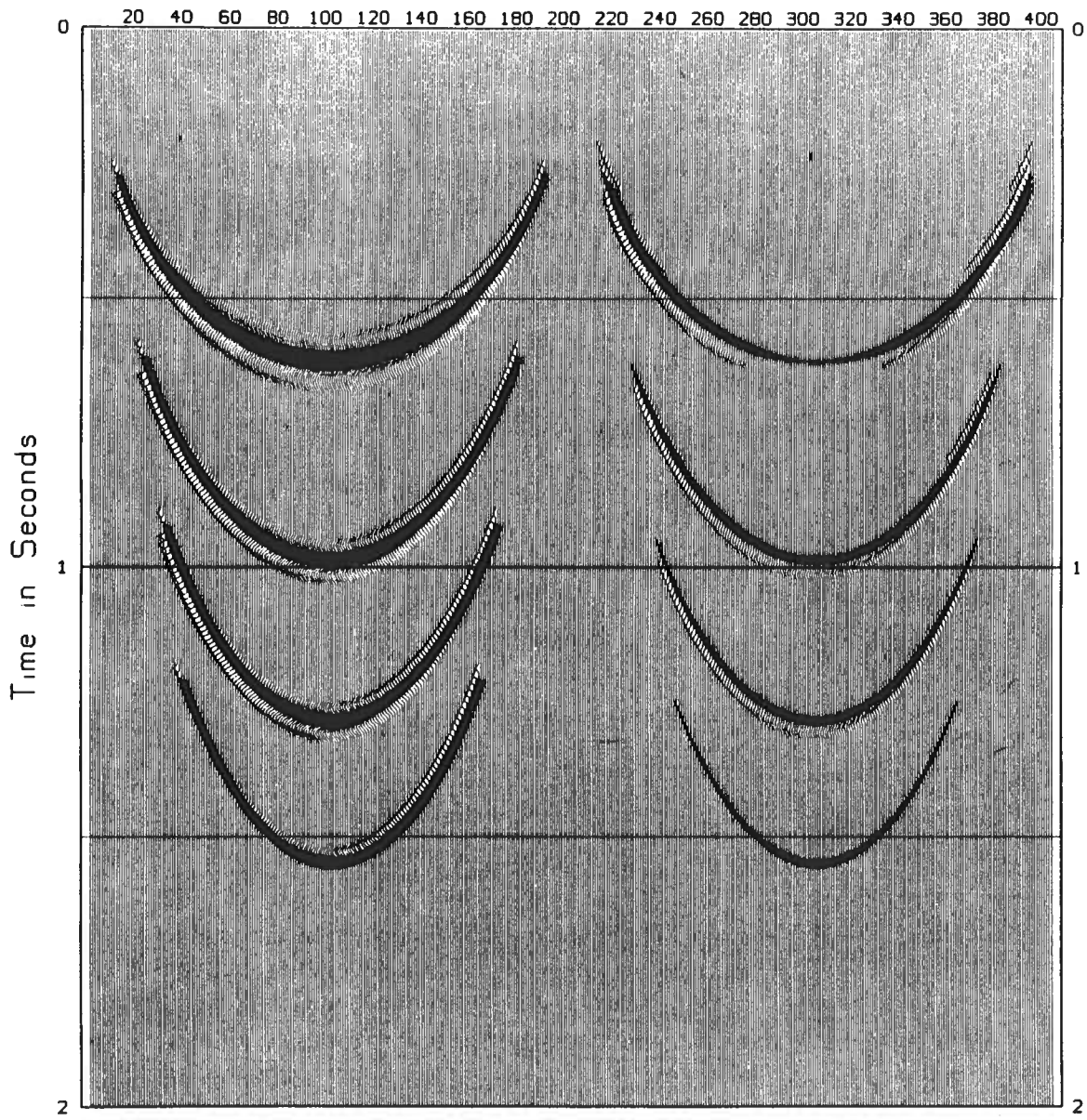


Figure 3.7b: Berg vs TZO Common Offset Impulse Response. Offset is 10000ft, receiver spacing 50ft, and velocity 8000ft. The TZO operator amplitudes increase along the limbs, and then taper smoothly to zero. These amplitudes are dictated by the behaviour of  $|h(x,\xi)|$ .

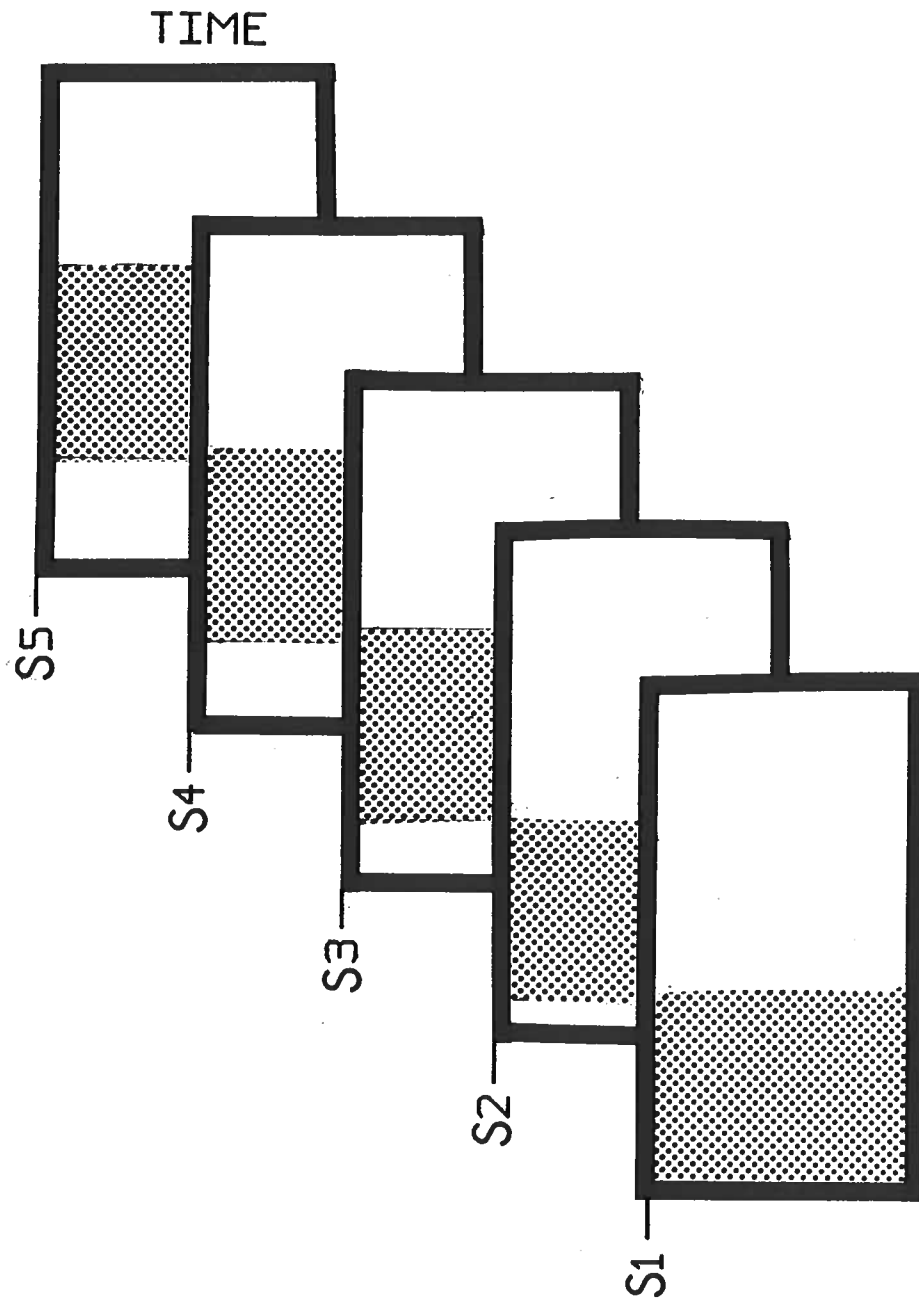


Figure 3.8: Domain of Influence of various shot records. Each shot can be pictured at the left of shaded region; the far offset at the right of shaded region. The shaded zone is the domain of zero offset traces affected by each shot.

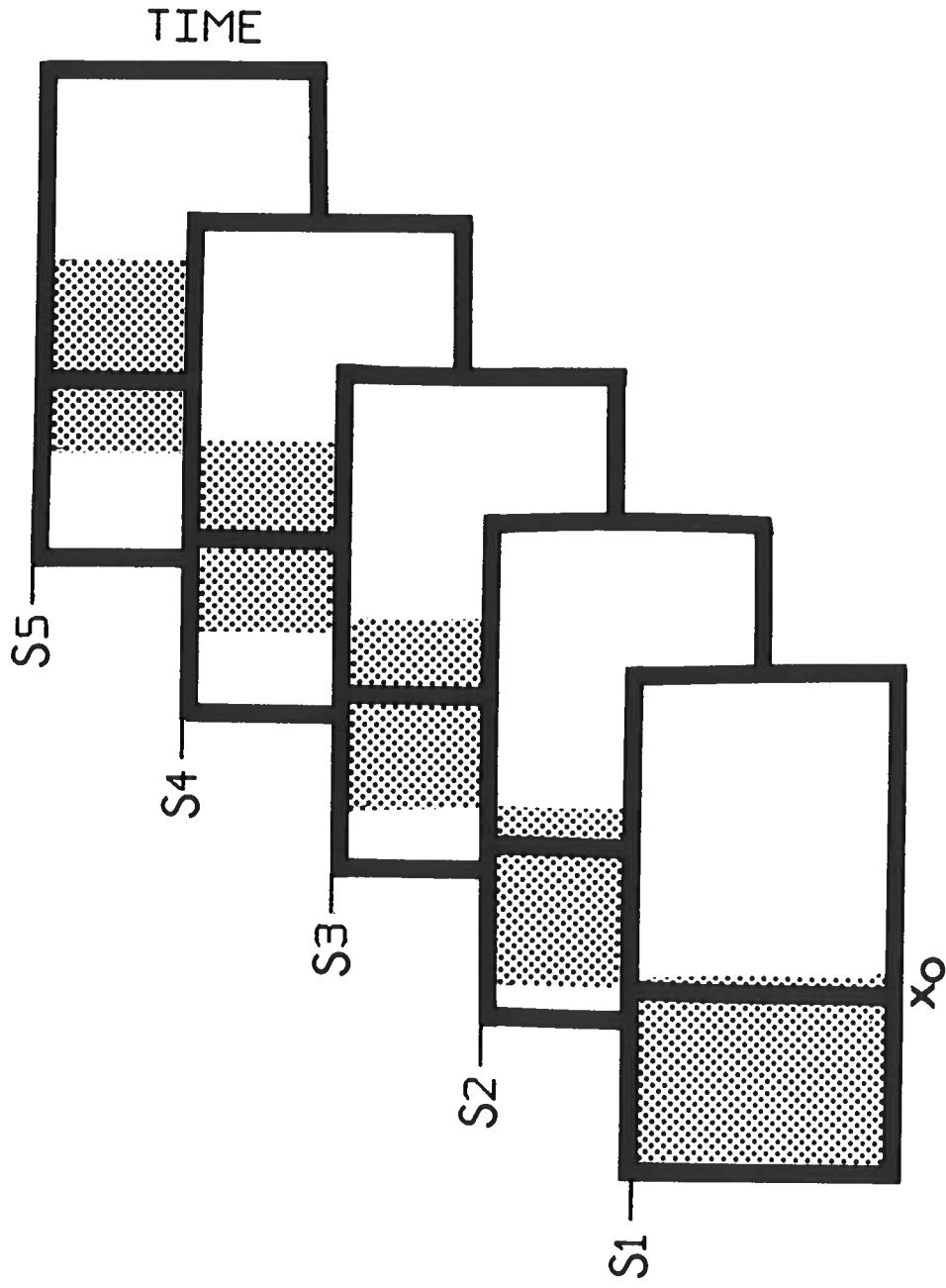
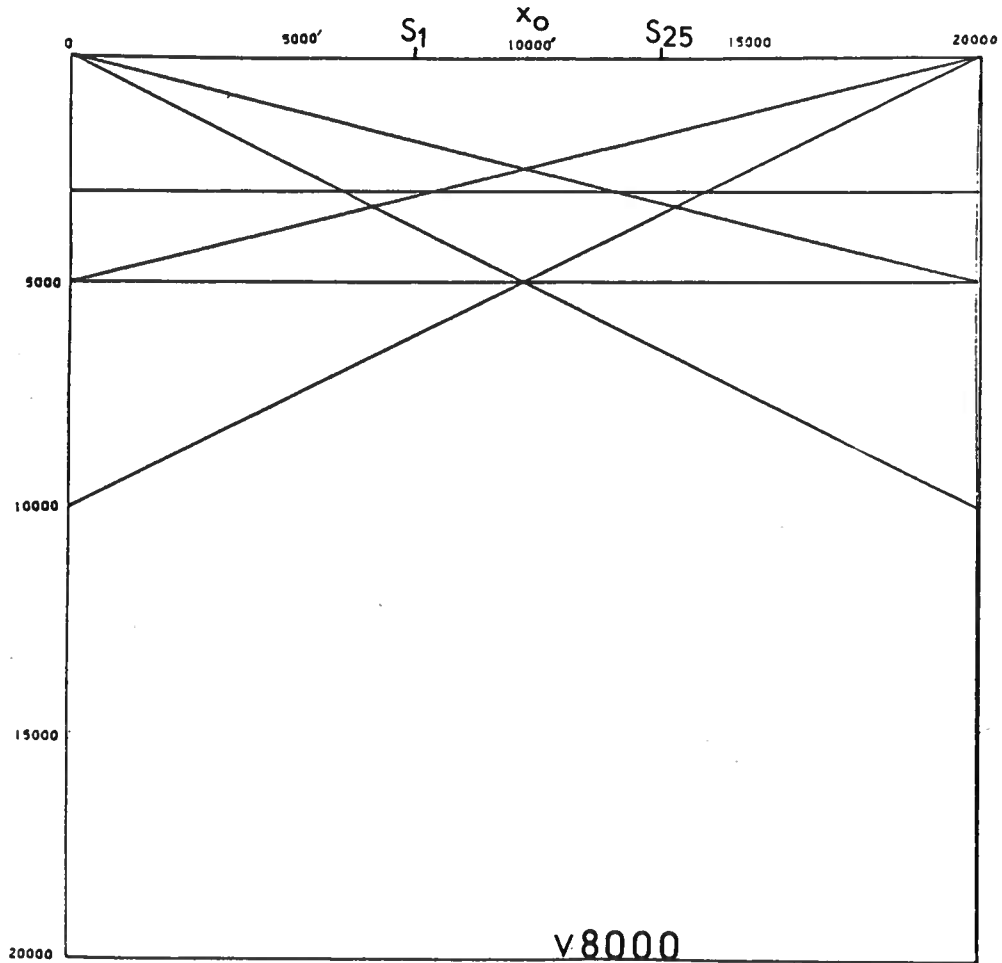


Figure 3.9: Schematic of velocity analysis. The location  $x_0$  receives a contribution from each of the 5 shots. Only when the velocity is correct should the traces generated from each shot be identical.



**Figure 3.10: Synthetic Model. 25 split spread records were generated. Geometry is 96 channel split spread, with near offset equal to 100ft, and far offset equal to 4800ft. First shot is at location marked  $S_1$ . Last shot is at  $S_{25}$ . Data were 4ms, with a 2.0 sec recording. Modeling algorithm is a constant velocity Kirchhoff integral code written by the author.**

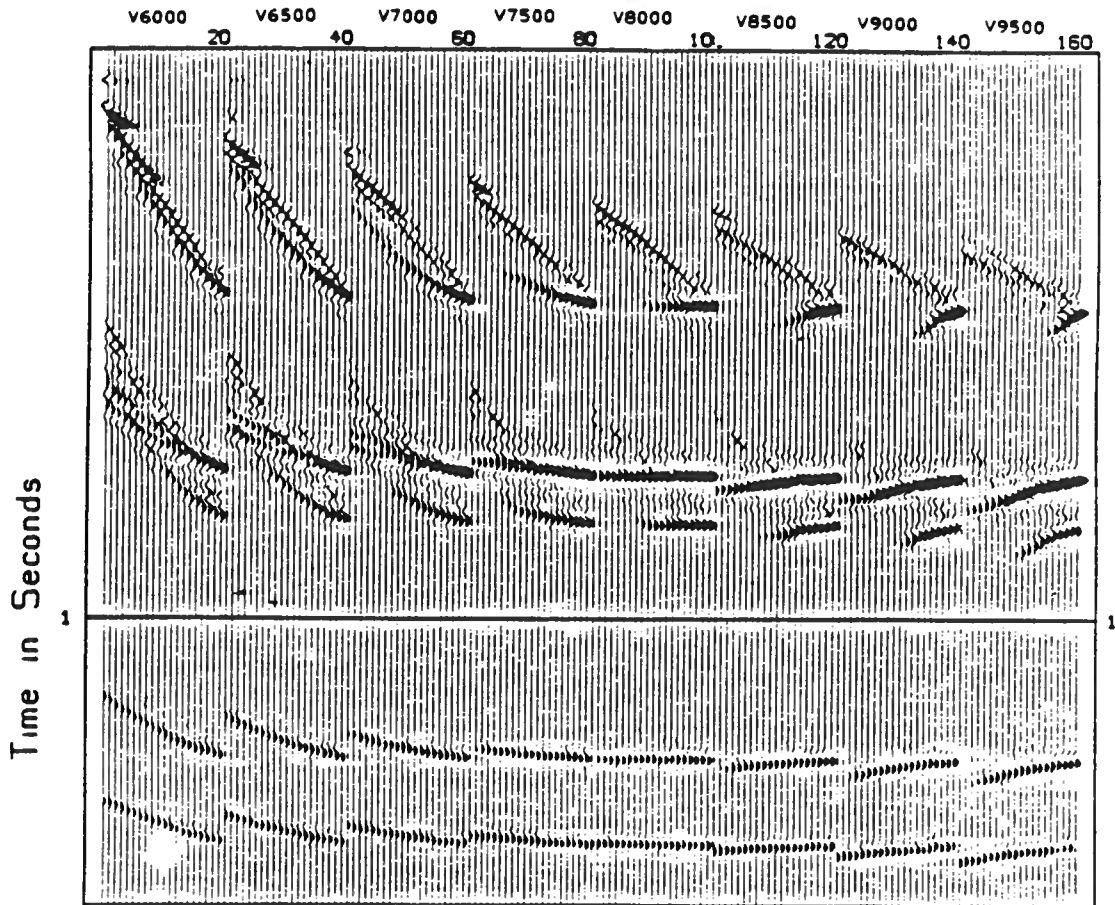
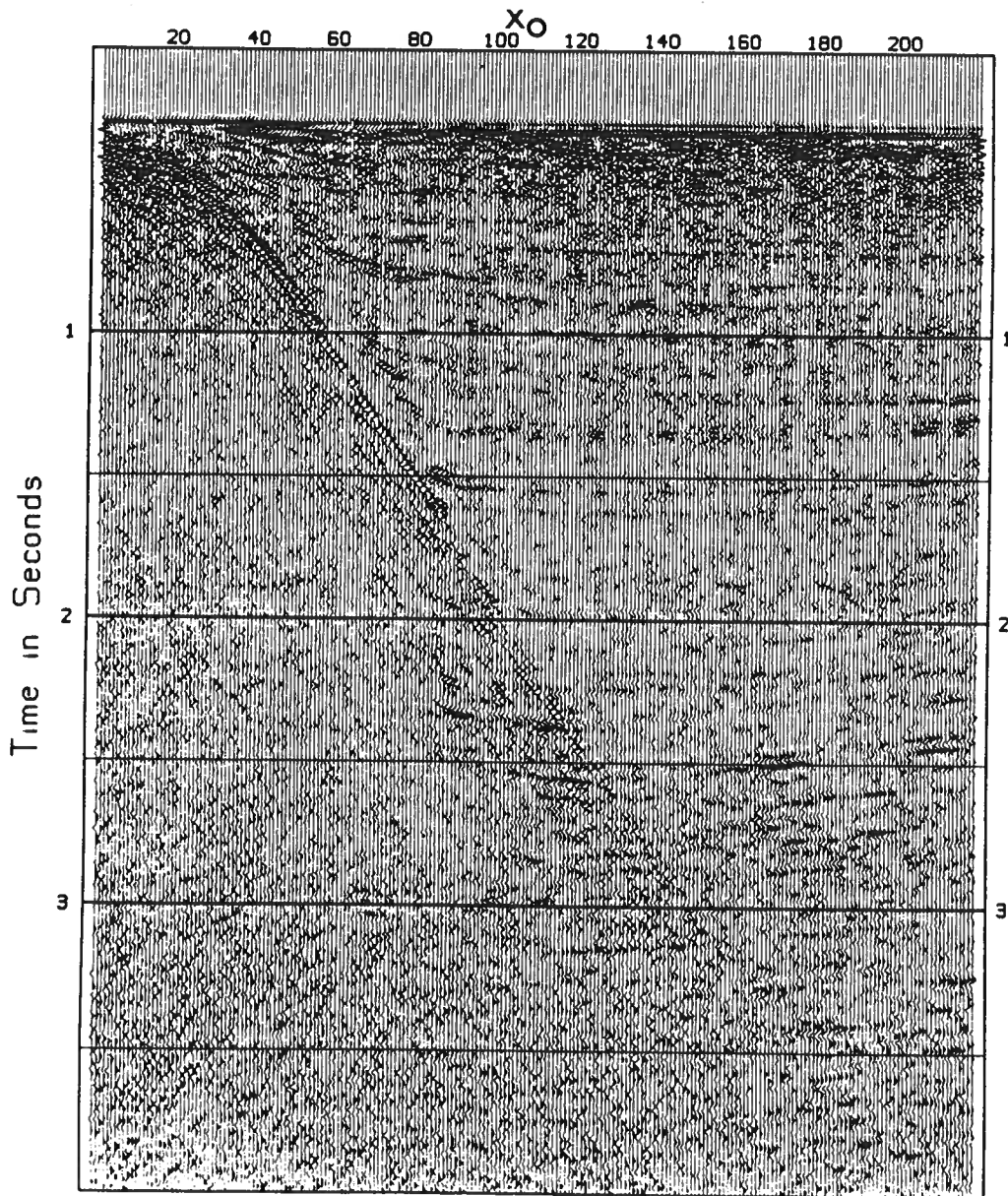


Figure 3.11: For the location marked  $x_0$ , velocity scans were done. For each indicated velocity, the 25 different contributors to  $x_0$  (one from each of the 25 shots) are saved and plotted side by side. When velocity is the correct velocity of 8000 ft/sec the 25 traces agree. Note that this is a dip independent velocity analysis (NMO+DMO) done on shot records. No CDP sorting is required.



**Figure 3.12: Salt Dome Data - Near Trace Display. Near trace offset is 1056 ft. Data were acquired from left to right with a 120 channel cable. Receiver interval is 82ft (25m). Data courtesy of Golden Geophysical and Anadarko Petroleum. (All displayed data in this and subsequent displays is plotted relative amplitude.)**

BERG  $\times 12500 \quad v = 5000 + 375t$

TZO  $\times 12500 \quad v = 5000 + 375t$

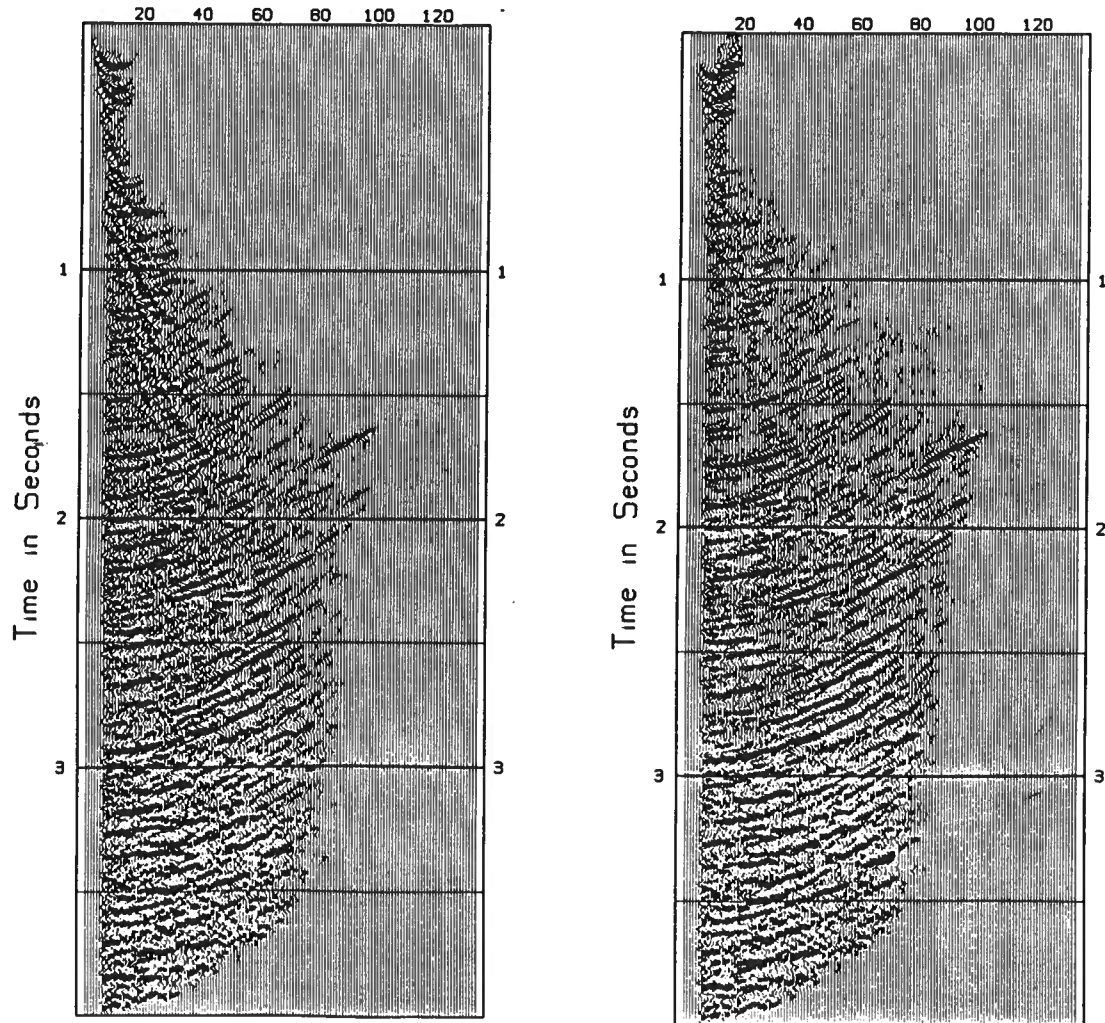


**Figure 3.13:**  $V=5000 + 375t$  velocity function for both Berg and Tzo algorithms. Velocity analysis is at location  $x_0$  of Fig. 3.12. The zero offset traces generated from each shot are plotted side by side. The traces smile up toward those shots whose contributions consist predominantly of far offsets. Thus, velocity is too slow.

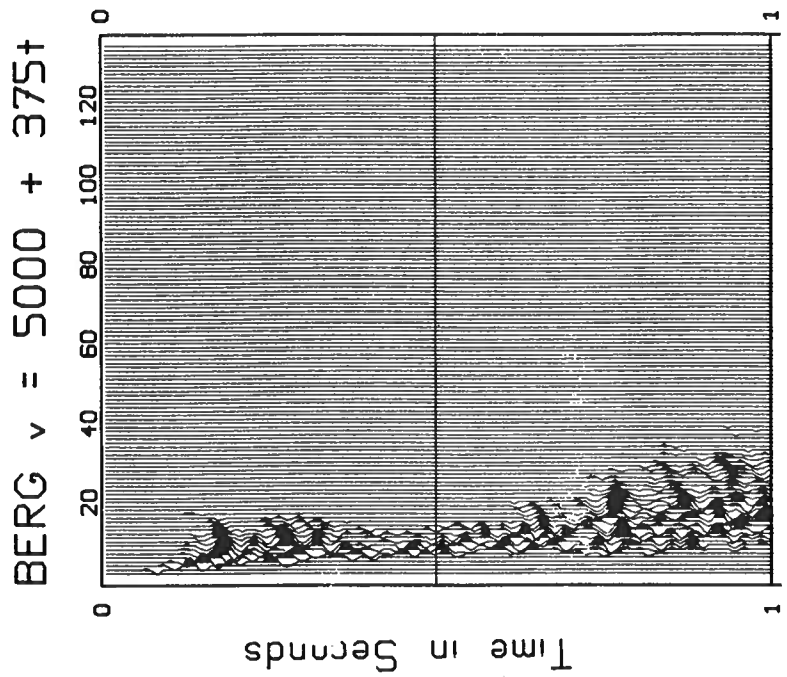
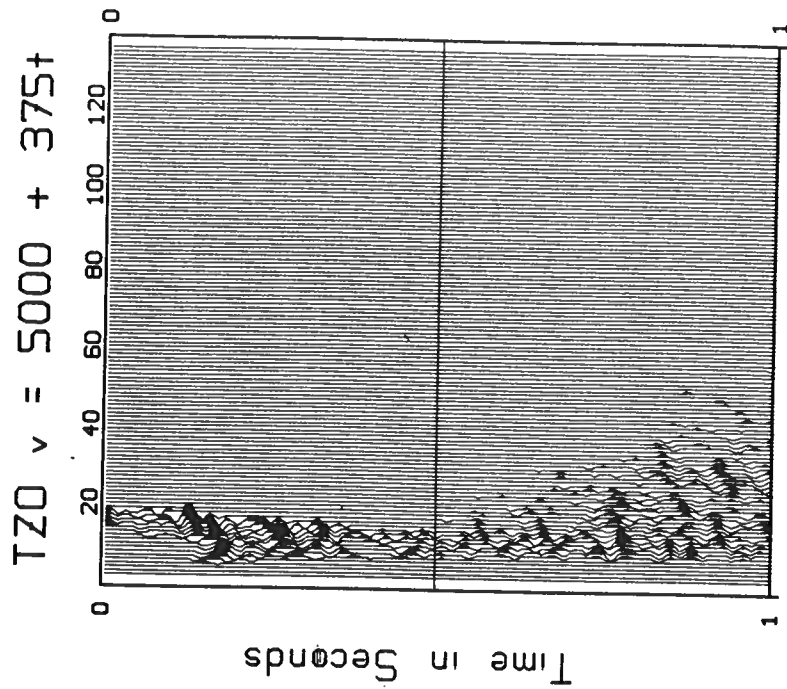


**Figure 3.14a: Enlarged view of 3.13 for 0 - 1 seconds.**

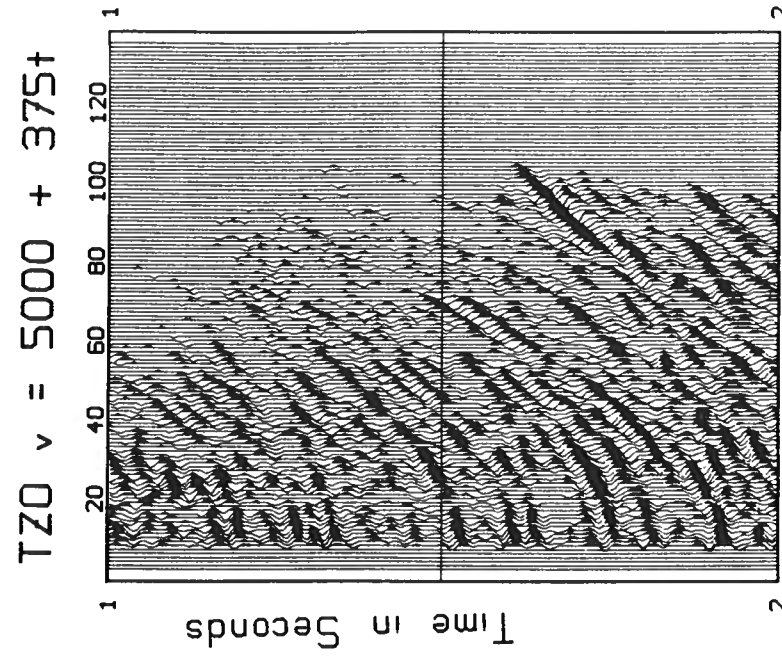
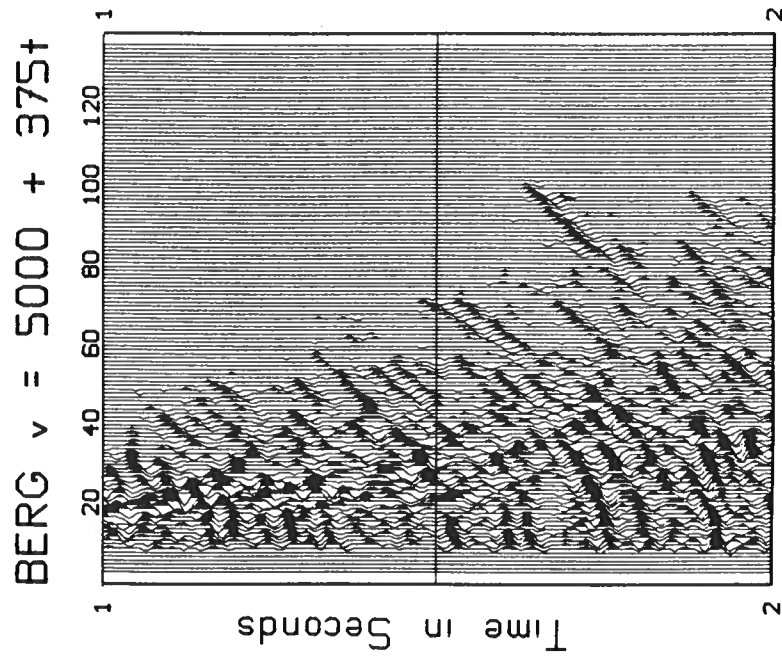


**Figure 3.14b: Enlarged view of 3.13 for 1 - 2 seconds.**

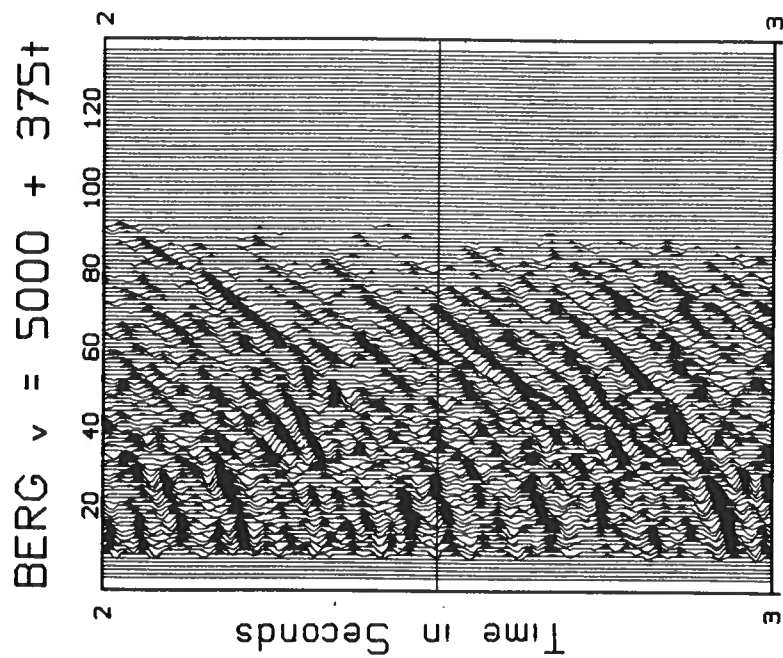
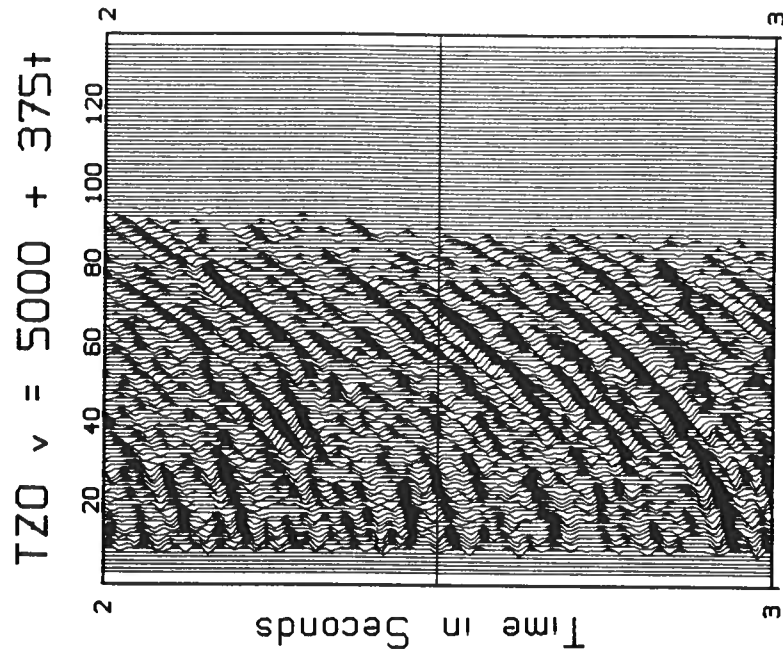


**Figure 3.14c: Enlarged view of 3.13 for 2 - 3 seconds.**

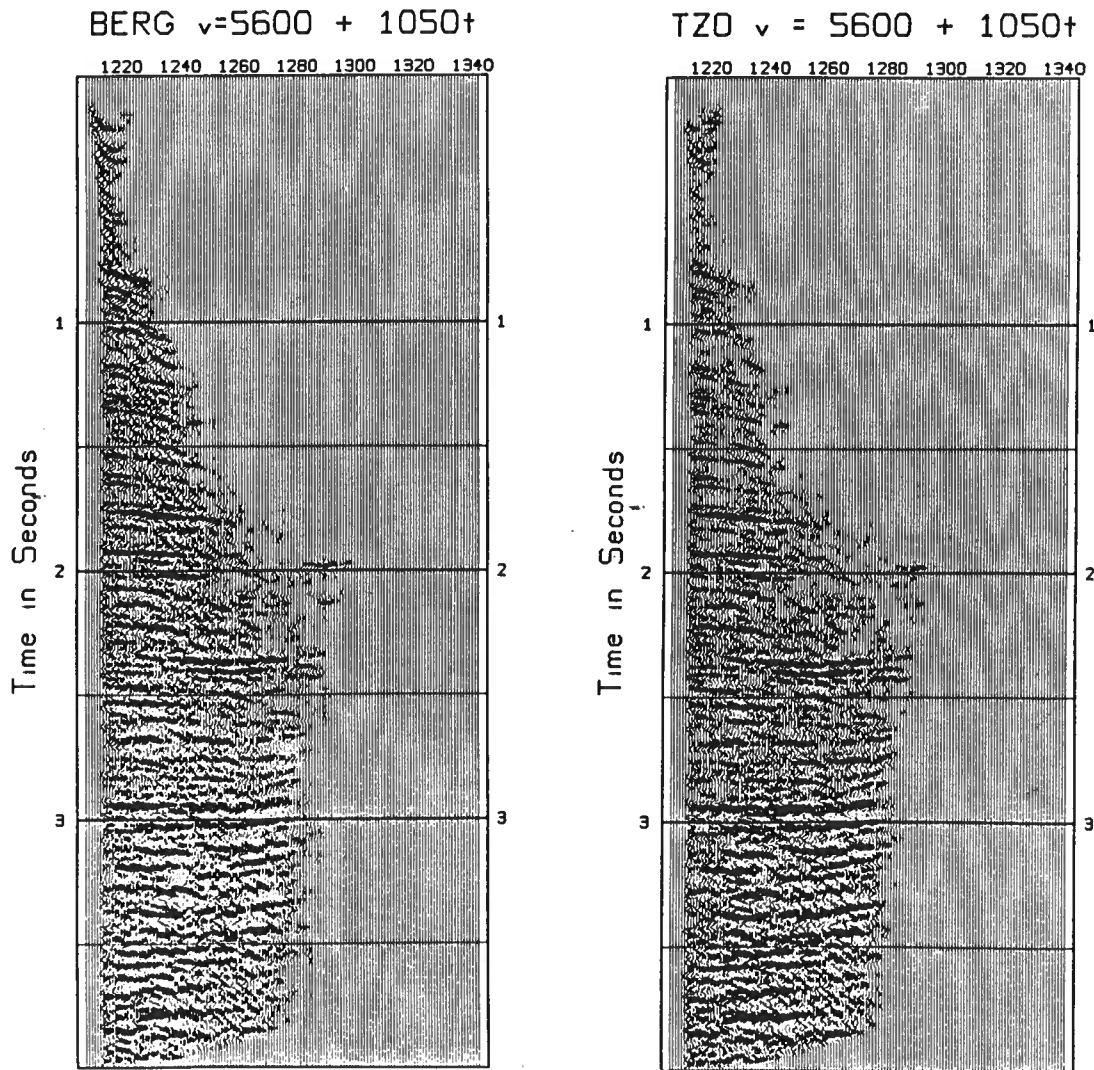


**Figure 3.15:  $v = 5600 + 1050t$  velocity panel for Berg and TZO algorithms. Here the function is approximately correct for the data between 2 and 3 seconds, as evidenced by agreement between traces from different shots.**

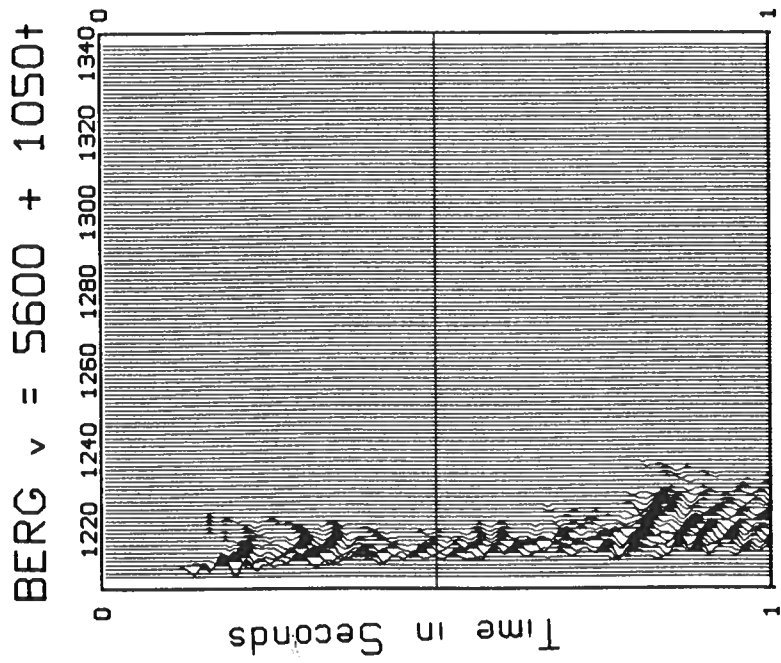
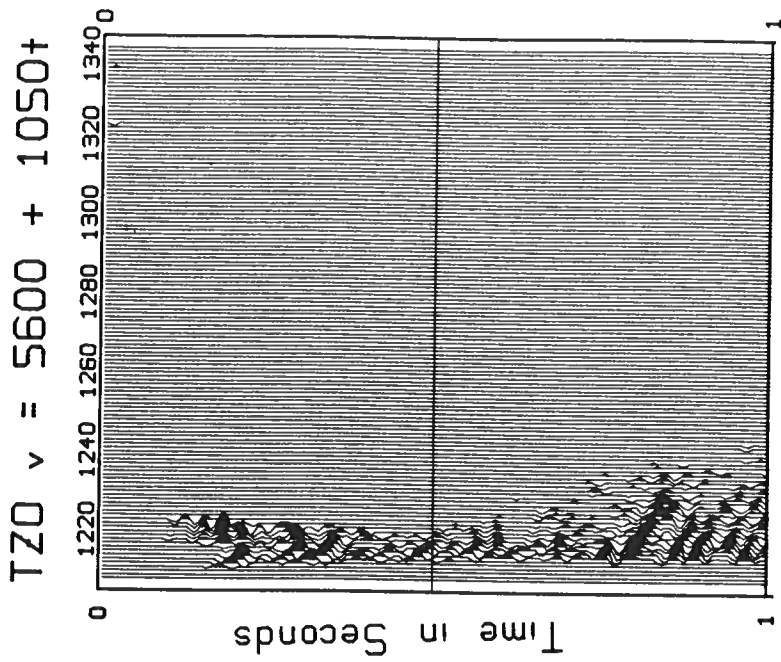


Figure 3.16a: Enlarged view of 3.15 for 0 - 1 seconds.

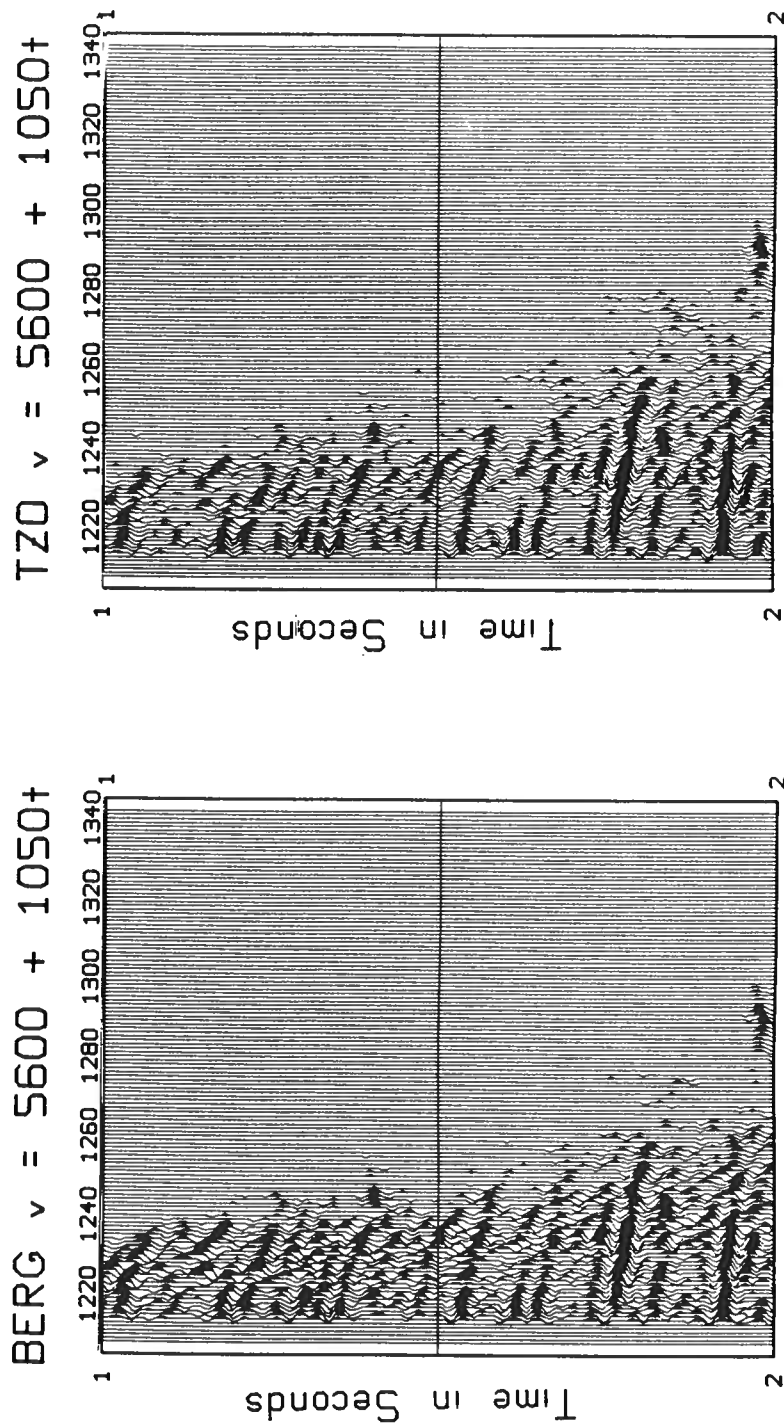
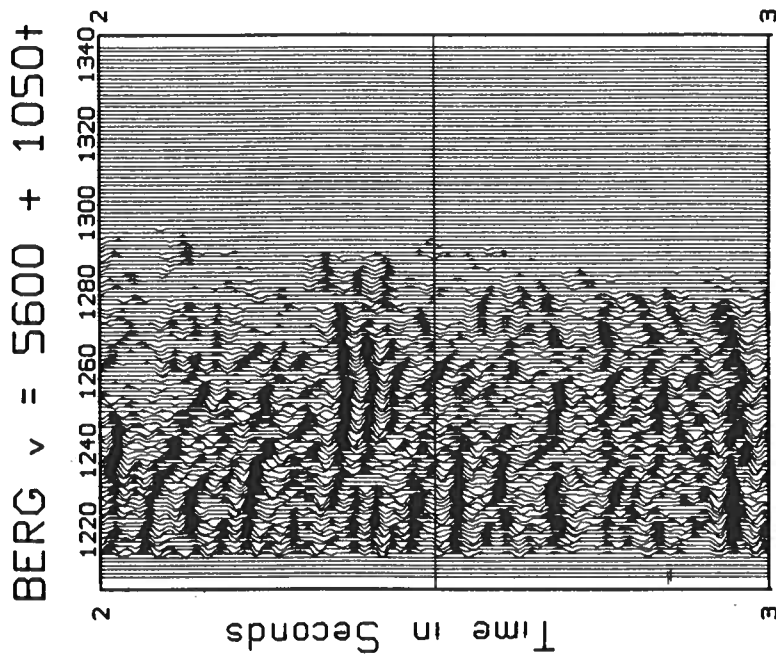
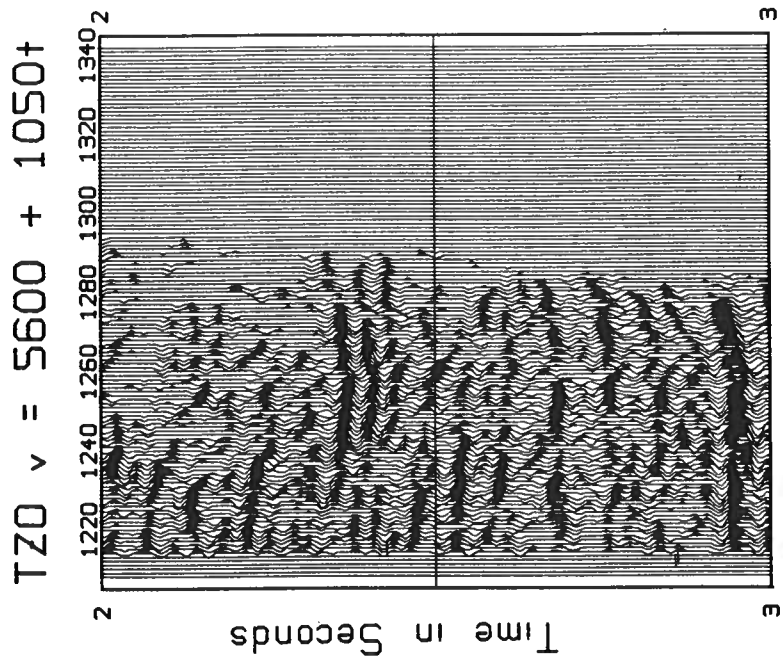
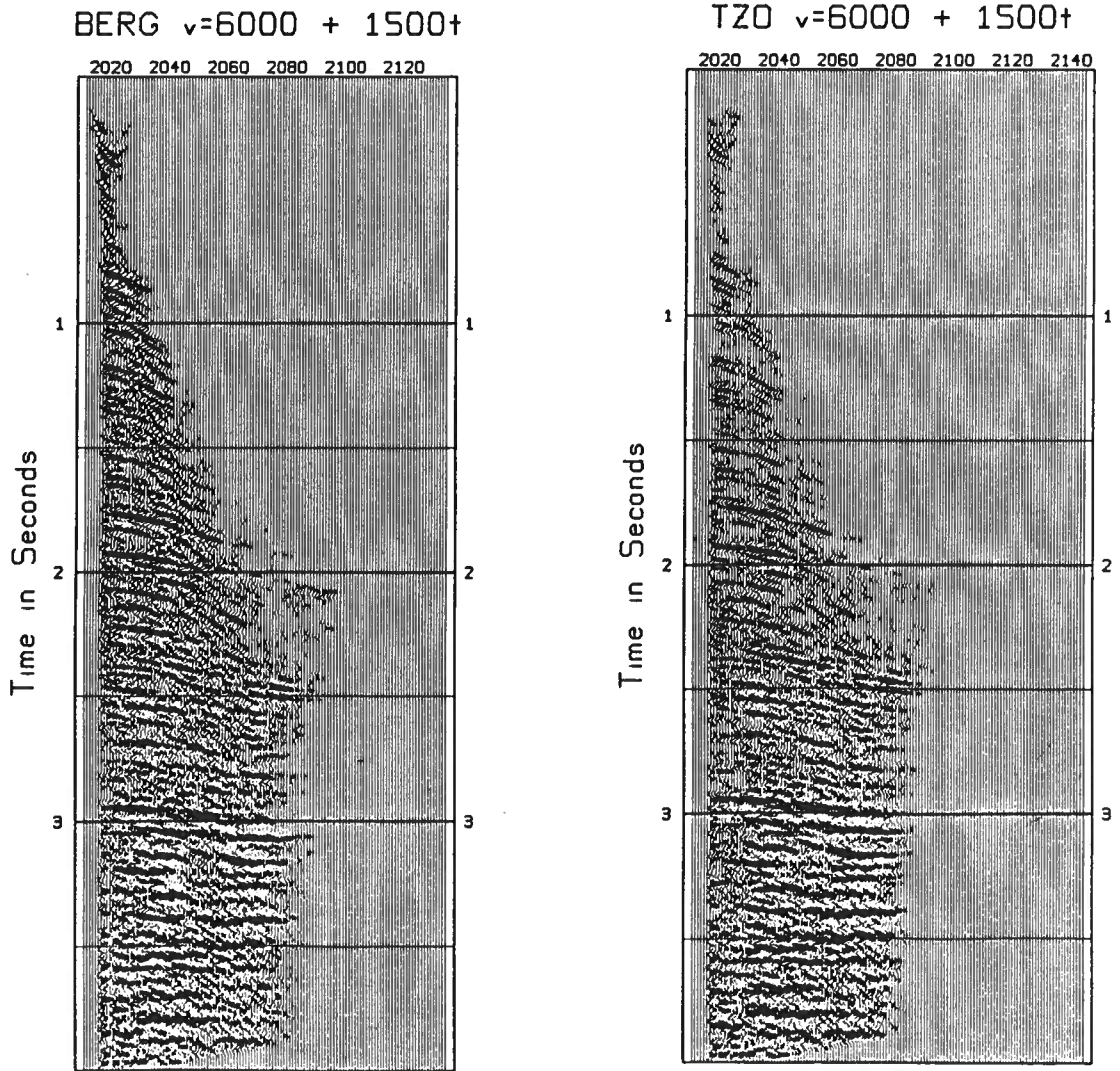


Figure 3.16b Enlarged view of 3.15 for 1 - 2 seconds.



**Figure 3.16c: Enlarged view of 3.15 for 2 - 3 seconds.**



**Figure 3.17:**  $v = 6000 + 1500t$  velocity panel for Berg and TZO algorithms. Here the function is too fast (as evidenced by traces frowning down towards those shots containing predominantly far offsets).

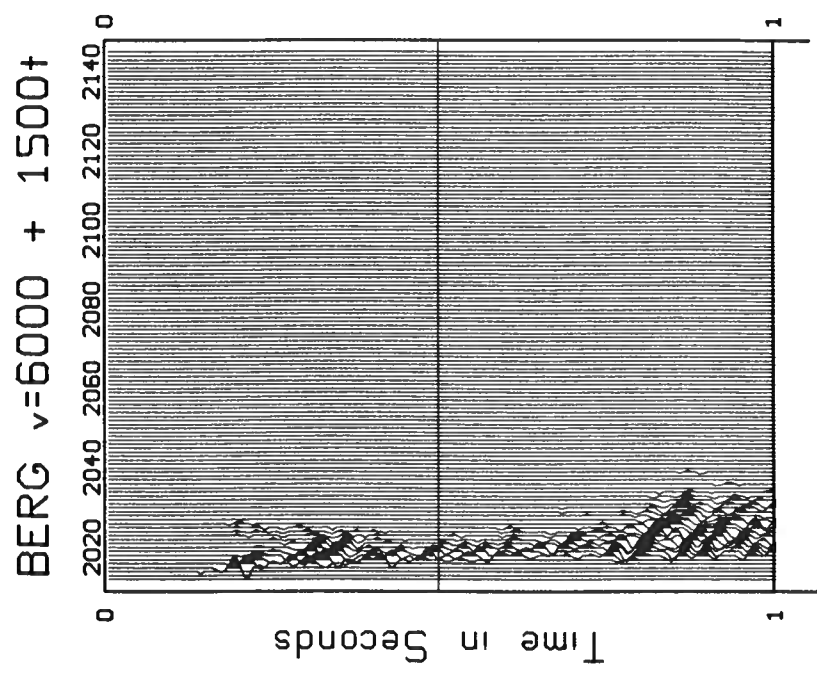
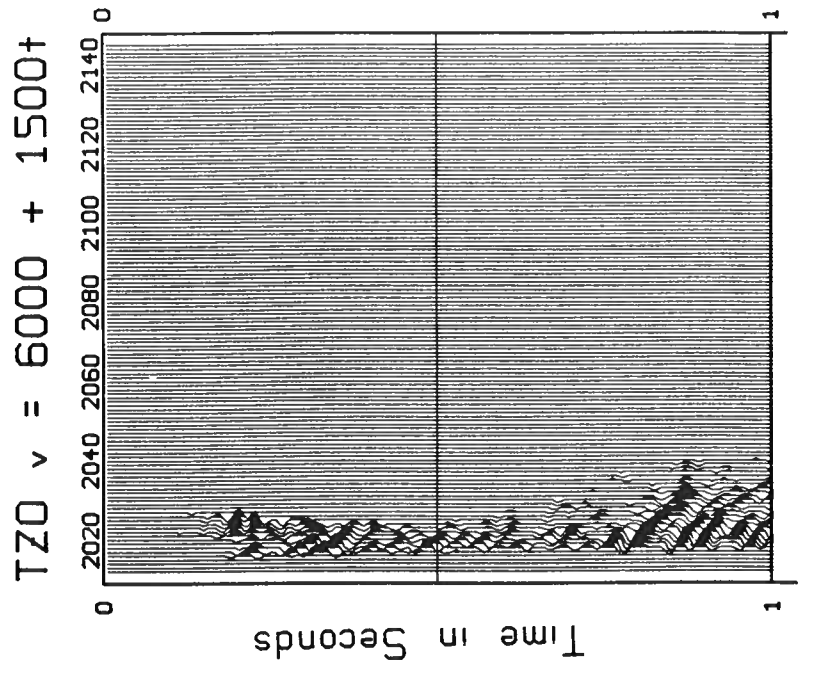


**Figure 3.18a: Enlarged view of 3.17 for 0 - 1 seconds.**

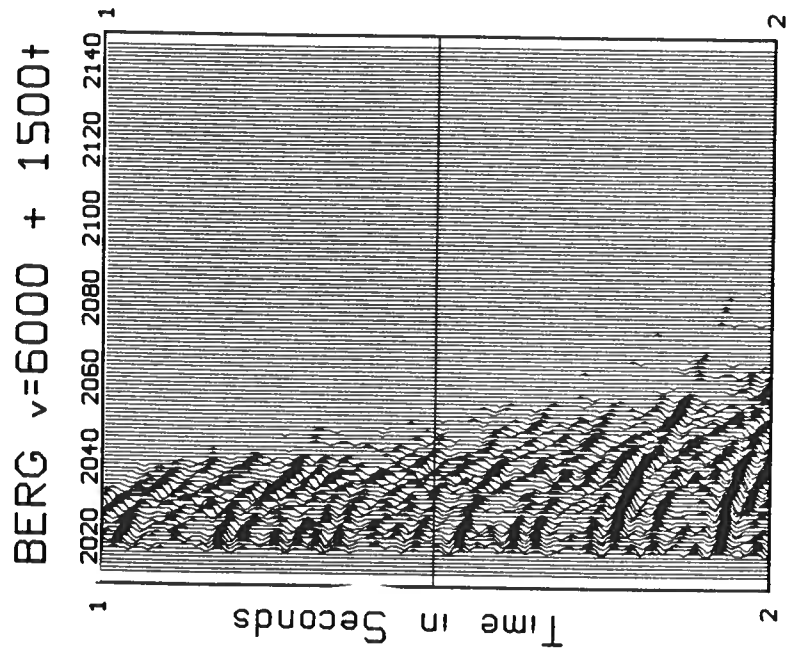
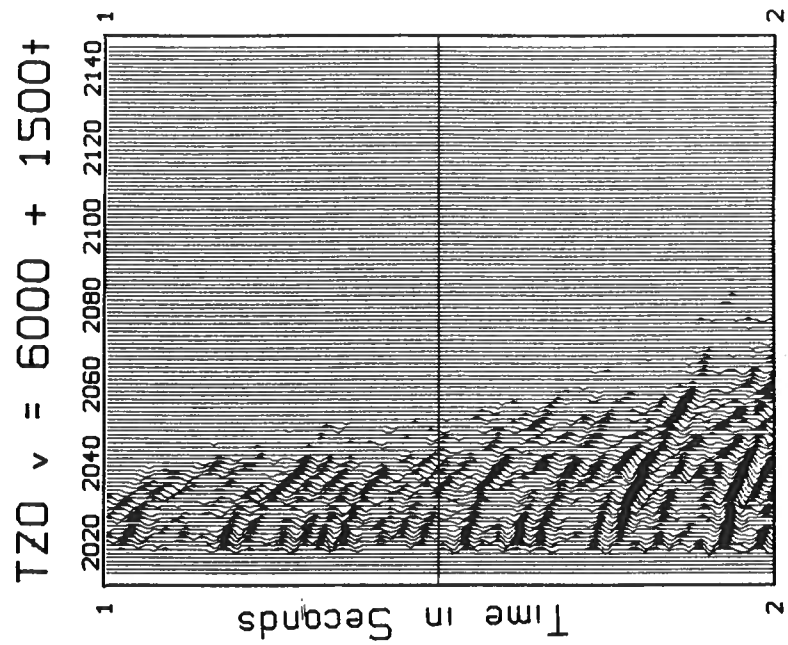


**Figure 3.18b: Enlarged view of 3.17 for 1 - 2 seconds.**

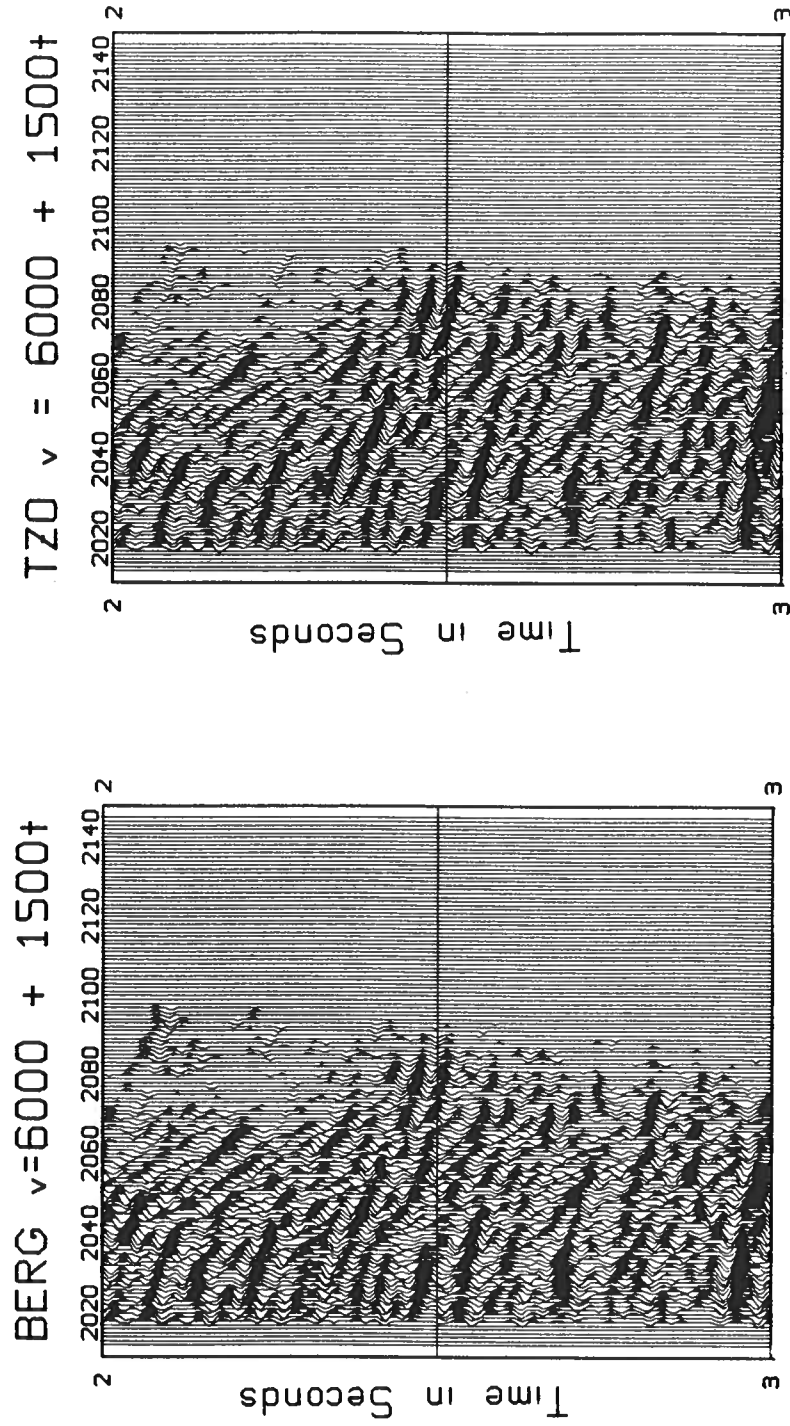


**Figure 3.18c: Enlarged view of 3.17 for 2 - 3 seconds.**

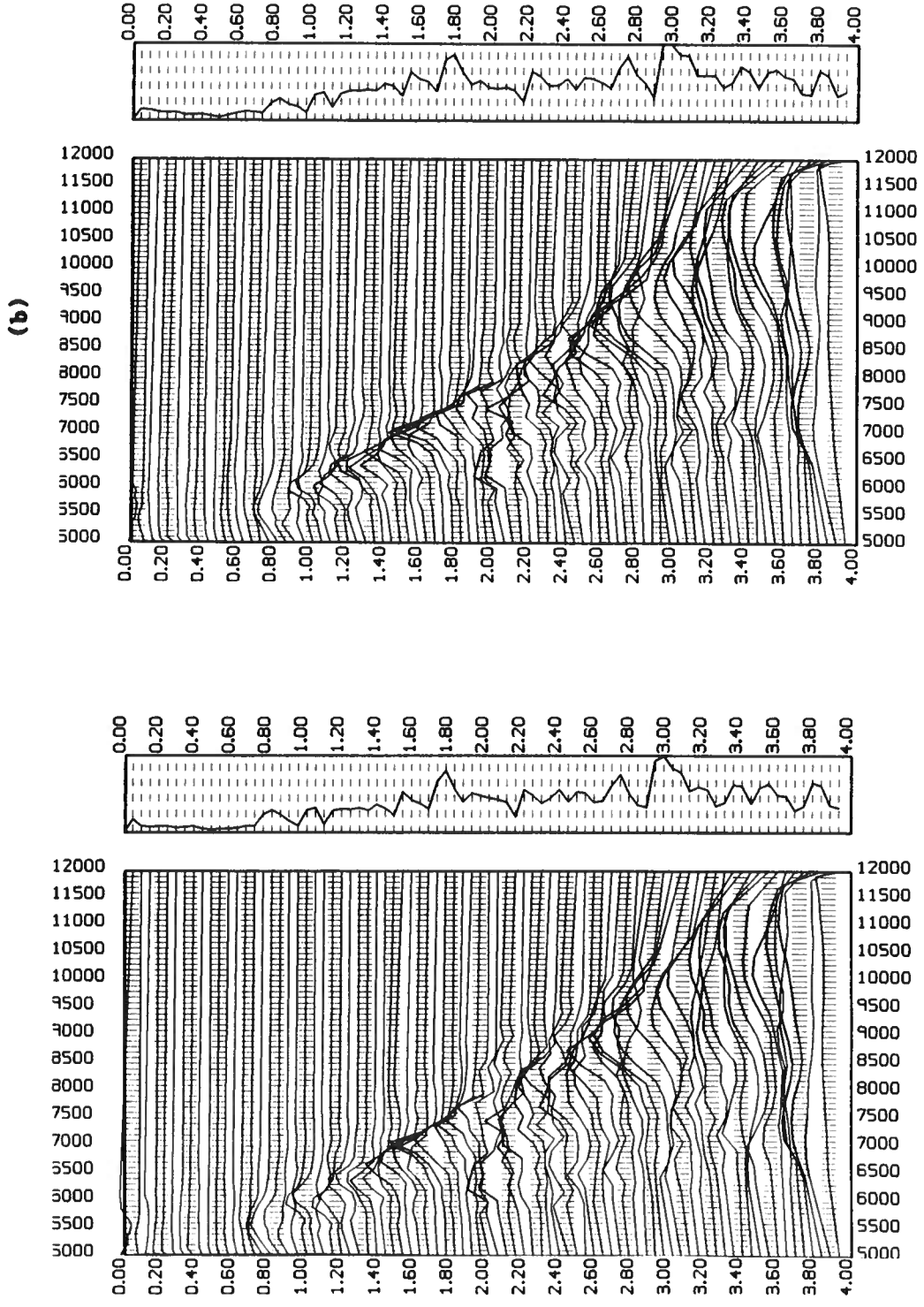


**Figure 3.19: Semblance displays of the velocity spectra for the Berg algorithm (a) and the TZO algorithm. The bar along the side of each spectrum plots the relative maximum semblance values at each time.**

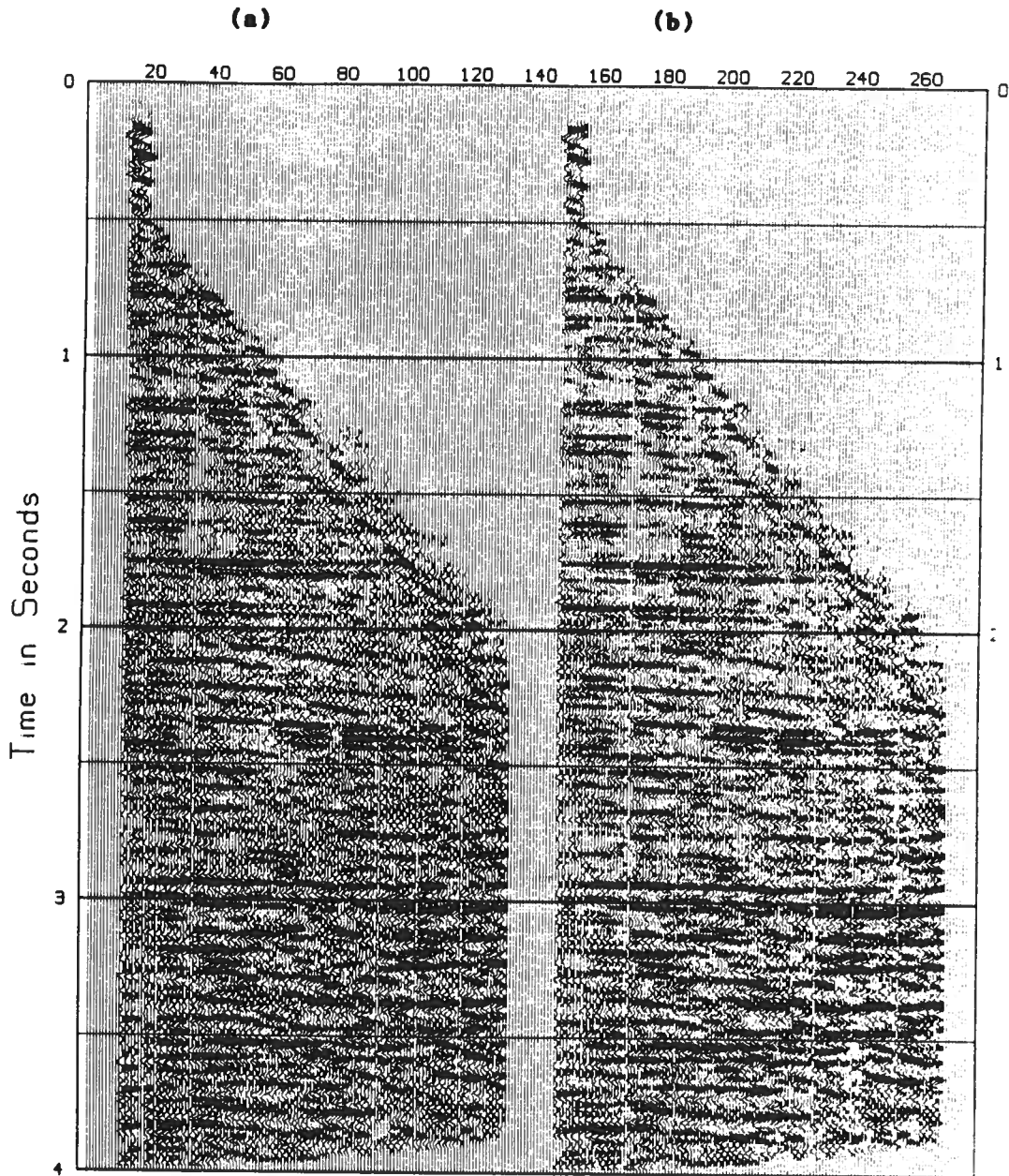


Figure 3.20: Offset panels for Berg (a) and TZO (b) algorithms. For the location  $x_0$  on Fig. 3.12 the contributions from each offset are saved and plotted side by side for comparison. Thus, this is equivalent to looking at the CDP  $x_0$  after the procedures NMO + DMO. Near offset is 1056 ft. Far offset is 10814 (receiver spacing 82 ft).

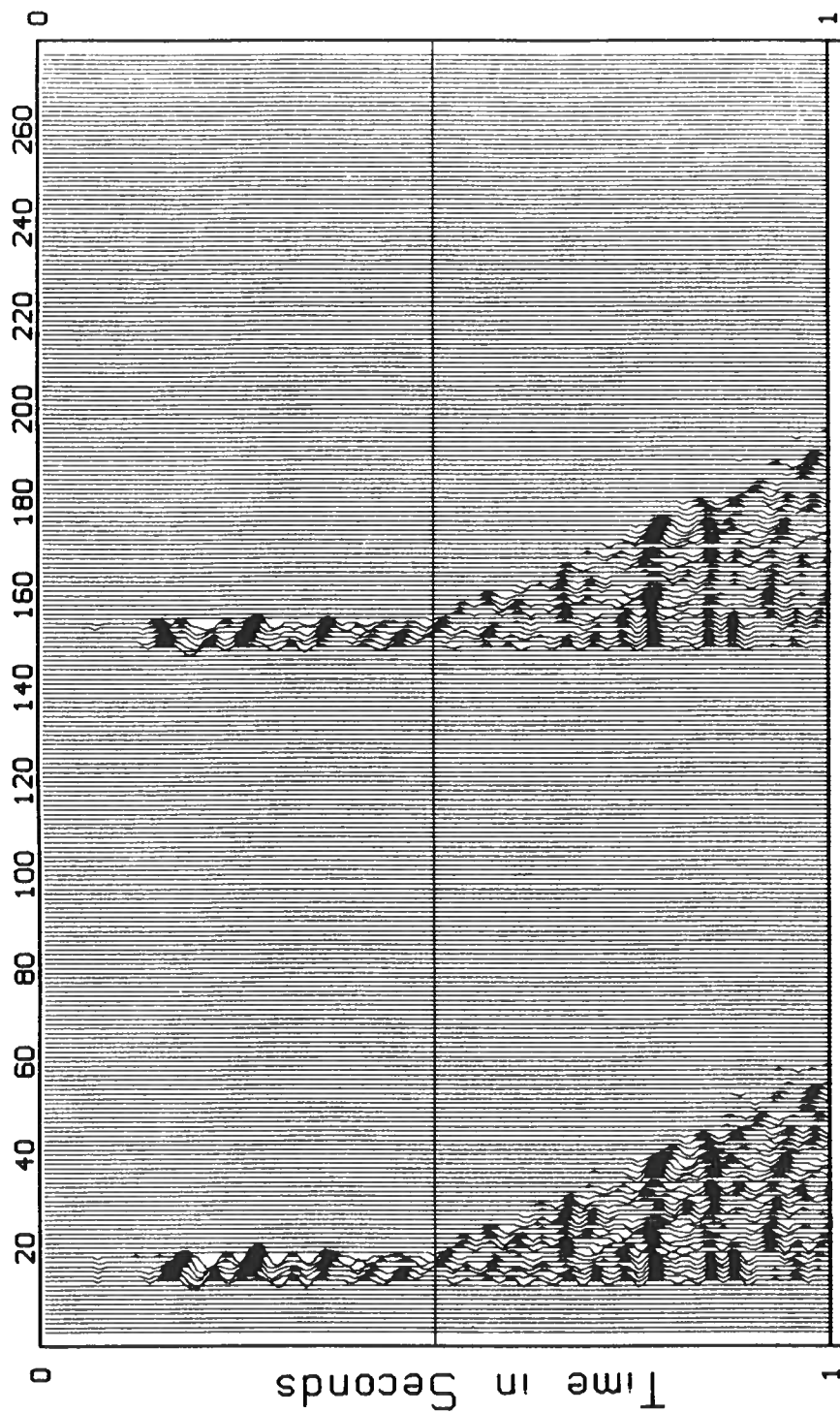


Figure 3.21a: Enlargement of Fig. 3.20 for 0 - 1 seconds.

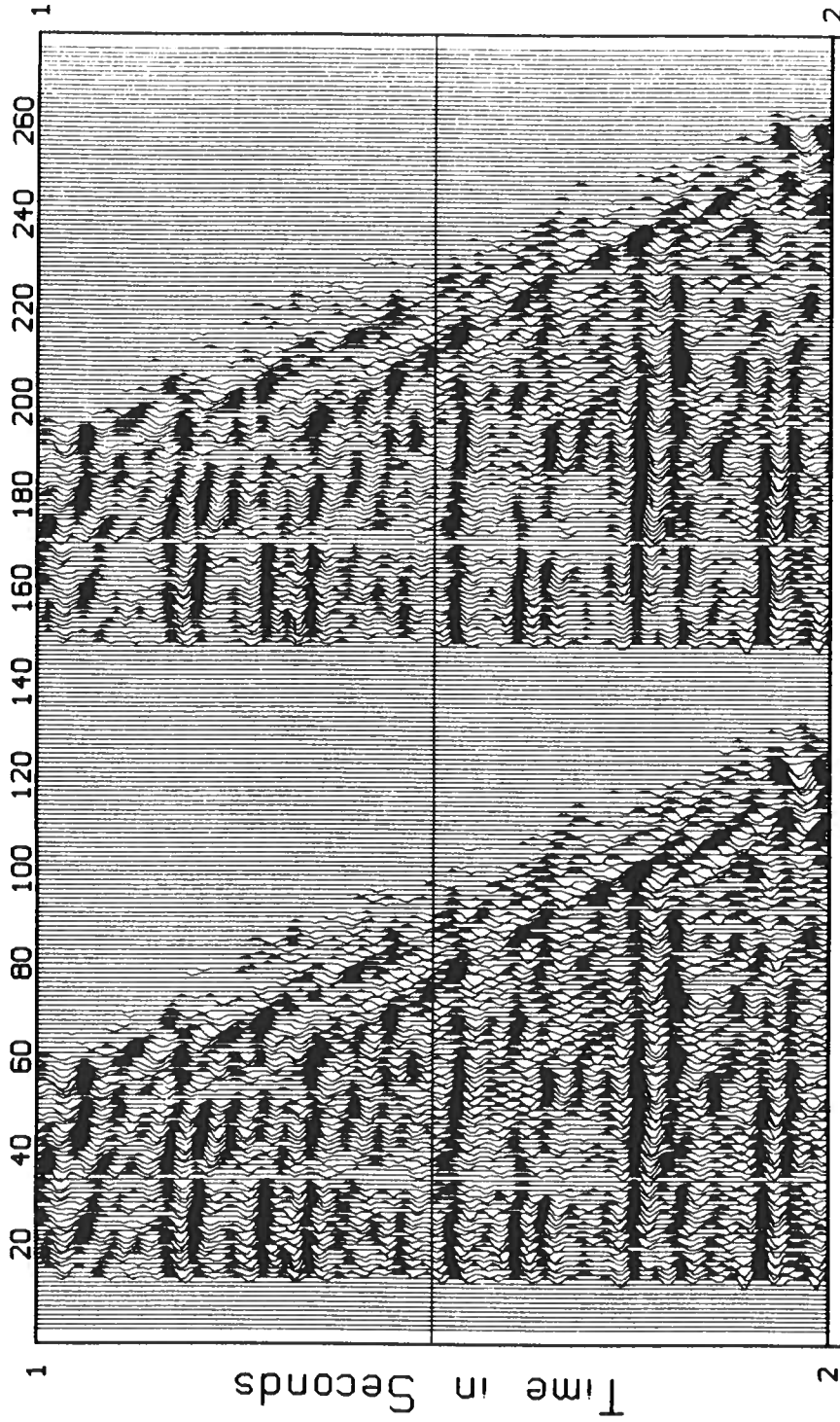


Figure 3.21b: Enlargement of Fig. 3.20 for 1 - 2 seconds.

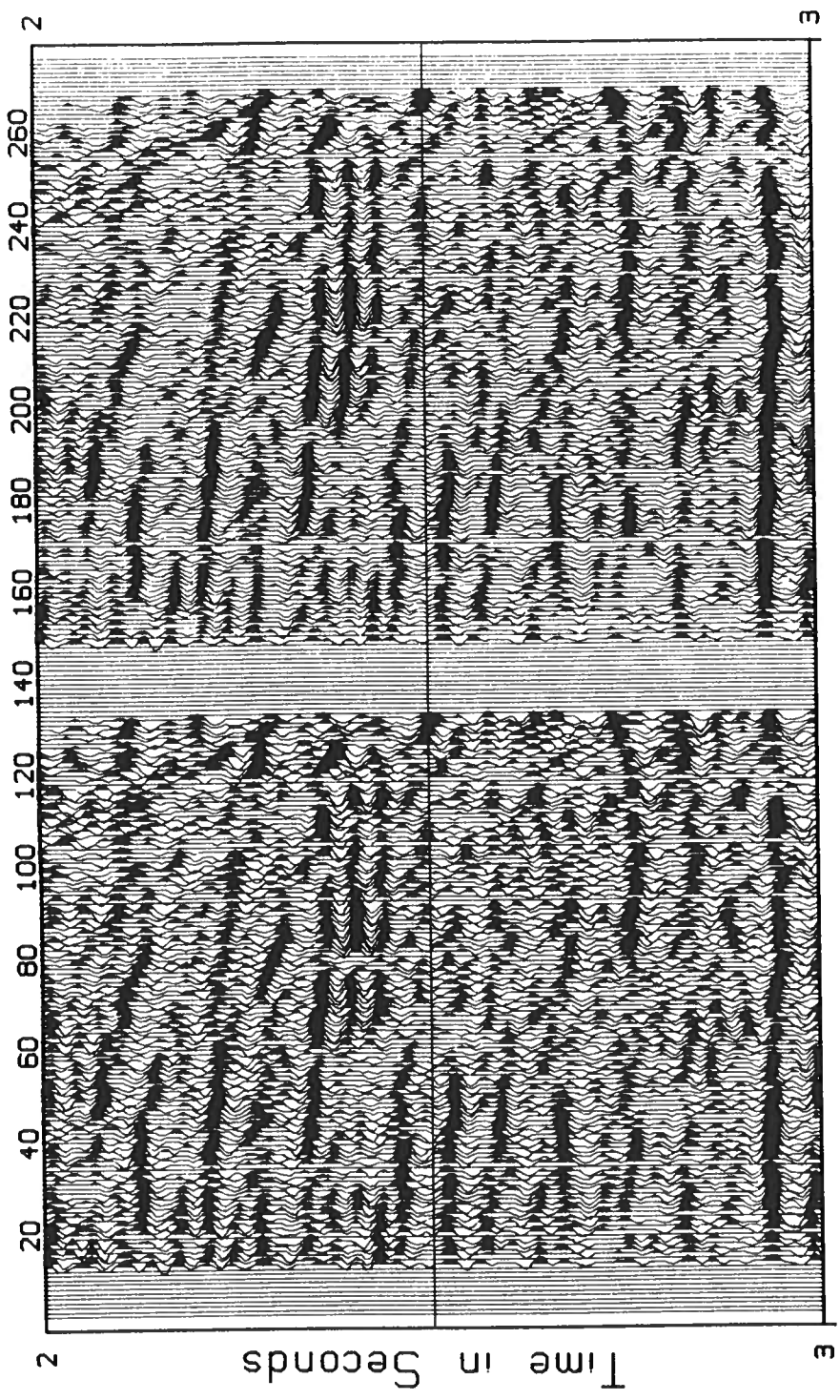
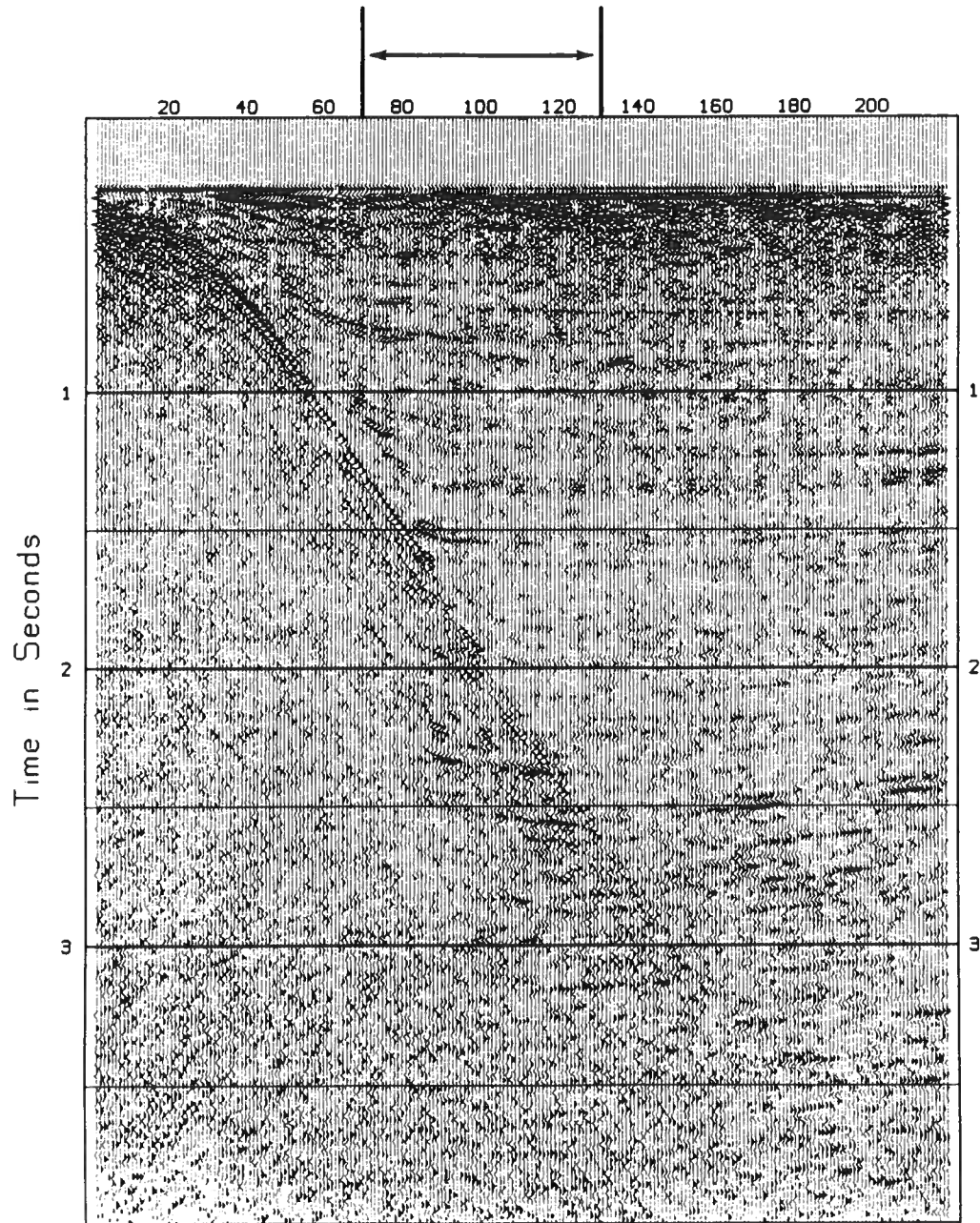


Figure 3.21c: Enlargement of Fig. 3.20 for 2 - 3 seconds.



**Figure 3.22: Near trace display showing region of stacked data.**

# BERG Stack vs TZO Stack

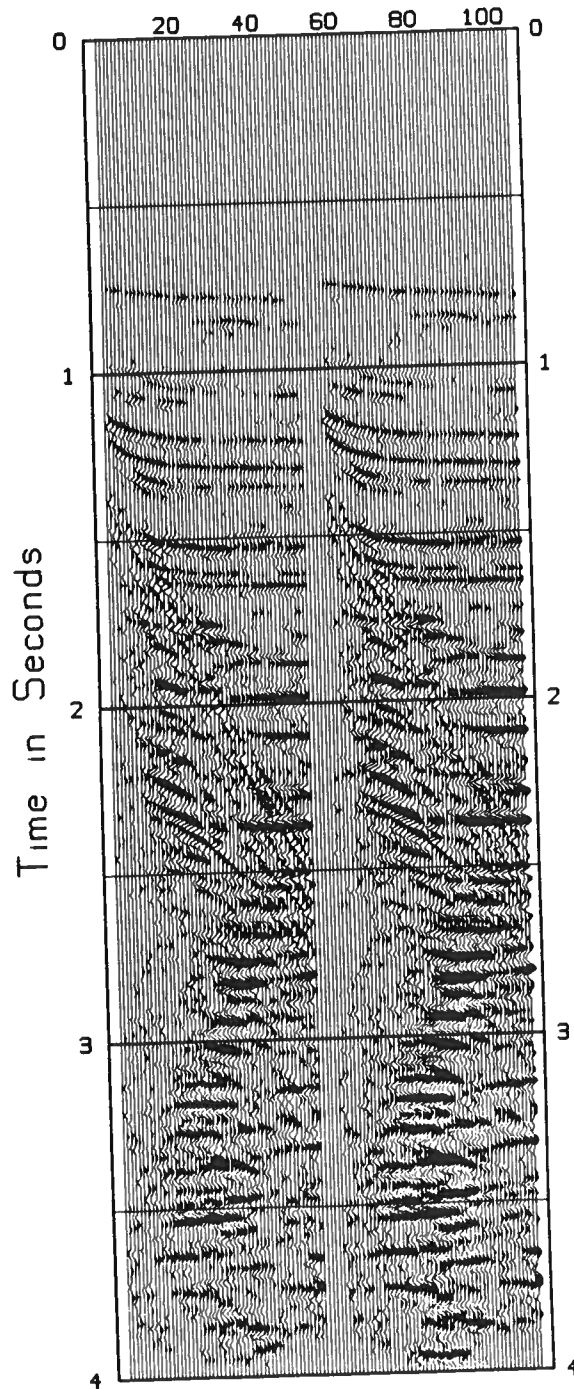
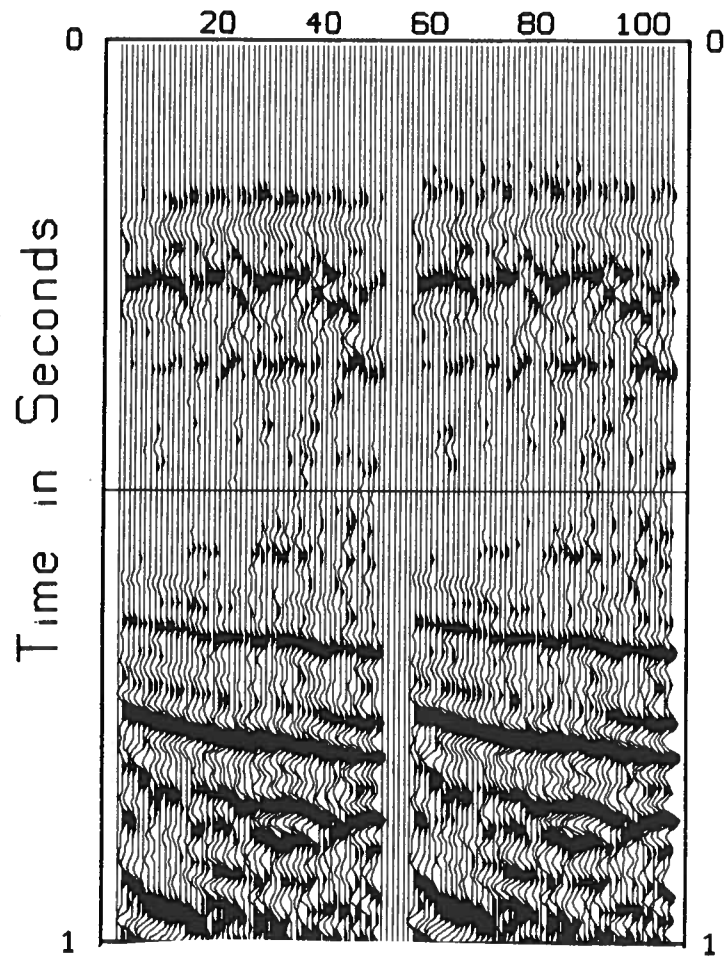
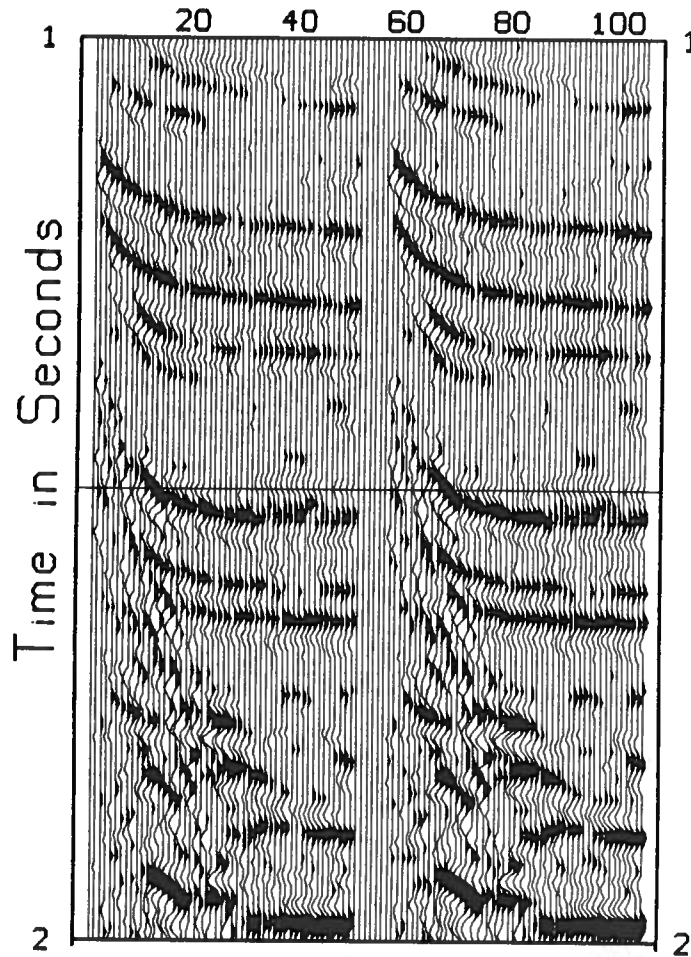


Figure 3.23: Comparison of Berg and TZO stacks over the range indicated in Fig. 3.22. The TZO operator used is the common offset domain operator.



**Figure 3.24a: Enlarged version of Fig. 3.23 for 0 - 1 seconds.**



**Figure 3.24b: Enlarged version of Fig. 3.23 for 1 - 2 seconds.**

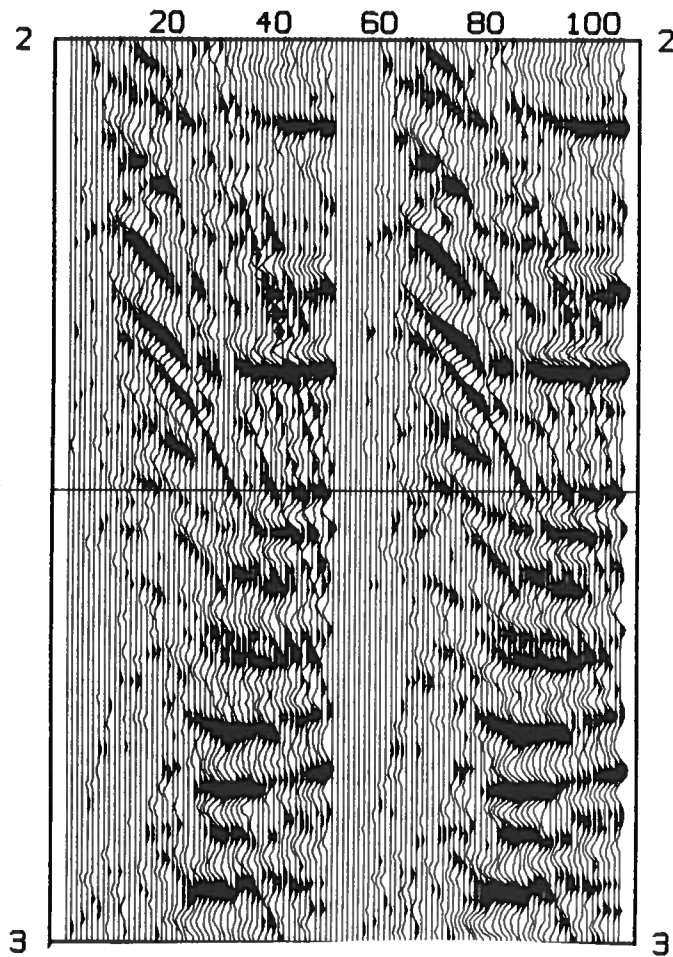


**Figure 3.24c: Enlarged version of Fig. 3.23 for 2 - 3 seconds.**

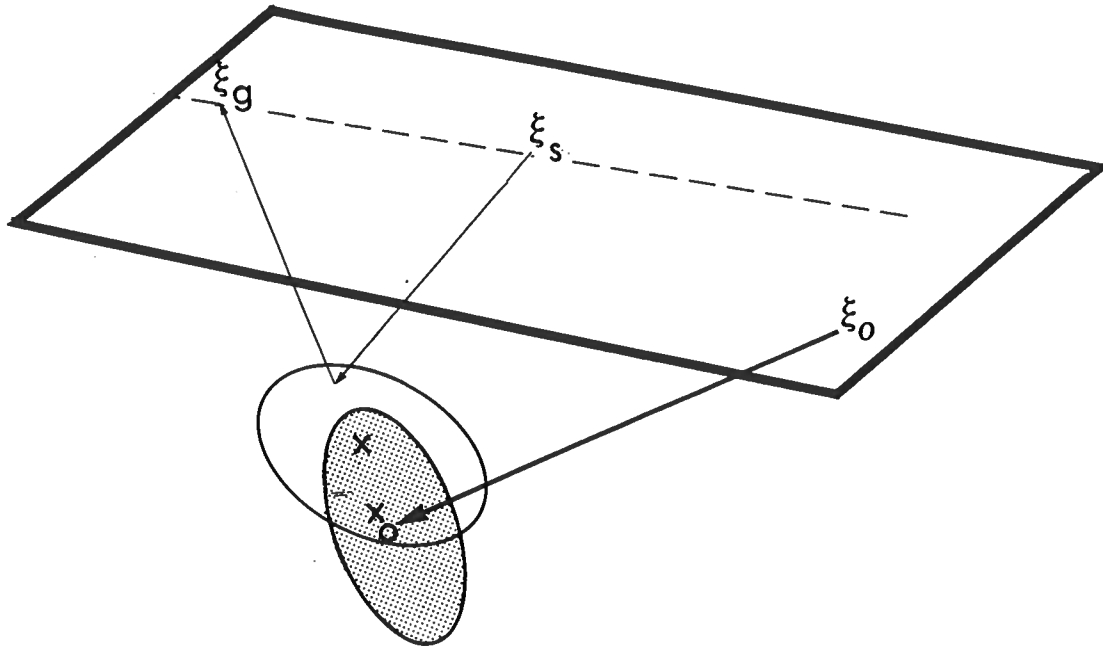


**Figure 3.25: Fresnel zone overlap for 3D transformation to zero offset. The problem is formulated as a pre-stack migration followed by a zero offset model. For a migrated output point  $x$ , all receivers  $\xi$  whose specular reflection is a Fresnel zone away from  $x$  will have a non-negligible contribution to  $x$ . In the forward modeling problem, the zero offset reflection point,  $x_0$ , gets a non-negligible contribution from those points  $x$  which are within a Fresnel zone of  $x_0$ . The result is that, in the 3D case, receivers  $\xi$  which are offline from  $\xi_0$  may produce a non-negligible contribution to  $\xi_0$ .**

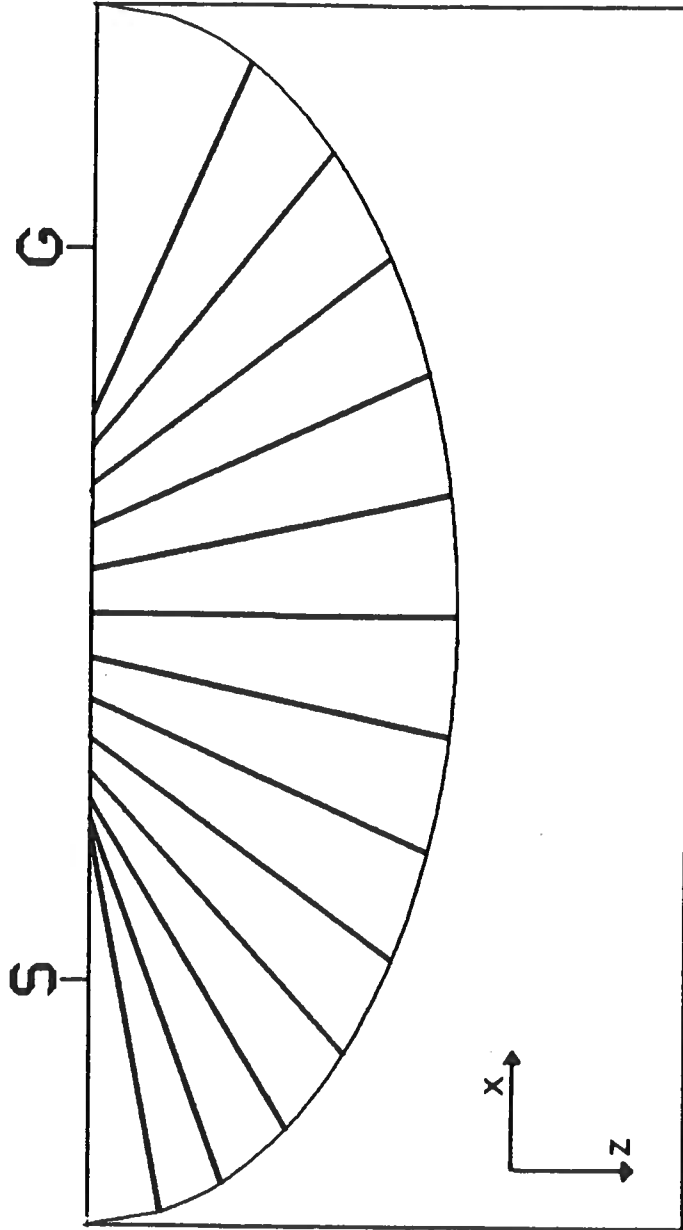


Figure A-1: The condition that the zero offset location,  $\zeta_0$ , be between the shot and receiver can be envisioned geometrically by the fact that all normals to an ellipse project to points between the foci. The ellipse is the pre-stack impulse response. The normals are the zero offset projections. (Exaggerated scale makes projections appear non-normal).

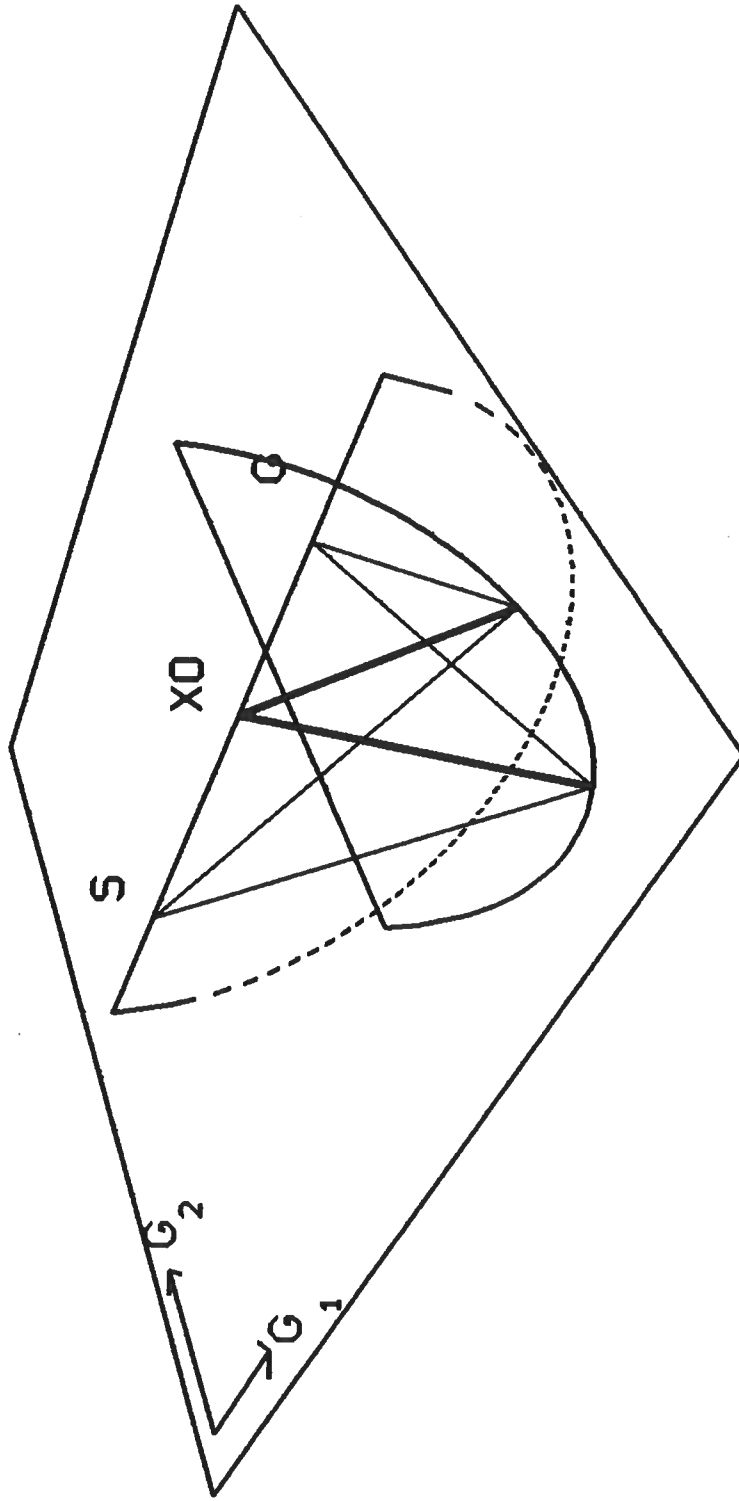
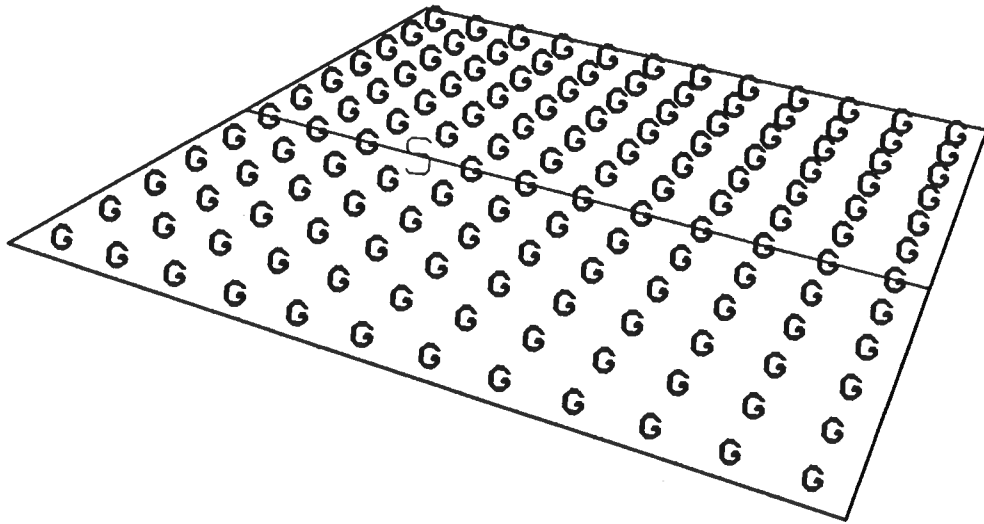


Figure B-1: Out-of-plane speculars. The condition of a specular reflection point is non-unique in transforming to zero offset. the specular reflection can be rotated in or out of plane leaving the zero offset location,  $x_0$ , unchanged.



**Figure B-2: 3D Common Shot. 3D common shot is defined as data with a fixed source point and receivers distributed over the acquisition surface.**

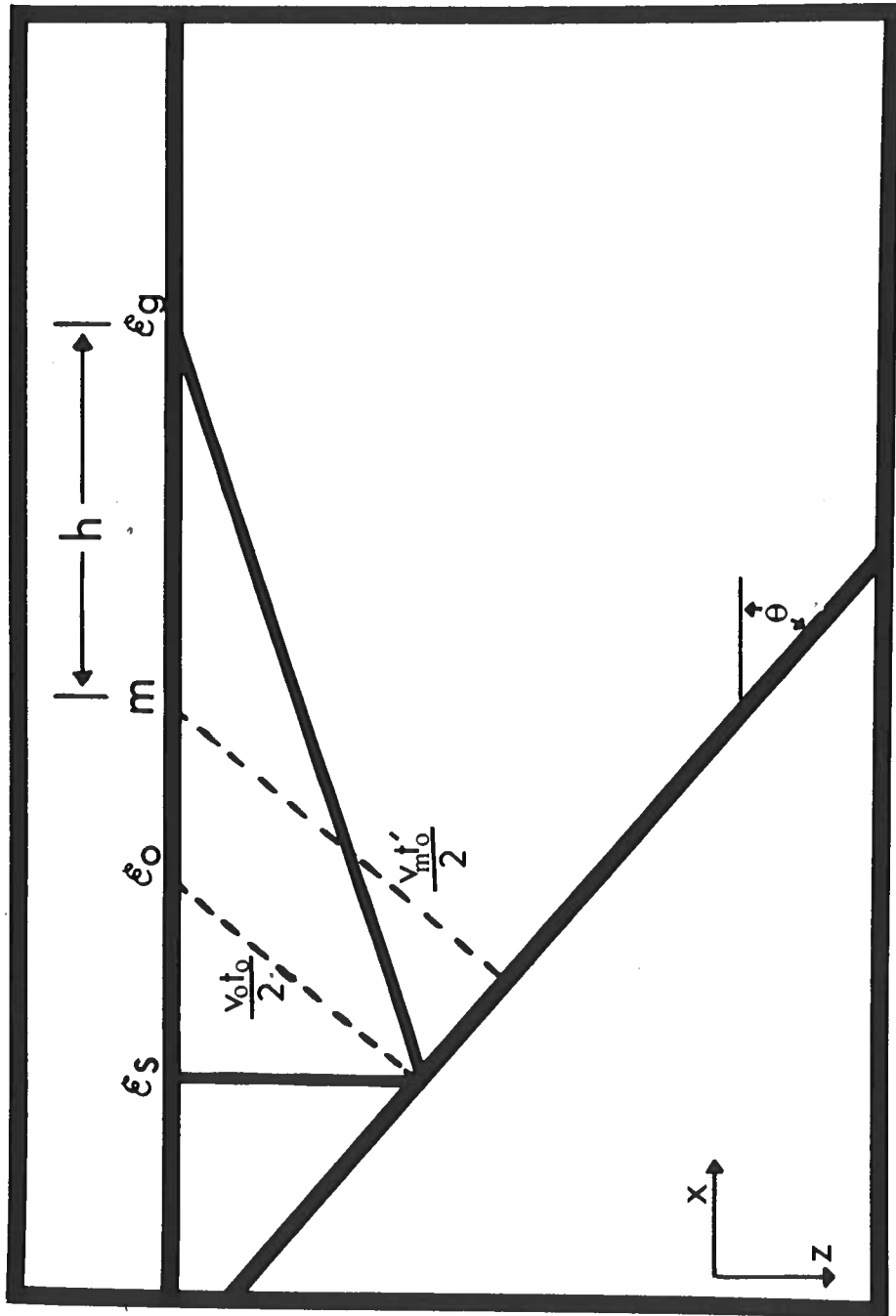
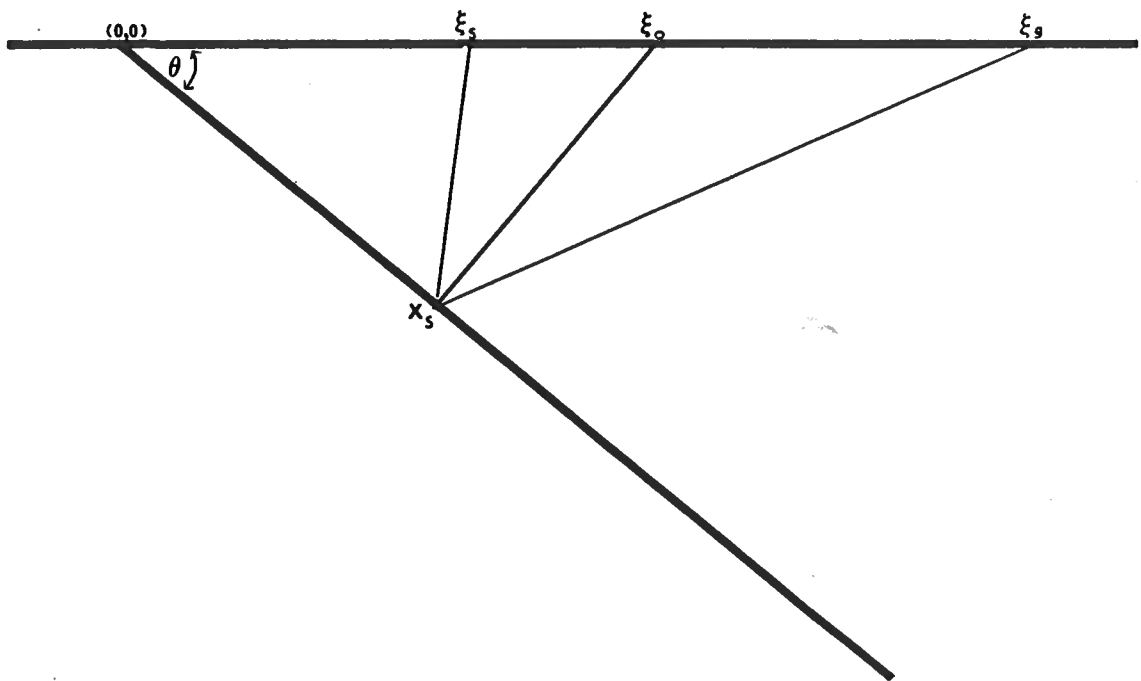


Figure D-1: Mapping geometry. The time  $t_o'$  is the two-way time at the midpoint,  $m$ . The time  $t_o$  is the actual zero offset two-way traveltime at the reflection point.



**Figure E-1: Specular reflection point corresponding to  $\xi_s$ ,  $\xi_g$ , and output point  $\xi_o$ .**

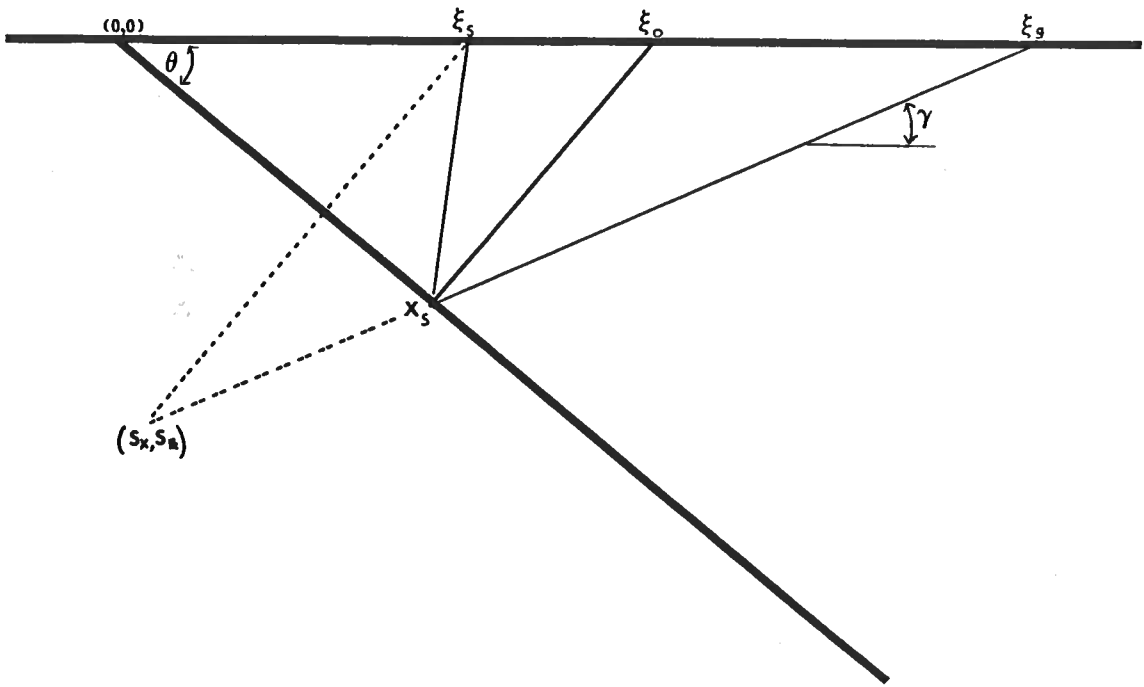


Figure E-2: Image source facilitates the solution of  $x_s$  in terms of known quantities

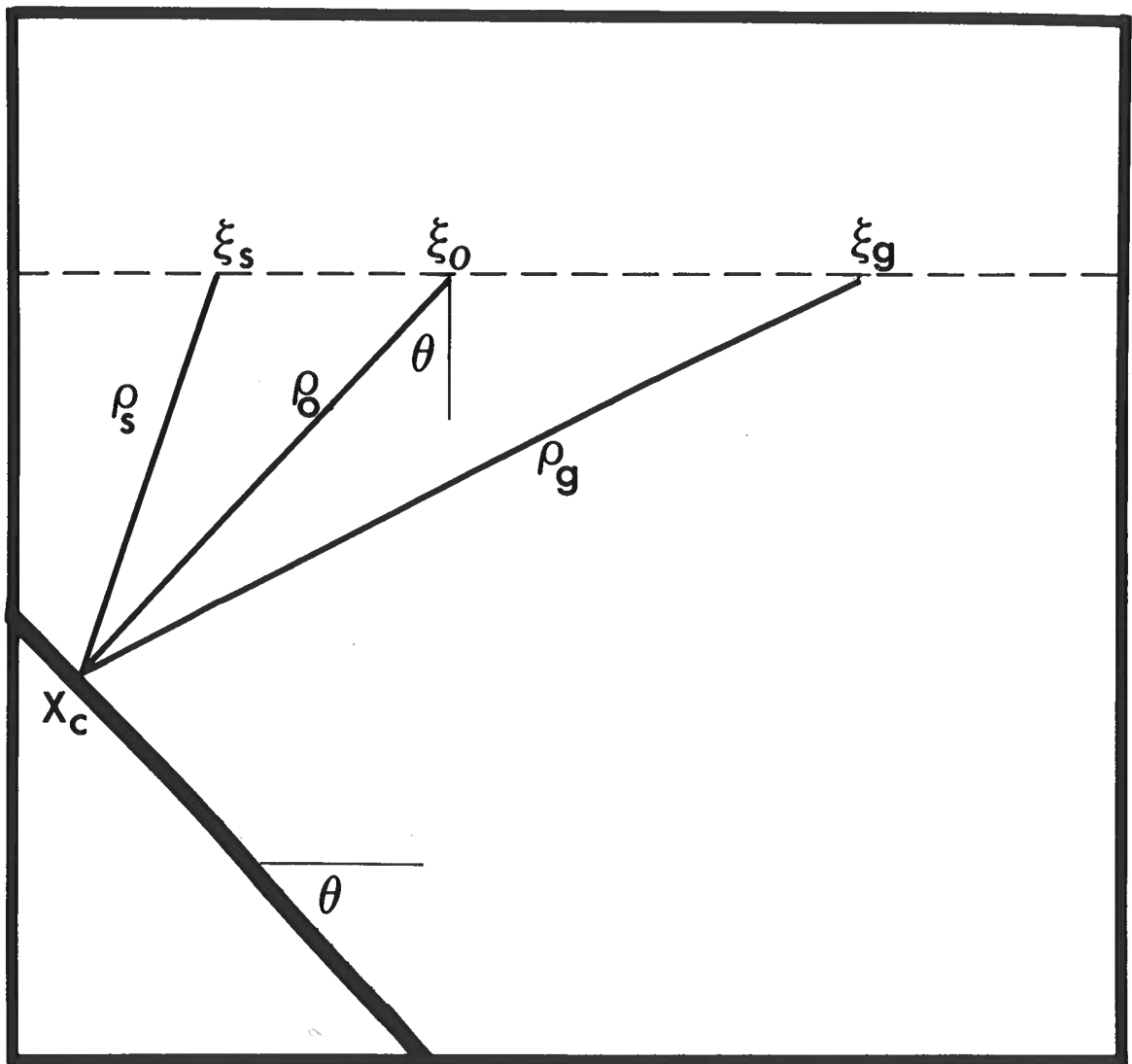


Figure F-1: Dip limits can be determined solely from geometrical considerations.